UNIVERSIDAD COMPLUTENSE DE MADRID
FACULTAD DE CIENCIAS FÍSICAS
DEPARTAMENTO DE FÍSICA DE MATERIALES

TESIS DOCTORAL

Tribological behaviour of DP600 dual phase steel on uni- and bi- directional discontinuos sliding wear.

Comportamiento tribológico del acero doble fase DP600 en ensayos de desgaste uni- y bi-direccionales por deslizamiento discontinuo

MEMORIA PARA OPTAR AL GRADO DE DOCTORA

PRESENTADA POR

Meritxell Ruiz Andrés

Director

Ignacio García Diego

Madrid, 2015

UNIVERSIDAD COMPLUTENSE DE MADRID

FACULTAD DE CIENCIAS FÍSICAS

DEPARTAMENTO DE FÍSICA DE MATERIALES

Doctoral Thesis

Tribological behaviour of DP600 dual phase steel on uni- and bi-directional discontinuous sliding wear.

Comportamiento tribológico del acero de doble fase DP600 en ensayos de desgaste uni- y bi-direccionales por deslizamiento discontinuo.

Meritxell Ruiz Andrés

Supervisor: Dr. Ignacio García Diego

Madrid 2015

CENTRO NACIONAL INVESTIGACIONES METALÚRGICAS (CENIM)

CONSEJO SUPERIOR INVESTIGACIONES CIENTÍFICAS (CSIC)

UNIVERSIDAD COMPLUTENSE DE MADRID

FACULTAD DE CIENCIAS FÍSICAS

DEPARTAMENTO DE FÍSICA DE MATERIALES

Doctoral Thesis

Tribological behaviour of DP600 dual phase steel on uni- and bi-directional discontinuous sliding wear.

Comportamiento tribológico del acero de doble fase DP600 en ensayos de desgaste uni- y bi-direccionales por deslizamiento discontinuo.

Meritxell Ruiz Andrés

Supervisor: Dr. Ignacio García Diego

Madrid 2015

CENTRO NACIONAL INVESTIGACIONES METALÚRGICAS (CENIM)

CONSEJO SUPERIOR INVESTIGACIONES CIENTÍFICAS (CSIC)

A mis padres.

“Lo que va davant, va davant, filla”

P. Andrés Clavell.

Este trabajo de investigación ha sido realizado gracias a la financiación proporcionada por los proyectos: Innpacto IPT-020000-2010-020, Ministerio de Economía y Competitividad (MINECO) y CONSOLIDER-INGENIO 2010 CSD 2008-0023 FUNCOAT.

Agradecimientos

Mi agradecimiento más sincero a Iñaki. Gracias por confiar en mi y por tu dedicación.

A Ana, Juan, Alfonso, Geles, Elena, Miguel, Mar, Manuel, Juan, Jose, Ana, Cristina y a todos los compañeros con los que he compartido estos años de investigación.

A mi familia y amigos por todo el apoyo mostrado durante todo este tiempo.

A mis padres y a mi hermano. Moltes gràcies pel vostre suport. Moltes gràcies per estar sempre al meu costat. Moltes gràcies per tot.

A Rafa por su motivación, comprensión y consejos. Gracias por estar a mi lado y hacerme feliz.

Y, especialmente, a Pascual, Remedios, Antonio y Asunción. Sé que us seguiu alegrant.

Abstract

Over the last decades, most of the tribological studies within the frame of the mild oxidative wear mechanism have suggested that the friction and wear behaviour are contact and sliding speed dependent. The wear model proposed by Quinn (1962, 1983, 1992, 1994, 1998) is responsible for addressing these analyses. In the case of unidirectional pin/ball-on-disc sliding wear tests, Quinn's model however does not distinguish between the contact conditions prevailing at the pin/ball and at the disc, which are completely dissimilar. At a macroscopic level, the pin/ball is in continuous contact with the disc. Conversely, each point of the wear track on the disc is only loaded when the pin/ball goes over it. Consequently, Garcia et al. (2003) proposed a modification to Quinn's model for mild oxidative wear, which was particularly adapted for the disc material. This new wear approach showed the significant role of contact frequency as an operational wear parameter.

The objective of this study is to ascertain whether the tribological behaviour in mild oxidative wear conditions where discontinuous sliding contacts take centre stage can be influenced by different materials, sliding geometries (uni- and bi-directional sliding tests) and even distinct approaches to wear measurement. For that, a thorough design of experiments was conducted to cover a range of parameters based on the sliding speed, contact frequency, and wear track diameter or stroke length. Besides, a dual phase steel, namely DP600, was chosen as the model disc material as it presents unique combination of mechanical properties that provides an optimal performance which maximised service life, and, therefore, makes it one of the advanced, interesting and useful high strength low alloy steels (HSLA).

Initially, to independently evaluate the effects of the operational wear parameters, i.e. contact frequency and sliding speed, on the wear rate of DP600 steel disc sliding against corundum ball, a series of conventional unidirectional ball-on-disc wear tests was

carried out at a given constant sliding speed but at different rotation speeds by modifying the wear track diameter; and viceversa. The coefficient of friction and wear rate exhibited not only a highly dependence on the sliding speed, but also on the contact frequency which appears to be the key factor determining the wear behaviour of the DP600 even at constant sliding speed. Furthermore, the validity of Garcia-Ramil-Celis model (Garcia et al., 2003) was confirmed for discontinuous sliding contact at contact frequencies below 7 Hz. However, above 7 Hz, the disc behaves as if it was subjected to a continuous sliding contact.

In a further step, analysis of the contact frequency effect on bi-directional sliding direction –i.e. reciprocating sliding- under discontinuous sliding contact conditions was evaluated. Moreover, it was also used for the first time the energy wear approach alongside the conventional Archard approach to study such contact frequency effect. For that, a set of bidirectional ball-on-plate tests were performed at a given constant sliding speed but at different contact frequencies by modifying the stroke length; and viceversa. This unusual way of setting the operational parameters on bidirectional ball-on-plate tests revealed that the coefficient of friction and wear rate also showed a strong dependence on the sliding speed and the contact frequency as occurs for unidirectional ball-on-disc tests. Once again, the contact frequency seems to be a key factor to define the wear behaviour of DP600 steel specimens. Besides, the wear volume as a function of the cumulative dissipated friction energy showed a directly linear relationship with the dissipated energy which indicates that the oxidation process of DP600 steels did not consume a considerable quantity of energy during testing. It was concluded that the heat generation at the interface is a significant factor to characterise the wear behaviour of the tribosystem, since it could contribute to a modification in the rheology or composition of the oxidised layer and thus, to the debris generated within the tribocouple.

Finally, the role of the sliding direction was further analysed by performing a third wear test method that is scarcely used, i.e. ball-on-disc continuously reversed (bidirectional) wear test. This test allowed one to compare both unidirectional and bidirectional motion at given sliding speeds and contact frequencies but taking into account the reversing sliding direction effect. According to the definition of cyclic number, CN, as proposed by Tang et al. (2011a), such CN indicates how often the rotation direction of the disc is reversed. The unidirectional sliding was thus represented by CN=0. Conversely, for

bidirectional wear tests, namely CN≠0. It was demonstrated that DP600 steel discs behaved differently to unidirectional and bidirectional sliding wear against corundum balls. The unidirectional sliding showed more severe wear damage than tests conducted under bidirectional motion. In addition, the Bauschinger Effect took place during the bidirectional sliding processes, being only noticeable when the sliding direction was reversed for some limited times, i.e. CN>5, where the wear volume loss decreased and was accompanied by a weak-strain-hardening effect. Moreover, the Bauschinger Effect in DP600 steel discs was directly affected by the sliding speed and contact frequency. The wear rate of the DP600 steel discs exhibited an inversely proportional relationship with the contact frequency, whereas it was directly proportional with the sliding speed.

Resumen

En los ensayos de desgaste en el que el mecanismo determinante del fallo es el desgaste oxidativo suave, los resultados de fricción y tasa de desgaste han mostrado una fuerte dependencia con la carga y la velocidad de deslizamiento aplicadas. El modelo en base al cual se ha podido analizar detalladamente la respuesta de los materiales ensayados durante las últimas décadas es el modelo de desgaste oxidativo leve propuesto por Quinn (1962, 1983, 1992, 1994, 1998). Este modelo, normalmente utilizado en el estudio del comportamiento tribológico de sistemas sometidos a ensayos unidireccionales de deslizamiento en seco de pin/bola-sobre-disco, no diferencia entre las condiciones de contacto de ambos cuerpos. Se considera que tanto el pin/bola como el disco se desgastan continuadamente, extrapolando ambos cuerpo a las condiciones de contacto del pin/bola. Sin embargo, esto no es del todo cierto puesto que el pin/bola se encuentra en continuo contacto con el disco durante todo el ensayo. En contraposición, cada punto del surco del disco solamente nota la carga del pin/bola cada vez que éste pasa sobre él, sufriendo así desgaste de manera discontinua. En consecuencia, García et al. (2003) propusieron una modificación del modelo de Quinn en el que se hacía una clara distinción entre las condiciones de contacto de los cuerpos (bola y disco) y que fue especialmente adaptado para caracterizar el comportamiento del disco durante el contacto. Este nuevo enfoque mostró que no sólo la carga y la velocidad de deslizamiento ejercen un papel determinante en el comportamiento frente a la fricción y el desgaste, sino que también la frecuencia de rotación (contacto) debe considerarse como un parámetro del ensayo.

El objetivo del presente trabajo de investigación es estudiar en qué medida nuevos materiales, diferentes geometrías de ensayo, así como distintos enfoques a la hora de analizar el desgaste, son relevantes y pueden afectar al comportamiento tribológico de un sistema sujeto a mecanismos de desgaste oxidativo leve, cuando dicho sistema es el disco del par tribológico. Para ello, se realizaron ensayos variando velocidad de deslizamiento y frecuencia de contacto utilizando como material objeto de estudio un

acero de doble fase ferritico-matensítico (DP600). Este acero fue elegido por sus excelentes propiedades mecánicas capaces de maximizar la vida en servicio del componente, lo cual hace de él uno de los aceros avanzados de baja aleación (HSLA) más destacados.

Con la finalidad de poder evaluar, por separado, los efectos que la frecuencia de contacto y la velocidad de deslizamiento ejercen sobre el desgaste de los discos de acero DP600 cuando deslizan frente a bolas de corindón, se llevaron a cabo dos tipos de ensayos de bola-sobre-disco unidireccional. En primer lugar, se estableció una velocidad de deslizamiento de ensayo constante a la vez que la frecuencia de contacto iba variando de acuerdo al diámetro del surco de desgaste. En un segundo tipo de ensayos, la frecuencia de contacto se eligió como parámetro constante y los ensayos de desgaste se realizaron a distintas velocidades de deslizamiento, ajustando nuevamente el diámetro del surco de desgaste. Los resultados de fricción y desgaste evidenciaron una fuerte dependencia con la velocidad de deslizamiento y la frecuencia de contacto, siendo esta última un factor clave a la hora de determinar el comportamiento tribológico de los discos de acero DP600, incluso a velocidades constantes. La validez del modelo propuesto por Garcia et al. (2003) para contactos discontinuos se confirmó en los discos de acero DP600 aunque solamente para frecuencias menores a 7 Hz. En los casos en los que la frecuencia de contacto es igual o superior a 7 Hz, los resultados mostraron cómo el disco deja de comportarse como un cuerpo sujeto a desgaste por contacto discontinuo y pasa a desgastarse como si se tratara de la bola, es decir, bajo condiciones de contacto continuo.

En segundo lugar, se analizó el papel de la frecuencia de contacto en el acero DP600 cuando este está sujeto a una geometría de ensayo diferente, concretamente en ensayos de movimiento bidireccional recíproco, utilizando para ello, y por primera vez, el criterio de la energía disipada por fricción para caracterizar el desgaste. Para ello, se realizaron ensayos bidireccionales de bola-sobre-plano siguiendo una metodología análoga a la descrita en la primera parte de este trabajo de investigación. Así pues, se estableció una velocidad de deslizamiento constante a la vez que la frecuencia de contacto iba variando de acuerdo a longitud de segmento desgastado. A continuación, la frecuencia de contacto se mantuvo constante y los ensayos de desgaste se realizaron a distintas velocidades de deslizamiento, ajustando la longitud de segmento desgastado. Los valores obtenidos del coeficiente de fricción y la tasa de desgaste del acero DP600

mostraron nuevamente una fuerte dependencia con la velocidad de deslizamiento y la frecuencia de contacto. De nuevo se pone de manifiesto el papel determinante que ejerce la frecuencia de contacto en el comportamiento frente a la fricción y el desgaste. Además, estos resultados mostraron la existencia de una relación de proporcionalidad entre el desgaste y la energía disipada, indicativa de que el proceso de oxidación del acero DP600 no consume mucha energía durante el transcurso de los ensayos. Se concluye así que el calor generado en las superficies de contacto durante el deslizamiento influye en el comportamiento frente al desgaste del sistema, puesto que parece contribuir a la modificación de la reología, de la composición de las capas oxidadas y, por lo tanto, de las partículas de desgaste producidas.

Finalmente, se llevaron a cabo una modalidad de ensayos que son el resultado de la combinación de los ensayos uni- y bi-direccional, utilizando la geometría de ensayo de bola-sobre-disco. Este tipo de ensayo añade la posibilidad de controlar los cambios de sentido mediante el parámetro número de ciclos, CN (Tang et al., 2011a). Este número indica la frecuencia de cambio en el sentido de la rotación. Un valor de CN=0 se corresponde con los ensayos unidireccionales, esto es, en los que el sentido de rotación no varía. Por otra parte, valores de CN≠0 indican un modo de ensayo bidireccional. Se ha demostrado que los discos de acero DP600 responden de forma diferente cuando se ensayan en condiciones uni- o bi-direccionales. De hecho, los resultados manifestaron, claramente, un mayor daño en los discos que se ensayaron unidireccionalmente, es decir en un mismo sentido de la rotación. Por el contrario, como consecuencia del modo de ensayo bidireccional, los discos de acero DP600 evidencian un marcado efecto Bauschinger, en particular, a partir de CN>5, mostrando tasas de desgaste inferiores a las obtenidas en el ensayo unidireccional, o bidireccional con valores de CN<5.

Contents

List of Abbreviations and Acronyms

AISI	American Iron and Steel Institute
BE	Bauschinger Effect
CN	Cyclic Number
COF	Coefficient of Friction
DP	Dual Phase
EDS	Energy Dispersive X-Ray Spectroscopy
FEG-SEM	Field Emission Gun Scanning Electron Microscope
HSLA	High-Strength Low-Alloy
SD	Sliding Direction
SEM	Scanning Electron Microscope
XRD	X-Ray Diffraction

List of Figures

List of Tables

Nomenclature

A_c	Oxidation activity factor
A_n	Nominal area of contact
A_r	Real contact area
α	Thermal diffusitvity of the metal
α_v	Wear rate in terms of wear volume and dissipated energy
β	Dimensionless parameter for bulk heating
D	Wear track diameter
d	Asperity contact area average diameter
d	Linear displacement
E	Young's modulus
E_d	Cumulative dissipated friction energy
E_i	Dissipated friction energy
F	Normal load
F_i	Tangential force
F_T	Frictional force
F	Normalised normal load
f	Contact frequency
H	Hardness (for metal)
H_o	Hardness (for material tested)
K	Constant of proportionality
k	Thermal conductivity
L	Sliding distance
M	Molar weight

μ	Coefficient of friction
N	Total number of contacting asperities
ξ	Critical oxide thickness
P_1	Parameter value chosen for fitting process in Garcia et al., 2003
P_2	Parameter value chosen for fitting process in Garcia et al., 2003
Q	Arrhenius activation energy for oxidation
q	Frictional heat
ρ	Density (for material tested)
R	Gas constant
r_a	Radius of an asperity
r_o	Radius of the ball
s	Stroke length
φ_{mol}	Molar energy wear
T_b	Bulk temperature
T_c^*	Effective equivalent temperature
T_f	Flash temperature or local temperature at the asperity
T_o	Sink temperature for bulk heating
τ	Designed parameter in Garcia et al., 2003
V	Volumetric wear loss
v	Linear sliding speed
v	Normalised linear sliding speed
W	Wear volume

1

Literature Review

1.1 Fundamentals of Tribology

1.1.1 Definition of Tribology

The science and technology of friction, lubrication, and wear between interacting surfaces in relative motion and related subjects and practices is known as Tribology (Hutchings, 1992; Bhushan, 2013). This word or concept is derived from the greek word *tribos* (Miyoshi and Chung, 1993) which means rubbing or sliding. Tribology is considered a multidisciplinary science that deals with the study of the thermal, mechanical, and chemical interactions occurring within two solid surfaces in contact when they are in relative motion with each other (Bhushan, 2013). Hence, it encompasses several parts of physics, chemistry, solid and fluid mechanics, heat transfer, materials science, lubricant rheology, reliability, and performance (Stachowiak and Batchelor, 2001).

The importance of this science was recognised by a committee of the Organisation for Economic Cooperation and Development in England on March 9th, 1966. The British government published the acceptance of a key report for the development of tribology, known as Jost report due to the researcher, Dr. H. Peter Jost who led the study. This report found a direct link between *"tribology education, and research and progress in industrial efficiency, and development."* Moreover, this report indicated that *"[...] Potential savings of £515 million per annum were estimated for industry by better application of tribological principles and practices."* (Jost, 2006).

The Jost report also addressed that about 89% of the total economic losses were directly or indirectly caused by the damage of components due to wear. Remaining 11% of these losses were however associated with friction problems (~9%) and insufficient use of lubricant (~2%).

This report was thus considered as the birth of tribology. After its publication, there was a great progress in understanding and modelling different aspects of tribology. Simultaneously, new surface technologies, materials and lubricants were developed. All of them with enhanced tribological characteristics.

Similar reports were published in West Germany in 1976 and in USA (Stachowiak and Batchelor, 2001). They revealed that tribological programs have to be established by both industry and governments to save costs. A brief summary is adressed in Table 1.1.

Table 1.1 Examples of savings due to significant enhancements associated with tribology programs (Stachowiak and Batchelor, 2001) .

Examples of savings due to changes related to tribology	**Savings (US $ / £)**
Tribology improvements in cars	18.6% total annual energy consumed in USA, ~14.3 billion US $/year
Application of tribological principles and practice to national energy	£468 to £700 million/year

Table 1.2 Areas of engineering and industry where tribology is present.

Aerospace	Fabric/Clothing
Agriculture	Flooring
Automotive	Lubricant manufacturers
Coatings providers	Body implants
Cosmetic	Military
Dental implants	Shoe manufacturers
Energy (Nuclear, Windy, Solar...)	Transportation

Tribology is all around us and provides answers to everyday questions (Figure 1.1), such as *which rubber grips the road better?* or *what material offers the longest life?*. Moreover, many areas of engineering and industry have a necessity to use and/or understand tribology (Table 1.2). For instance, an analysis of machine break-downs

shows that in the majority of cases failures and stoppages are associated with interacting moving parts such as gears, bearings, couplings, sealings, cams, clutches, etc. The majority of problems accounted for are tribological. Our human body also contains interacting surfaces, e.g. human joints, which are subjected to lubrication and wear (Stachowiak and Batchelor, 2001).

Figure 1.1 Wear damage in soles caused by friction –shoes against floor- as a result of a daily use.

1.1.2 Brief Historical Review of Tribology

Interacting surfaces in relative motion and the practices related thereto are in general associated with different dissipation phenomena, such as energy dissipation which, in turn, connect friction and wear. Over the past centuries, the study of these dissipation phenomena -friction and wear- and, also, lubrication caught the attention of eminent scientists.

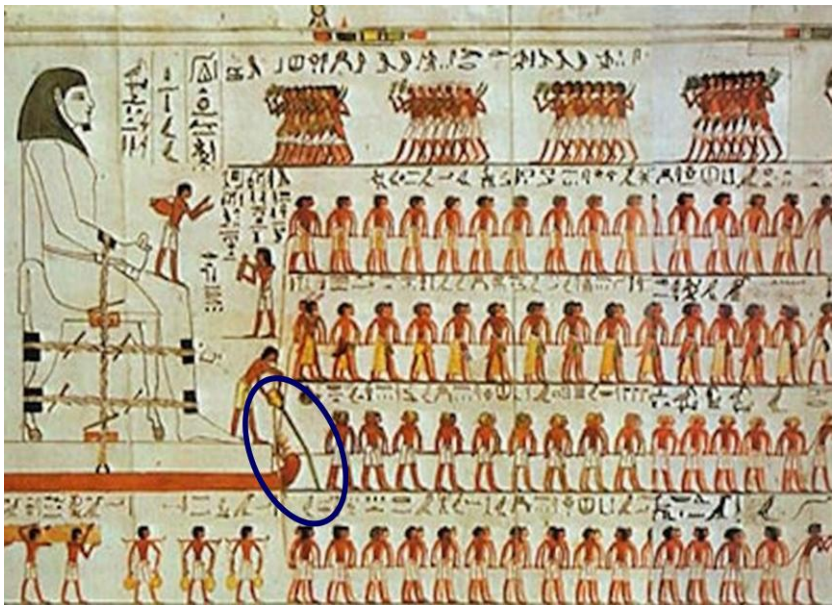

Figure 1.2 Egyptians pouring lubricant in front of the sledge in order to transport the statue of Ti at Saqqara, Egypt (Ibáñez, 2014).

The early recorded tribologists are dated in 2400 B.C. Historical manuscripts show images about how Egyptians transported the statue of Ti at Saqqara (Egypt) by pouring a liquid (lubricant) in front of the sledge (Figure 1.2). They clearly used a practical way to move those large heavy stones easily by reducing friction. This could be viewed as one of the very first lubrication engineers (Bhushan, 1997).

However, there were no clear friction laws available at that time. Several thousands of years after, Leonardo Da Vinci (1452-1519) evolved significant tests, i.e. sled friction, ball bearing or 4-ball geometry, that helped to define the two basic laws of friction. His valuable work turned him the father of modern tribology.

These two laws related to friction were experimentally rediscovered by Guillaume Amontons (1663-1705) in 1699 (Bowden and Tabor, 2001). Other pioneer tribologists were John Theophilius Desanguliers (1683-1744), Leonard Euler (1707-1783), and Charles Augustin Coulomb (1736-1806). In 1781, Coulomb confirmed Amontons' observations and went a step further by making a clear distinction between static friction (force required to start sliding motion) and kinetic –dynamic- friction (force required to maintain friction during sliding motion). He observed that kinetic friction is normally lower than the static friction, and also indicated that this kinetic friction can be nearly considered as independent of the sliding speed.

Therefore, tribology is one of the oldest engineering discipline. Notwithstanding, it is one of the least developed classical sciences to date. The reason is that tribology is neither certainly a single discipline nor well represented by steady state processes. It is also true that tribology is a field of science which applies an operational analysis to problems of great significance such as reliability, maintenance and wear of technical equipment ranging from household appliances to spacecraft (Stachowiak and Batchelor, 2001).

1.1.3 Surfaces In Contact

The scientific and engineering study of surfaces is a key issue, since the solution of many tribological problems requires an early understanding of fundamental surface properties such as-the structure and roughness. By looking closely at a surface, it can be observed that it is neither simple nor flat, as illustrates Figure 1.3. A mated surface is normally formed by a series of layers such as oxides, adsorbed contaminants, and lubricants, which cover and protect the bulk material.

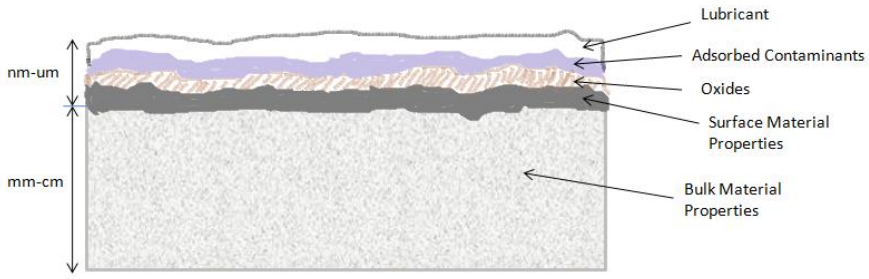

Figure 1.3 Schematic depiction of a representative engineering surface where all their layers are clearly identified.

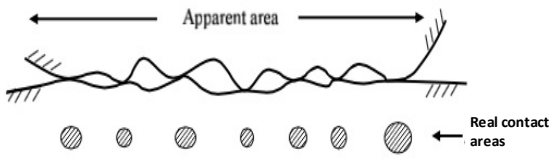

Figure 1.4 Schematic representation of the contact area between two rough surfaces; adapted from (Zhang, 2006).

In all engineering applications the surface of a component comes into contact with the external environment. According to tribological systems the importance of the

interfacial configuration is crucial. Therefore, it is necessary to choose a proper bulk material with both structural and economic criteria, together with surface properties able to withstand environmental conditions. Despite the accuracy to achieve the desired surface, i.e. a macroscopic flat surface under thorough examinations reveals that any surface presents certain roughness at micro- or mesoscale (Persson et al., 2005) which plays an important role in tribology. This surface roughness, or rather the asperity geometry and distribution, normally results from the manufacturing method, main rubbing history and handling. Even on carefully polished surfaces, asperities -hills and valleys- are large compared with the size of a molecule. If two solids are placed in contact, the upper surface will be supported on the peaks of the irregularities, and large areas of the surfaces will be separated by a distance which is great compared with the molecular range of action (Persson, 2000; Bowden and Tabor, 2001), as shown in Figure 1.4.

Generally, the rougher the surface the greater the wear. On the other hand, very smooth surfaces, less than about 10 microinches (RMS) lack the ability to store wear debris (and lubricants) due to the absence of valleys between asperities. In addition, very smooth surfaces increase molecular interaction forces that promote cold welding and increase the strength of welds (Lipson, 1969; Schumacher, 1977). It has been noted that, when initially formed, adhesion welds are small and the motion across the surface finish lines minimises the growth of welds, as opposed to paralleled motion (Hirst, 1973).

1.1.4 Friction

The conceptual definition of friction is known by the resistance to relative motion between two bodies in contact produced when one body moves against another (Hutchings, 1992). This resistance comes from the objects that are touching each other and the corresponding microscopic forces between them, i.e. molecular adhesion (Van der Waals, electrostatic, metallic bonds) and mechanical abrasion (elastic and plastic deformation). To complete the concept of friction, it should be make a clear distinction between sliding and rolling friction (Figure 1.5). It is known that sliding friction occurs when two rigid bodies relatively move one against another at the contact area. Whilst, in rolling friction, one body -or both- freely moves in the sliding direction, allowing it to ‘rotate’ or ‘roll’. Due to other factors such as misalignment or relative movement of asperities within the interacting surfaces, the sliding friction is always involved when rolling wear takes place (Stephens, 2001).

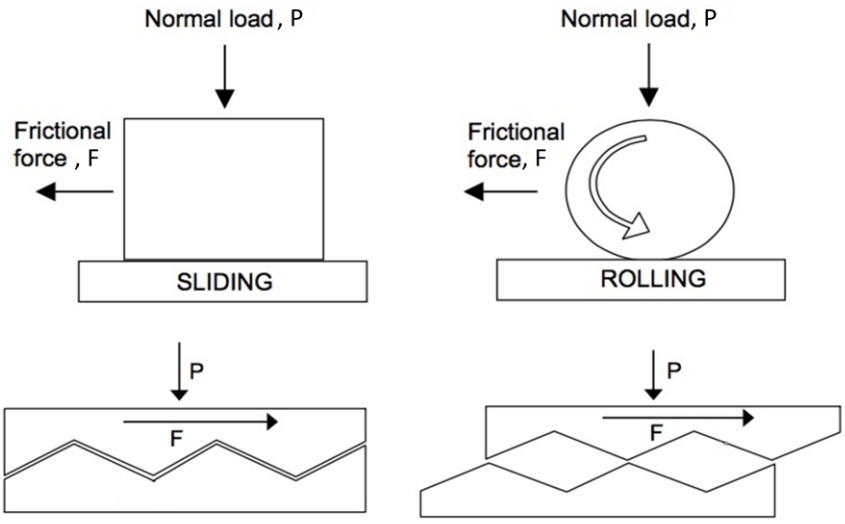

Figure 1.5 Schematic illustration of the mechanisms related to relative motion, i.e. sliding and rolling (Stephens, 2001).

Friction is not a material property but a tribological system property (Basu and Kalin, 2011). Thus, it needs to be controlled, since excessive friction could lead to fracture the material.

As aforementioned in Section 1.1.2, there are historically three widely accepted laws of friction, also known as Amontons-Coulomb laws. The first two laws of friction were truly defined by Leonardo da Vinci. However, they were redefined by Amontons, as follows:

1. *Frictional force is proportional to normal load.*

This statement can be translated empirically as:

$$F_T = \mu \cdot F \tag{1.1}$$

where F_T is the frictional force, μ is the coefficient of friction (COF), and F is the normal load.

In terms of COF, μ is rewrite as:

$$\mu = F_T/F \tag{1.2}$$

The coefficient of friction is thus the ratio between the frictional force that a surface exerts on an object moving over it and the normal load pushing this object toward the

surface (Hutchings, 1992). In other words, the COF is the force required to move an object through a surface which tends to resist the motion of this object.

Despite the simplicity of the COF equation, measuring this COF correctly requires a profound data processing. The COF is different if an object is in motion or not. The objects which are static, i.e. there is no movement within the contacting surfaces, in general require greater force to initiate the sliding than that required to maintain them in motion. In fact, once the motion starts the COF substantially diminishes. Hence, it is interesting to notice that the COF is comprised by the sum of two different factors, i.e. the static and kinetic coefficient of friction, as shown in Equation 1.3.

$$\mu = \mu_s + \mu_d \tag{1.3}$$

being μ_s the static coefficient of friction, and μ_d the kinetic –or dynamic- coefficient of friction.

2. Frictional force is independent of apparent area of contact.

Subsequently, Coulomb (Stephens, 2001) proposed the third law of friction which states:

3. Frictional force is independent of sliding velocity.

These three laws suitably fit the experimental data over a particular range of conditions. However, it is important to point out that their use can be limited due to any chemical or mechanical variations directly produced within the interacting surfaces during sliding, such as oxidation. These alterations could modify, for instance, the adhesion properties at the contact area and, consequently, affect the overall COF value. Table 1.3 shows a comparison of COF values for a range of materials tested under dry sliding conditions.

Table 1.3 COF values for various materials tested under dry sliding conditions (Peterson and Winer, 1980).

Material	Counterbody surface	COF (μ)
Mild steel	Mild steel	0.62
60/40 Leaded Brass	Tool Steel	0.24
PTFE	Tool Steel	0.18
Stellite	Tool Steel	0.60
Ferritic Stainless Steel	Tool Steel	0.53
Polyethylene	Tool Steel	0.53
Tungsten Carbide	Tungsten Carbide	0.35

1.1.5 Lubrication.

The role of lubrication is various: reduces friction; prevents or minimises sliding wear; transports debris away from interface, and provides cooling. It has another substantial benefit, a layer of lubricant, –gas, solid or liquid- introduced between the interacting surfaces exhibits low shear strength.

The lubricated systems are characterised into different categories. These types of lubrication are (Hutchings, 1992; Campbell, 1969):

· Hydrodynamic lubrication: A fluid film separates the surfaces in contact. In general, this fluid is thicker than the asperity heights appearing on the bearing surfaces.

· Elastohydrodynamic lubrication: It occurs when the surfaces are significantly deformed.

· Boundary lubrication: In this case, the adsorbed molecular films, i.e. oily or grease comprised films, separate the sliding surfaces. Notwithstanding, asperity contact and junction formation are perceived.

· Solid lubrication: Solid lubricant films or coatings that provide low shear strength.

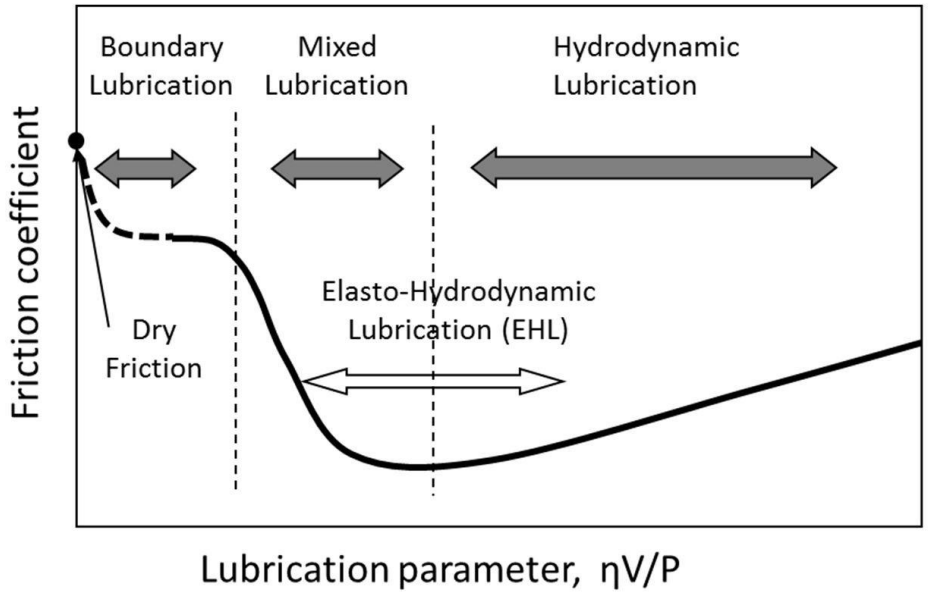

Figure 1.6 Schematic representation of the Stribeck curve: COF as a function of the lubrication parameter, ηV/P (Kondo, 2013).

The Stribeck curve (Figure 1.6) clears up the understanding of the wear behaviour in wet systems, i.e. with lubrication. This curve is a detailed plot where the friction (vertical axis) is related to a parameter that combines viscosity, speed, and load (horizontal axis).

1.1.6 Wear.

Wear is a complex process that implies the removal –or displacement- of material from one body when it is subjected to contact and relative motion with another body. There are large amount of variables or factors that are greatly influence on friction and wear phenomena, conditioning the COF and wear rate under specific conditions. Therefore, they must be carefully controlled and assessed. The most significant factors are usually classified into the categories which are listed below (Kivioja et al., 2001; Peterson and Winer, 1980; Chang, 2005; Bhushan and Gupta, 1991; Stachowiak and Batchelor, 2001):

- Material characteristics: Composition, properties and microstructure

Alloying elements, hardness, impact strength, toughness, modulus of elasticity, corrosion resistance, fatigue resistance, crystal structure, grain size, grain boundaries

- Operating conditions

Normal load, sliding speed, time, temperature, lubrication

- Geometrical variables

Surface roughness, surface topography, particle size, particle shape

- Environmental surroundings

Ambient air temperature, relative humidity, contaminants

1.2 Dry Sliding Wear

1.2.1 Simple Theory of Sliding Wear. The Archard Wear Equation

A simple and one of the pioneer models to predict the sliding wear phenomenon that occurs between sliding bodies was the Archard wear approach (1953), also known as the linear wear law, which was based upon an earlier work proposed by Holm (1946).

According to Johnson et al. (1972), this model is based on the theory of asperity contact, i.e. when two surfaces in contact slide over each other, one or both of the surfaces will suffer wear. It postulates that the wear rate is defined by the wear volume as a function of the normal load, sliding distance, and hardness.

The Archard wear equation states that the wear volume, W, is directly proportional to both the normal load, F, and the sliding distance, L, and is inversely proportional to the hardness of the softer body, H. This wear equation is expressed as follows:

$$W = \frac{K \cdot F \cdot L}{H} \tag{1.4}$$

where K is a constant of proportionality known as the wear coefficient which measures the probability of debris production (Peterson and Winer, 1980) and, therefore, describes the severity of wear. K is always less than unity.

This model was originally focused on the wear behaviour of metals. However, it can be extended into other materials, such as ceramics and composites (Hutchings, 1992).

1.2.2 The Wear Mechanism Maps. Mechanisms of Wear

Traditionally, normal contact load and sliding speed are considered the most important parameters in tribological systems. These parameters are commonly used to construct contact wear maps, which are a useful tool to predict the conditions under which a tribosystem can operate safely (Zhang and Alpas, 1997).

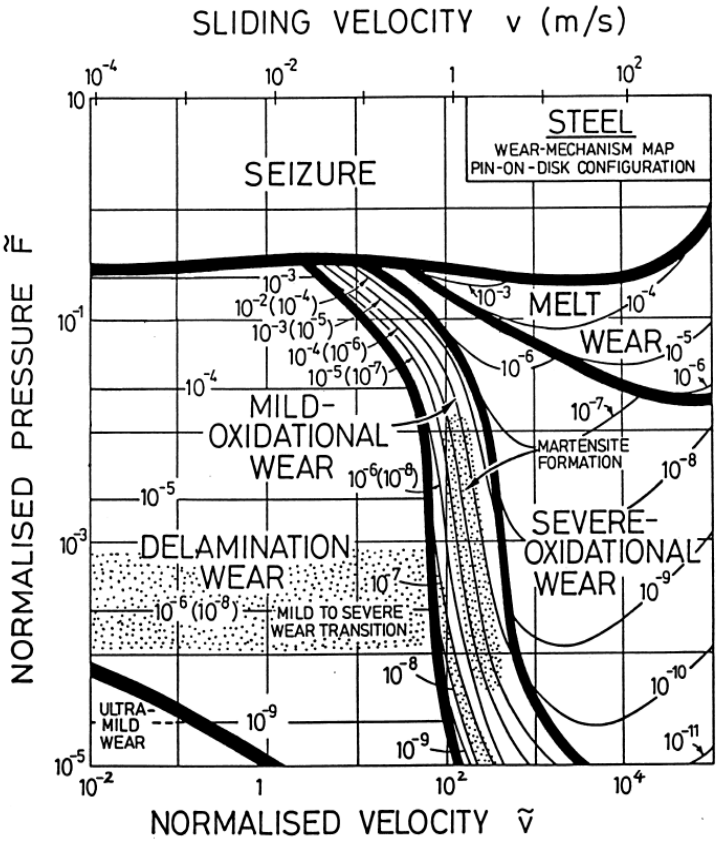

Figure 1.7 Wear mechanism map for steels proposed by Lim and Ashby (1987).

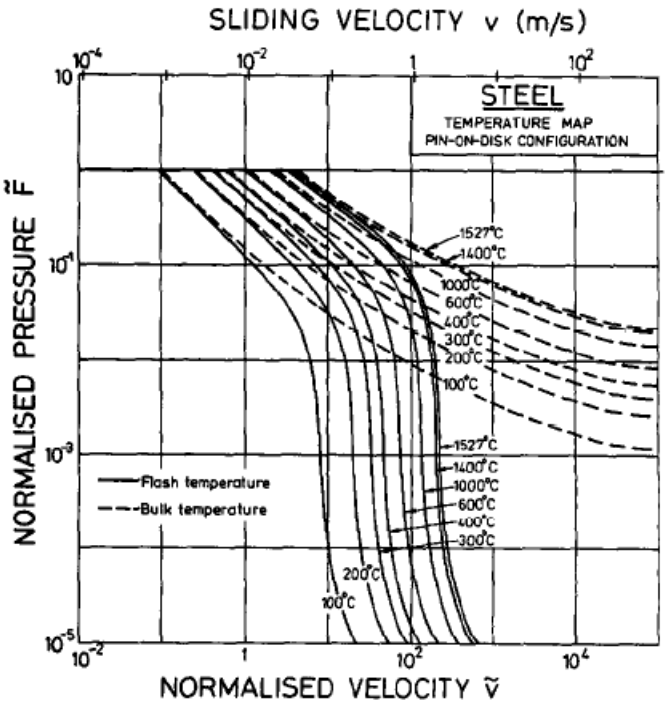

Figure 1.8 Temperature map for steels proposed by Lim and Ashby (1987).

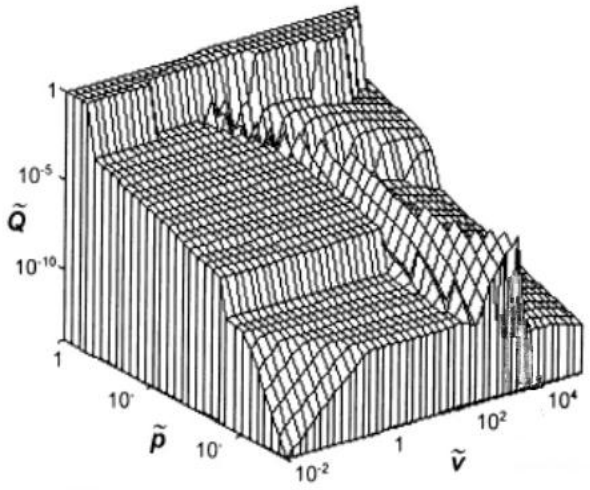

Figure 1.9 3D-wear mechanism map proposed by Põdra (1997).

In 1987, Lim and Ashby (1987) presented their wear mechanism maps –or diagrams- which show the wear rate, and the dominant wear mechanism regime for certain testing conditions (Figure 1.7). In these maps, a small variation in the normalised contact pressure, and/or in the normalised sliding speed, may result in a significant transition between two distinct wear mechanisms. Moreover, the temperature plays a key role in these transitions (Bhushan, 2000), as can be easily observed in the surface temperature maps proposed also by Lim and Ashby (Figure 1.8). Wear maps have been

experimentally and theoretically constructed for systems based on technologically important materials, such as steel sliding versus steel (Lima and Ashby, 1987), steel versus nitrided steel (Kato et al., 1994), and also aluminium alloys versus steel (Zang and Alpas, 1997; Liu et al., 1991).

Based on Lim and Ashby (1987) work, Põdra (1997) built a 3D wear mechanism map (Figure 1.9) from which, it is easily inferred that the normalised wear, increases gradually as the wear mechanism varies. In addition, it can be observed that within each wear mechanism regime the wear directly depends on the normalised pressure. However, the normalised sliding speed is slightly wear dependant.

Tabla 1.4 Comparison of the various classification of wear (Quinn, 1980).

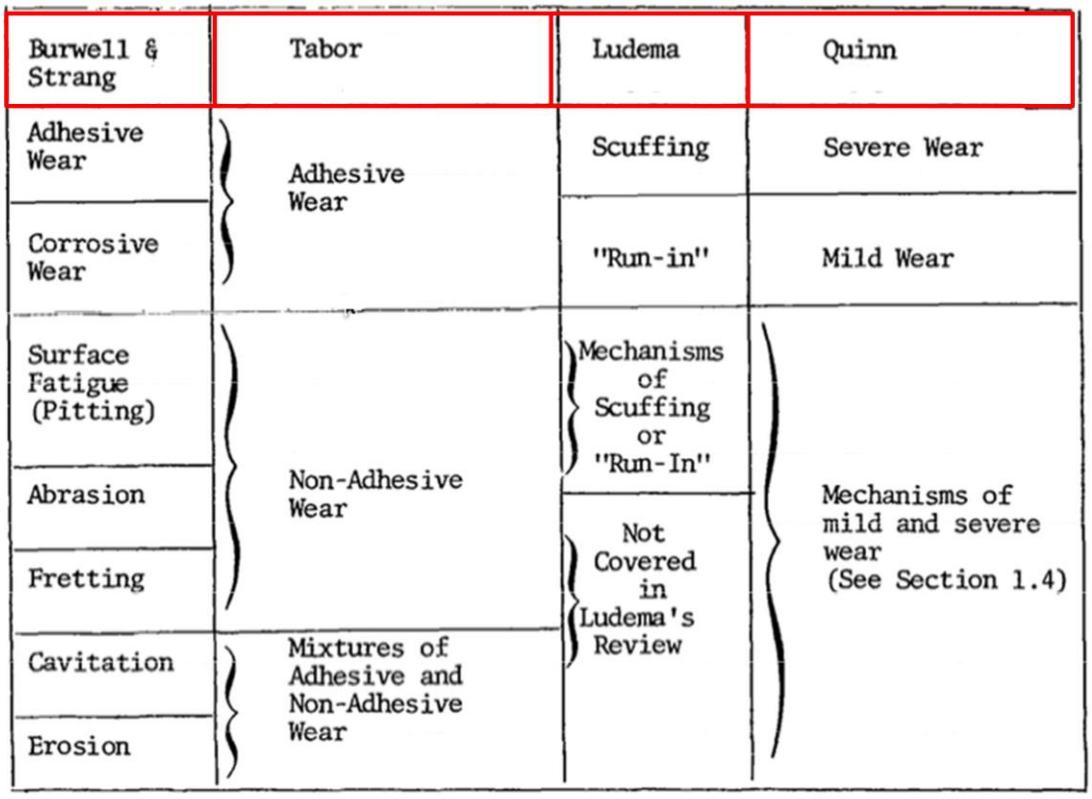

Wear mechanisms occurring in dry sliding tests have been classified into different types. All these classifications are strongly related to the previous classifications proposed by Burwell and Strang (1952), with seven wear types; and Archard and Hirst (1956), with only two. Tabor (1978) just distinguished three types: adhesive, non-adhesive, and a mixture of both. The author discussed the nature of the atomic forces at

the interface but also the way the interface deforms under the action of a pull-off force (for adhesion) or a tangential force (for sliding), and how the bond itself breaks under shearing. Ludema (1981) defined scuffing, namely the roughening of surfaces by plastic flow whether or not there is material loss or transfer. Whilst Quinn (1980) established mild and severe wear as the two main mechanisms of wear.

As above reviewed, there is not yet any agreement in the literature to classify overall the wear mechanisms. However, most of the wear mechanisms are encompassed in the following classification:

· Abrasive wear

The term abrasive wear is used to describe situations where the main cause of wear is scratching or cutting by abrasive particles (Bayer, 2002). It occurs when the asperities of a rough, hard surface or hard particles slide on a softer surface and damage the interface by plastic deformation or fracture. Figure 1.10 illustrates five of the most common mechanisms of abrasive wear.

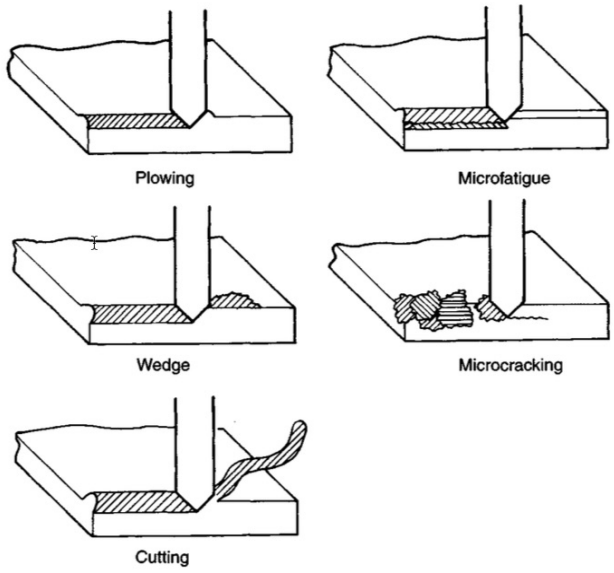

Figure 1.10 Schematic description of five mechanisms of abrasive wear (Tylczak and Oregon, 1992).

There are usually two situations for abrasive wear (Tylczak and Oregon, 1992):

1. Two-body abrasion: One surface is harder than the other surface in contact. It normally takes place in mechanical operations such as grinding, cutting, and machining.

2. Three-body abrasion: In general, the hard surface is a small particle –third body- of grit or abrasive that tend to lodge between the two interacting surfaces. This abrasive particle abrades one or both of these surfaces.

· Erosive wear

Erosion is known as the wear caused by a fluid, a stream of particles, or bubbles. This way of material removal does not take place by contact between two solid bodies (Bayer, 2002). The erosion mechanism is simple and causes severe damages. Normally, a solid erosive particle impacts on one solid surface and consequently, material from this surface is removed. In Figure 1.11, a schematic classification of erosion wear modes is presented.

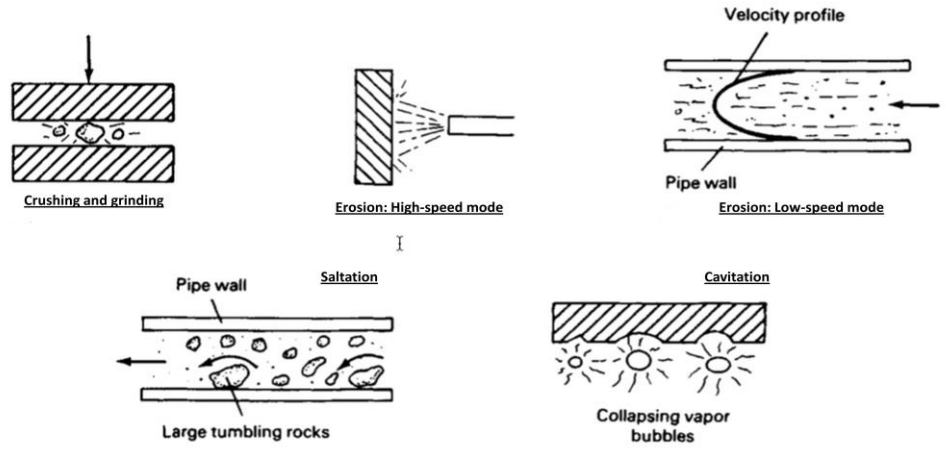

Figure 1.11 Classification of erosion wear modes; adapted from (Davis, 2001).

Conversely, cavitation erosion occurs when a solid and a fluid are in relative motion. The fluid then deteriorates the surface material due to generation of vapor or gas pockets (Davis, 2001) inside the flow of liquid. The damage is caused by the continuous impingement of vapor bubbles on the surface (Bhushan and Gupta, 1991).

The response of materials to the impact of solid particles or liquid drops greatly depends on the material properties, and the environmental surroundings (D'Errico et al., 1999, Tu and Matsumura, 1999).

· Adhesive wear

This wear mechanism was firstly assigned by Burwell and Strang (1952), and it was also probably based on the Bowden and Tabor (1954) cold-welding mechanism of friction. Adhesive wear occurs when two bodies are in sliding contact, whether lubricated or not, involving adhesion between the asperities at the interface (Figure 1.12). As is known, there is strong adhesive bondings through the contact area. When these adhesive bondings are able to resist the relative sliding produced between both interacting surfaces, large plastic deformation, i.e. severe wear (Quinn, 1983), can be caused by dislocation slide due to the compression and shearing. Consequently, the asperities in contact are broken off by sliding and leads to the detachment of parts from one surface by adhesive forces. Then, those fragments are transferred to the opposite surface, where they can become into wear particles or return to their original surface in a manner of back-transfer mode (Bhushan 2000, 2002).

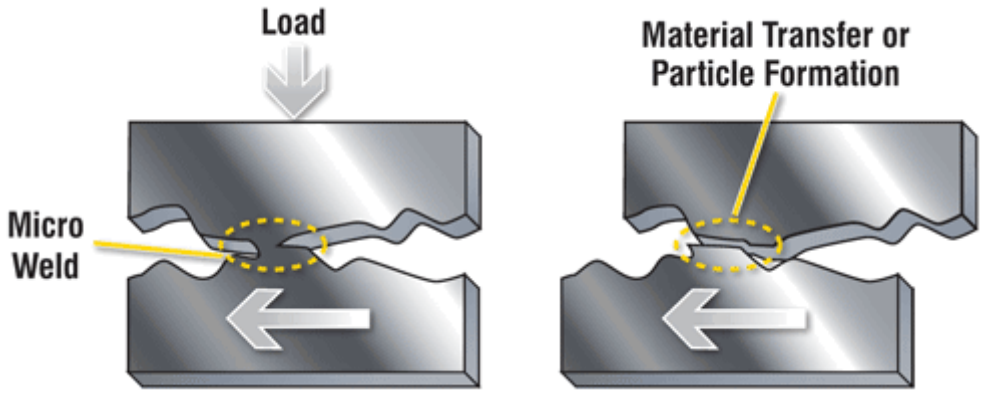

Figure 1.12 Schematic illustration of the adhesive wear process (Troyer, 2010).

The formation of loose wear particles are often originated from chemical variations. The chemical products form a protective layer -less than a micrometer thick on the surface- which tend to reduce adhesion and promotes the debris loss (Bhushan, 2002).

This chemical modification by friction or mechanical energy is referred as oxidation -or mild wear (Quinn, 1983)- and the wear process controlled by this reaction is then named oxidative wear.

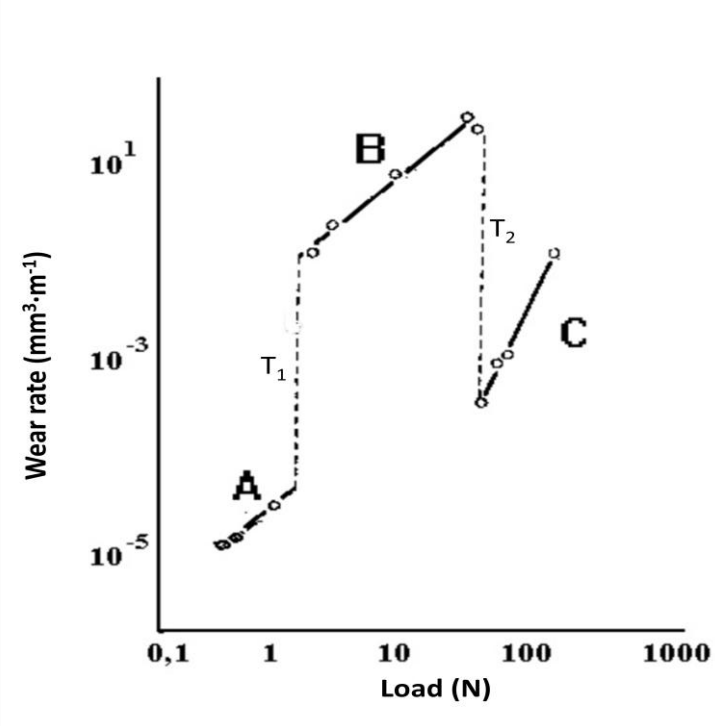

Figure 1.13 Correlation between wear rate and load for a medium carbon steel pin sliding at 1 m/s in air against a tool steel in a pin-on-ring test (Hutchings, 1992).

Based on the pioneering work of Welsh (1965), Hutchings (1992) reported an example of transitions in the wear behaviour of medium carbon steel during dry sliding pin-on-ring tests, at a constant sliding speed.

It can be observed in Figure 1.13 that the wear rate undergoes a slight increase at low applied loads. During this load interval, the wear rate remains in a low range. Oxidised wear particles are formed and, hence, the regime can be described as mild wear.

As the applied load increases, a steep transition (T_1) to severe wear is clearly perceived. The wear rate noticeably increases by a factor greater than 100, and metallic debris is produced.

Subsequently, a second transition (T_2) takes place at higher loads, where the wear rate falls abruptly. Once again mild wear is encountered, since only oxidised debris are collected after testing.

· Fatigue wear

The effect of failure by fatigue wear process is related to repeated stress cycles during sliding and rolling contact. The damage occurs due to stress-reversal effects (Czichos, 1978).

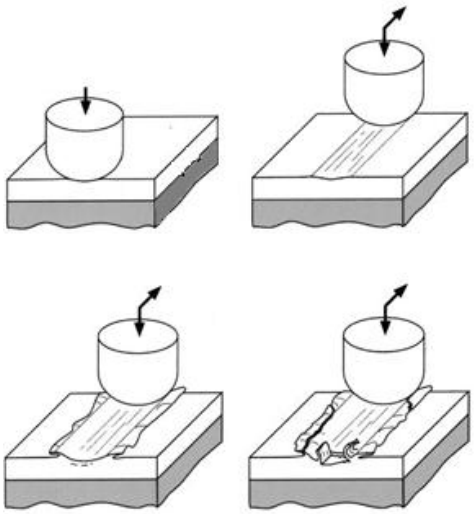

Figure 1.14 Schematic representation of fatigue mechanism (Wang et al., 2003).

The repeated loading and unloading cycles normally induce the formation of subsurface or surface cracks (Figure 1.14), which are nucleated at/or below the surface as the deformation goes on (Bhushan, 2000, 2002). As a result, a large quantity of wear particles is formed, leaving considerable pits in the surface.

- Experimentally, more than one of these mechanisms can operate at any given time or sequentially during the wear process. However, one of them always plays the dominant role in failure due to wear. It is common to observe that abrasive wear can result from initial adhesive wear. In other words, adhesive wear produces wear particles that are trapped between the contacting surfaces, leading to a three-body abrasive wear mode (Bhushan, 2002).

1.2.3 Wear Test Methods

In general, the wear tests are employed for quality control issues (Kennedy and Hashmi, 1998), such as thickness, porosity, ductility, hardness, adhesion, and wear resistance.

The main purpose of these tests is to compare and predict the wear behaviour of two interacting materials in relative motion subjected to different stress conditions during service. However, the assessment of the wear experienced by those materials under any real situation is really complex. For that reason, the process of selecting the most convenient test for a specific purpose is crucial to make significant interpretations (Axén et al., 2001). Therefore, it is appropriate to plan and design in detail the wear test methods based on their degree of realism in order to mimic as closely as possible the conditions of a real application in the laboratory.

Table 1.5 Most common wear test methods (Kennedy and Hashmi, 1998; JIS, 1989).

Pin-on.disc	Alumina slurry test
Pin-on-drum (abrasive wear test)	Rubbing test
Block-on-ring	Taber test
Pin-on-plate	Dry sand rubber wheel test
Repeated impact wear test	Amsler test

Over the last decades, innumerable wear test methods with different contact geometries have been internationally standardised since they provide identical conditions to those in service. The most common contact geometries are summarised in Table 1.5.

Moreover, wear test methods can be characterised by multiples categories according to different configurations. One may differentiate between sliding wear tests (Neupane et al., 2014) or those tests that involves contact by impact (Iwai et al., 2006).

In other situations, wear tests are distinguished relying on the sliding direction. These tests are normally defined as unidirectional (e.g. ball-on-disc (Cosemans et al., 2003) or block-on-ring (Ruiz-Andres et al., 2015a) or bidirectional. The bidirectional wear tests can be, in turn, distinguished between reciprocal motion (e.g. ball-on-plate (Eddoumy et al., 2011) or fretting (Chen et al., 2002)) or continuously reversed sliding (Tang et al. 2011a, 2011b; Harea et al., 2013). It is interesting to noticed that the sliding direction is a crucial factor when it comes to decide which is the most efficient manner to perform machining, cutting or grinding. For instance, Wu et al (1999) studied the wear behaviour and tribocorrosion of TiN coatings sliding against corundum in two different

wear tests, namely ball-on-disc (unidirectional sliding) and ball-on-plate (reciprocating motion) where both were performed in air and water at a constant applied load. Results showed that the TiN wear rate is higher under bidirectional sliding than in unidirectional tests.

Furthermore, wear tests are also characterised by their wear track, i.e. open or closed tribosystems. In other words, if the counterbody follows the same sliding track, the system is closed. Whilst, an open tribosystem is considered when the wear track is constantly renewed (e.g spiral wear tests (Rice et al., 2013)).

It should be pointed out that in most of the sliding wear test methods, specially in those where the tribopair is formed by two asymmetrical bodies (e.g. a sphere slides against a disc in ball-on-disc tests), there is one of these two bodies which is continuously in contact as the test progresses, namely the ball; whereas the other one, i.e. the disc, does not. In this case, each point of the wear track belonging to the disc is only damaged when the ball passes over it. It is observed that the contact configuration clearly differs between both bodies since they are not equivalent.

1.2.4 Quinn's Mild Oxidative Wear Model

Oxidative wear is a form of mild wear, one of the two basic classifications for non-lubricated sliding wear firstly proposed by Archard and Hirst (1956). While mild wear is characterised by oxidised wear debris generation and smooth oxidised wear surfaces. This type of wear clearly involves a reaction with the environment, in particular with oxygen (Quinn, 1983). Moreover, the oxidative wear mechanism occurs when sliding surfaces are subjected to thermal oxidation. The heat is externally provided with a heat source, or internally by the frictional heat produced in the sliding contact.

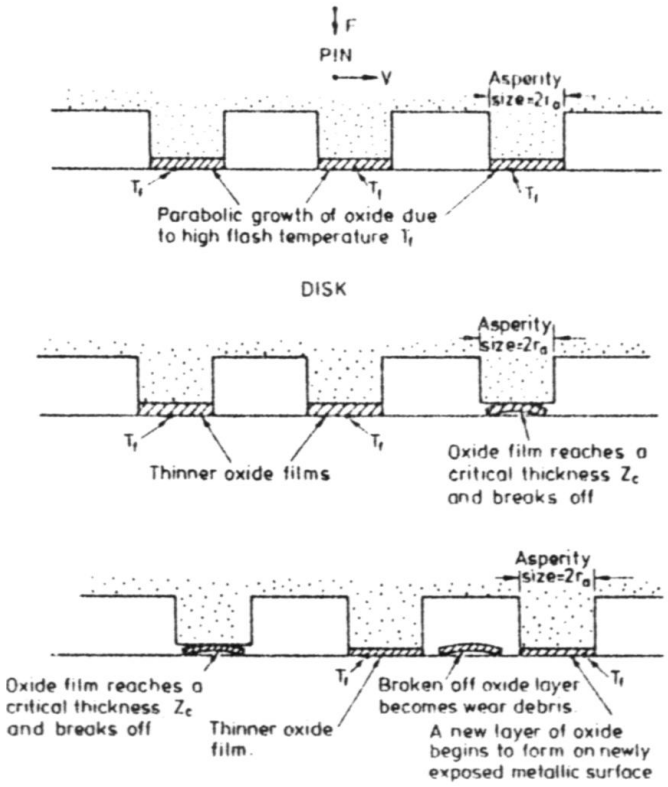

Figure 1.15 Schematic depiction of the explanation about the formation and growth of oxide layers due to high flash temperature between two interacting surfaces (Stott, 1998).

The mild oxidative wear model proposed by Quinn (1980, 1983, 1994, 1998) for a tribosystem comprised by a pin/ball sliding against a disc provides extensive information about the behaviour of oxide films under continuous sliding contact conditions (Quinn 2002; Archard 1986). Under these specific sliding conditions, the contact area of the pin/ball is in continuous contact with the disc in pin/ball-on-disc tests. It is known that this model takes place in two successive steps. Initially, the asperities on both surfaces the body (pin) and the counterbody (disc) oxidise as a consequence of a high local rise in temperature due to friction. The oxide layers formed at these asperities usually grow following a parabolic trend or linear growth law (Godet, 1984). Then, when locally a critical oxide thickness is reached at the asperities, the oxide layer breaks off and a new oxide layer is generated on the freshly exposed metallic surface, as indicates Figure 1.15. Thus, the expression for the volumetric wear loss in a pin, W, leads to as follows:

$$W = \frac{dA_c exp\ -Q\ \ RT_f}{\xi^2 \rho^2 v} \frac{F}{H} L \qquad (1.5)$$

where d is the asperity contact area average diameter, A_c the oxidation activity factor, Q the Arrhenius activation energy for oxidation, R the gas constant, T_f the local temperature at the asperity, F the normal load, L the sliding distance, ξ the critical oxide thickness, ρ the density for the material tested, v the sliding speed, and H the hardness for the material tested.

Once the oxide layer is broken off, the oxide particles formed from the layer may agglomerate to generate a protective layer establishing equilibrium between formation and delamination or fragmentation of the layer (Fromhold, 1976; Fehlner and Mott, 1970). When performing wear tests using a pin/ball-on-disc configuration, the pin/ball is under continuous contact with the disc, and consequently, as the contact load and the sliding speed are considered the controlling operational wear parameters which best define the wear test conditions for a wide range of materials, the material of the pin would become fully characterised.

1.2.4.1 Iron Oxides

A great majority of metals tends to form oxides at high temperatures, and also at moderate and room temperature during sliding. The oxidative mechanism for those metals has been thouroughly characterised in the literature (Birks et al., 2006; Cornell and Schwertmann, 1996; Marston et al., 2004; Chen and Yuen, 2003; Fromhold, 1972).

In particular, ferrous alloys easily react with oxygen during the initial stage of oxidation due to iron is thermodynamically unstable when it is exposed to the atmosphere (Caplan and Cohen, 1966). Layers of different oxides are formed on the top of the metal surface when iron is oxidised. Iron forms pure oxide compounds in three main forms, listed as follows:

1. Wüstite ($Fe_{1-x}O$)
2. Magnetite (Fe_3O_4)
3. Hematite (Fe_2O_3)

The variation in the iron oxide form is attributed to a significant change in the temperature (Hurricks, 1972, 1974). Based on the iron-oxygen phase diagram (Kubaschewski and Hopkins, 1962), wüstite (FeO) is thermodynamically stable at temperatures greater than 570 ^{o}C. At lower temperatures, the wüstite phase decomposes to magnetite and α-iron (Kubaschewski and Hopkins, 1962). Magnetite (Fe_3O4) is an

oxide usually found when the temperature range reached during sliding is between 450ºC and 600ºC (Quinn et al., 1980, Tyagi et al., 2002, 2004; Sullivan et al., 1980; Sullivan and Athwal, 1983). Whilst, hematite (Fe_2O_3) is the expected oxide found when a low temperature below 450ºC is reached.

1.2.5 Modification to Quinn's Mild Oxidative Wear Model

When the aim in a pin/ball-on-disc research work is to study the wear behaviour of the disc material, the contact clearly varies since the disc and ball are not equivalent, as indicates Table 1.6.

Table 1.6 Contact conditions for two interacting bodies -disc and pin/ball- in a pin/ball-on-disc wear tests.

Body 1: The disc	**Body 2 (or counterbody): The pin/ball**
Each point of the wear track on the disc is only loaded for a limited time interval between successive rubbing events, i.e. the disc is not constantly suffering wear damage during testing.	The pin/ball is in continuous contact with the disc as rubbing proceeds.

Garcia et al. (2003) thus proposed a Quinn's model modfication in order to take into account this fact. They introduced a new operational wear parameter, namely the contact frequency (or rotation speed), registered between the ball and each point of the disc wear track in ball-on-disc tests. They developed a novel approach to sliding ball-on-disc wear tests considering that, from the viewpoint of the disc, each part of the wear track is in discontinuous contact with the counterbody. Hereto, a series of ball-on-disc wear tests was performed at constant sliding speed, v, but for different contact frequencies, f, and viceversa. This is possible by adjusting the wear track diameter, D, as follows:

$$v=\pi \cdot f \cdot D \tag{1.6}$$

According to their results, it should be noticed that only one of these three operational parameters, i.e. v, f, and D, is independent, and it is not relevant for studying the wear rate. In other words, they observed that the wear rate in tests performed at different combinations of sliding speed and contact frequency did not present any clear dependence on the wear track diameter. Consequently, the wear track diameter seemed to be this non-influencing parameter and, therefore, it was discarded as a controlling wear parameter.

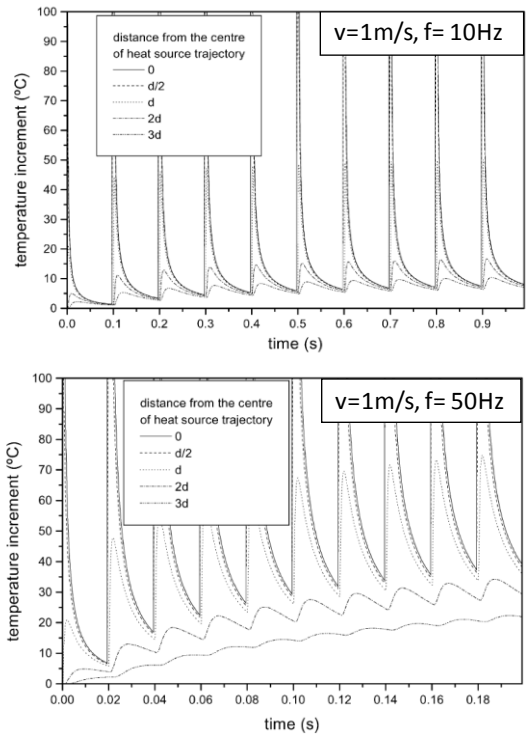

Figure 1.16 Comparison of simulated temperature increments of TiN-coated disc surfaces at 1m/s and different contact frequencies -10 and 50 Hz- by the cycling passing of a heat source (Garcia et al., 2003).

Over the last decades, the assessment of the flash and bulk temperature during pin/ballon-disc wear tests only considered the effects of the sliding speed (Cowan and Winer, 1992; Archard 1958; Greenwood and Alliston-Greiner, 1992; Kuhlmann-Wilsdorf, 1987a, 1987b). Therefore, the authors performed a new simulation of the wear track surface heating in order to include specifically the rotation frequency together with the sliding speed (Figure 1.16).

They also reported that the heat reached at any point of the disc during the trajectory of the ball is assumed to be generated due to the friction energy within both interacting bodies, and it can be simulated by a square wave.

For that reason, Garcia et al. (2003) stated a simplification of the equation for the surface flash temperature, T_f, in a disc, which in turn, is in discontinuous contact with a pin/ball, by computing the heat transmission equation:

$$T_f = \tau v^{1\ 2} \tag{1.7}$$

where τ contains all the parameters not related to either sliding speed or contact frequency.

Therefore, the expression for the volumetric wear loss of a disc material, *W*, in Garcia-Ramil-Celis model (Garcia et al., 2003) leads to the following:

$$W = \frac{A_c exp\ -Q\ \ RT_f}{\xi^2 \rho^2 f} \frac{F}{H} L \tag{1.8}$$

where ξ is the critical oxide thickness, ρ the density, f the contact frequency, H the hardness of the material tested, F the normal load applied, L the sliding distance, R the gas constant, T_f the local temperature in the asperities, A_c the activity factor, and Q the Arrhenius activation energy for oxidation.

The authors found that their wear rate results were not consistent with the mild oxidation model by Quinn, since they were not sliding speed dependent. This model provides a congruent evolution of wear rate regardless of it is expressed as a function of contact frequency or sliding speed in contrast to Quinn's model that does not fit for discontinuous sliding contacts (Garcia et al., 2003). Thus, they concluded that the contact frequency, defined by the rotation frequency of the disc, became the most influencing parameter on the wear rate of TiN coated steel discs when tested in a pin/ball-on disc configuration.

Navas et al. (2006) later confirmed the role of the contact frequency in ball-on-disc wear tests on tool carbon steel discs sliding against a chemically inert ball, namely corundum.

The need of considering contact frequency on tribocorrosion systems has been also pointed out in recent mathematical models for sliding wear in both gaseous and aqueous environments (Jiang and Stack, 2006). In nuclear pressurized water reactors (PWR), wear damage on some tubular components have been found to be also sensitive to the activation or latency time (inverse of the contact frequency) resulting from vibrating contacts (Reynier et al., 2005).

1.3 Wear in Dual Phase Steels

1.3.1 Dual Phase Steels. Definition

Evolution of newer materials with improved combinations of mechanical porperties such as strength, ductility and toughness has led to the development of a series of microstructure-strengthened steels One of these important new advanced high strength low alloy (HSLA) steels is Dual Phase steels which are characterised by being a ligther and higher strength steel grade (Hulka, 2000) widely used in the automotive industry due to the necessity of improving fuel efficiency (Cui et al., 2011; Meng et al. 2014; Han et al., 2011), with its subsequent energy saving and environmental protection (Pritchard and Trowsdale, 2002; Wang et al., 2014).

Moreover, a noticeable increase of the highly demanding collision safety standards have been developed in the vehicle body frame parts (Futamura et al., 2011), e.g. panel reinforcement, bumper beam and door beam. DP steels have been also employed in the field of mineral processing, mining, and pipeline transportations of slurry (Sui et al., 1992). In a recent study it has been also found that DP steels hold appropiate potential for use as farm implements where strength and wear resistance become of great concern (Wayne and Rice, 1983).

The DP steel microstructure consists of about 75-85% continuous ductile ferrite matrix phase with the remainder being a mixture of harden martensite islands randomly distributed, and lower amounts of other phases such as bainite and retained austenite (Rashid, 1981).

This characteristic microstructure leads to different unique properties, as high tensile strength, low yield strength ratio followed by continuous yielding behaviour (no-yield point elongation), and high work-hardening rate at early stages of plastic deformation, which is attributed to the austenite-to-martensite transformation within the constraints

of the ferrite matrix (Sun and Pugh, 2002) as well as good ductility (Wu-rong et al., 2011; Ozturk et al., 2009). In addition, the absence of the yield point elongation provides DP steels with a high crash resistance, good formability and excellent surface finish (Ramazani et al., 2013).

1.3.2 Wear behaviour

A number of researchers (Wayne and Rice, 1983; Blau, 1981; Sawa and Rigney, 1987; Basak et al., 1998; Modi et al., 2003; Tyagi et al., 2001, 2002, 2004; Abouei et al. 2007a) have been working on the tribology of DP steels, although there is a necessity of developing a more comprehensive understanding of their friction and wear behaviour due to it has not yet been researched extensively.

Blau (1981) detailed the initial sliding behaviour of DP steel, studying the friction break-in, i.e. the coefficient of friction average as a function of the stroke number. Significant differences were observed when tests were performed in flowing argon or run entirely in air. The author also found that the presence of more than one maximum value for friction may be a consequence of sequential work hardening of the microstructural constituents.

Sawa and Rigney (1987) reported that, under air conditions, the wear behaviour of DP steels depends strongly on its morphology, i.e. shape, size, and distribution of martensite. Basak et al.(1998), as well as Modi et al.(2003), and Tyagi et al. (2001, 2002, 2004) indicated that the wear resistance of DP steels increases with increasing the volume fraction of martensite.

Wayne et al. (1983) showed the dependence of wear on microstructure and concluded that the duplex microstructure of the DP steel offers higher wear resistance than that observed in steel with spheroidal carbides. Abouei and co-workers (2007a, 2007b, 2008) analysed the worn surfaces and debris of DP steels, and reported that the friction, the wear rate and the wear coefficient are explained as a function of the microstructure and the wear mechanism, e.g. mild oxidative or delamination.

1.4 The Energy Approach to Wear Measurements

Most of ASTM (American Society for Testing and Materials) wear standards and wear mechanism models, such as Archard's equation (Archard, 1953), express wear rate by means of volume units, i.e. in terms of removed or loss material. This approach provides high accuracy results and is often used to quantify loss volume in irregular worn scars (Bayer, 1994). A simple alternative to measure wear is to weigh the specimen before and after the wear test (Ruscoe, 1987) with an easy mass difference estimation. Other wear approaches are based on linear dimensional measurements (Bergman et al., 1997; Glaeser, 1976) or contact areas (Mehrota, 1983; Matsunga et al., 1972). The wear scar depth/width or the changes in specimen sizes (e.g the possible pin length reduction in a pin-on-disc test) behaves as an indicator of wear.

Moreover, there are some other approaches to quantify wear, known as either independent or complementary approaches, that include vibration analysis (Martin, 1992), lubricant analysis (Lockwood and Dalley, 1992), and motor-current signature analysis (Eissenberg and Haynes, 1992). In recent years, energy analysis has also gained considerable attention (Huq and Celis, 2002; Fouvry et al. 2003, 2007) to determine wear damage related to the dissipation of frictional energy in sliding contacts operated under unidirectional or bidirectional mode.

This energy approach is based on the dissipated frictional energy due to friction through the surfaces in contact. Mohrbacher et al. (1995) first presented the definition of the cumulative dissipated friction energy, Ed, for bidirectional sliding contact conditions. This is based on the idea that a particular tribochemical wear process requires characteristic mechanical activation energy to proceed (Wu et al., 1999). The dissipated friction energy, E_d, is obtained by summing up the energy dissipated during each reciprocating cycle over the whole test duration:

$$E_d = \sum F_t \cdot d \tag{1.9}$$

where F_t is the tangential force and d is the linear displacement.

Likewise, the wear equation is expressed as follows:

$$V = \alpha_v \sum E_d \tag{1.10}$$

A linear relationship between the energy dissipated per cycle and the generation of surface damage is noticed. The energy wear coefficient, αv, represents the wear rate in terms of the wear volume vs. the dissipated energy and is expressed as the volumetric wear loss per joule.

1.5The Bauschinger Effect

Based on the machining processes of new hard materials, Tang et al. (2011a, 2011b) recently addressed the question concerning whether it is more efficient to perform machining/grinding under unidirectional or under bidirectional (back-and-forth) sliding conditions. Their results on specimens of Cu-Zn alloys, tested against steel, in a modified wheel abrasion tester, showed that there is a remarkable difference in the wear rate. They reported that reversing the sliding direction decreases the wear damage. They thus concluded that unidirectional sliding could be more effective than bidirectional when used for machining or grinding materials. This result was attributed to the Bauschinger effect (BE) that can take place on the Cu-Zn alloy.

The BE is generally defined as the phenomenon whereby the flow stress applied to plastically deform a material, in the reverse direction, is lower than that in the original direction (Goel et al., 1983), i.e. the BE is characterised by a decrease in yield strength after a change in the load path (Demir and Raabe, 2010).

In metals, the BE primarily results from the directionality of the mobile dislocations in their resistance to motion (Davoudi et al., 2014), and their annihilation when new dislocations with opposite sign are generated by reversed applied stress. This annihilation leads to a reduction in the strain energy and is, therefore, a favourable energy process (Zhu et al., 2013). Both the reversible movement of dislocations and their annihilation can derive in softening during stress reversal.

Consequently, the BE clearly affects any plastic deformation when materials are subjected to cyclic back and forth strain path and/or to variations in the applied load (Demir and Raabe, 2010). At macroscopic scale, many mechanical processes are associated with the BE. For instance, most of the operations related to metal forming which, in turn, involve reverse strain cycles, such as plate fabrication or pipeline-making processes (Sowerby et al., 1979). Hence, this information is of significant importance for the enhancement of machining or grinding processes with higher

efficiency and their associated energy consumption via the work direction. Moreover, it may be helpful to control the wear damage in a component which is in constant dynamic contact with others (Zhu et al., 2013). At microscopic scale, components such as microelectromechanical devices (MEMS) also show BE (Demir and Raabe, 2010).

In LiF single crystals, Harea et al. (2013) found that the wear is higher under unidirectional sliding. The authors concluded that these results are related to the BE and also, to a redistribution of the contact spot as a result of the ploughing and adhesion of debris to the interacting surfaces.

1.6 Concluding Remarks

The application of mild oxidation wear model based on discontinuous heat inputs, i.e. Garcia-Ramil-Celis model, has demonstrated to be a valuable method to study the wear behaviour for the disc material in uni-directional pin/ball-on-disc wear test methods. There is now clear evidence that differences between the effects of sliding speed (traditional-considered operational parameter) and contact frequency (new-considered operational parameter) are possible when the wear rate of the disc material is analysed, at least in mild oxidation wear conditions. However, there are still many open questions concerning interesting wear features, such as the following:

- Are the material system properties reasonably significant in relation to discontinuous tribological contacts during uni-directional pin/ball-on-disc wear tests?

- How do approaches to wear measurements such as dissipated energy analysis affect the effects of the sliding speed and contact frequency?

- How do testing methods different from uni-directional pin/ball-on-disc wear tests influence the operational wear parameters, i.e. the sliding speed and contact frequency?

1.7 Outline of this Dissertation

Chapter 2 introduces the motivation and objectives of this research work.

Chapter 3 provides an overview of the main experimental techniques and materials used in this thesis.

Chapter 4 discusses the friction and wear behaviour of dual phase steels sliding against corundum balls in dry discontinuous sliding contact conditions as a function of sliding speed and contact frequency by means of unidirectional ball-on-disc wear tests.

Chapter 5 analyses the role of the contact frequency when tests are performed on reciprocating sliding, in particular, under bidirectional ball-on-plate tests. The study has been carried out using the energy wear approach.

Chapter 6 studies the influence of sliding direction changes, operational wear parameters and others factors such as hardness and Bauschinger Effect on the wear of dual phase steels.

Chapter 7 presents the conclusions extracted from this investigation

.

2

Motivation and Objectives

2.1 Motivation

Tribological studies are found in almost all industrial sectors due to the relevance of a surface failure, which can negatively alter the performance of industrial facilities, shorten their service life and comprising safety issues (Pritchard and Trowsdale, 2002). The knowledge about the nature and extent of wear as a consequence of the ever increasing demand for better performance of components has gained importance in recent years. For instance, in manufacturing processes, the inspection and control of machining, cutting, or coating are required to detect possible wear damage caused by techniques or tools as well as to guarantee surface quality of products.

In order to solve this fact, engineers and designers have joined efforts to make optimal decisions associated with tribological considerations -e.g. operational wear parameters, sliding directions, or approaches to wear measurements. Specially, tribologists agree that there should be a need to concentrate fundamental research in order to understand the complexity of wear process. Despite many wear models have been developed so far, adequate attention has not been paid to some crucial factors such as the right description and differentation of both material bodies that interact at the contact area, critical operational wear parameters, sliding contact conditions or sliding directions. Thus, it is of sum importance to analyse all these factors associated with the wearing conditions and determine which are the most suitable requirements for testing, since they can be decisive to maximise the performance of a wear resistant material, enhance machining effectiveness or reduce energy consumption.

2.2 Aim of the Study and Summary of the Work

In this research work, we have contributed to solve these open issues by studying the effect of traditional and new operational wear parameters –i.e. sliding speed and contact frequency, respectively- operating under dry sliding conditions in order to extend current knowledge on a proposed Quinn's modification wear approach, i.e. Garcia et al. [ref] mild oxidation wear model, where discontinuous sliding contact conditions take centre stage by focusing on the study of the disc material. DP600 steel was chosen as the model material due to its unique combination of mechanical properties such as strength, ductility (Wu-rong et al., 2011; Ozturk et al., 2009), toughness, good formability and excellent surface finish (Ramazani et al., 2013) that provides an optimal performance which maximised service life, and, therefore, makes it to one of the most important recent advances in high strength low alloy steels (HSLA).

In particular, this investigation was firstly aimed at ascertaining whether different materials can influence and modify the tribological behaviour in mild oxidation wear conditions under discontinuous sliding contact conditions. For this, friction and wear behaviour in DP600 steel discs sliding against corundum balls were evaluated. Initially, ball-on-disc wear tests were performed at several sliding speeds while maintaining the contact frequency at a fixed value, and viceversa. The effect of the contact frequency on friction and wear in DP600 steel discs was thoroughly discussed. Then, these results were compared to those obtained from previous works (Garcia et al., 2003; Navas et al., 2006) where different materials were analysed.

Secondly, it is known that several attempts were made to assess the wear behaviour by means of complementary to the Archard or independent wear approaches (Wu et al., 1999). One of these approaches is the energy model which is, in turn, based on the dissipated frictional energy due to friction through the surfaces in contact. However, the number and variety of these studies focused on discontinuous sliding contacts seem to be lacking. Therefore, we also aimed to report for the first time the effect of the operational wear parameters, specifically the contact frequency, in the frame of different wear approaches, i.e. Archard and energy models, when the tribological configurations are discussed under discontinuous sliding contact conditions.

Finally, the third objective of this work was to expand the still scarce knowledge on how the sliding direction together with the operational wear parameters can affect wear, in particular when the study is focused on the discontinuous sliding contact conditions. For this reason, different wear test methods such as unidirectional, bidirectional and continuously reversed wear tests were performed.

3

Methods and Materials

3.1 Materials

The selected pair of materials studied for all the wear tests analysed in the present work were:

- Dual phase (DP) steel as the disc or plate (*body*)
- Corundum (Al_2O_3) as the ball (*counterbody*)

3.1.1 Dual Phase Steel

A commercial high strength low carbon dual phase (DP) steel, namely DP600, was used in this work. The chemical composition of this DP600 steel (Table 3.1) was analysed at Laboratorio de Análisis Químico (CENIM-CSIC, Madrid, Spain) by optical emission spectrometry (OES) using arc/spark excitation to perform elemental analysis of the specimen. In order to obtain the carbon content of the DP steel an elemental analyser was also employed.

Table 3.1 Chemical composition of DP600 dual phase steel (% wt.).

	C	Si	Mn	Cr	Ni	Mo	Al	Nb	V	Fe
DP600	0.122	0.38	0.91	0.021	0.045	<0.01	0.043	<0.005	<0.01	Balanced

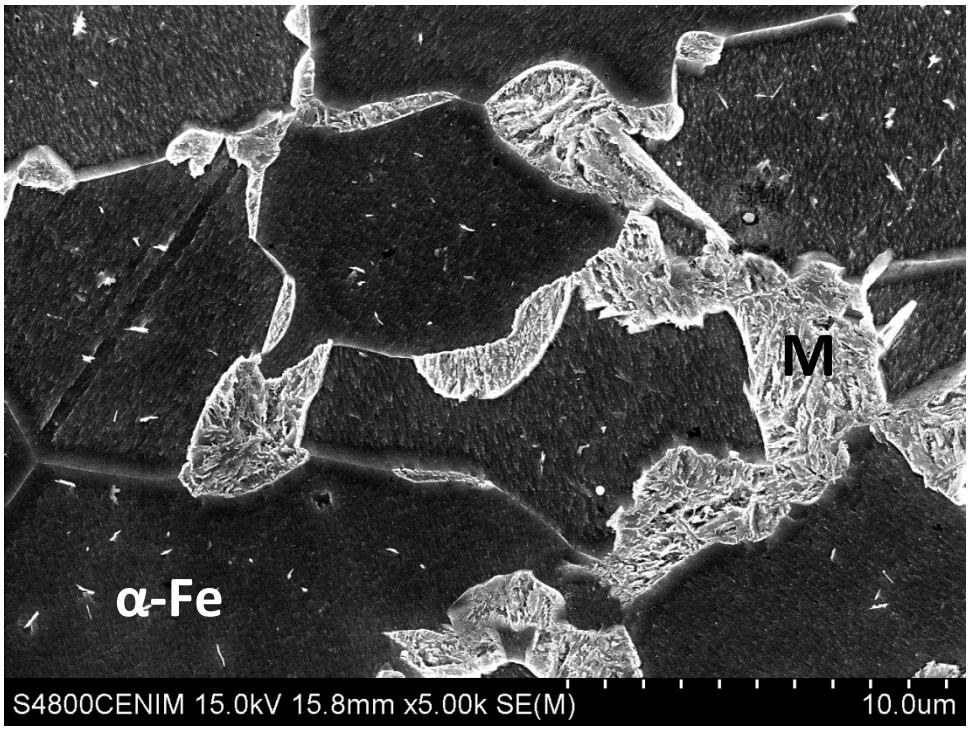

Fiugre 3.1 SEM image of the DP600 steel microstructure, etched at 2% Nital: Ferrite (α-Fe) – dark contrast; martensite (M) –bright contrast.

DP steels microstructure is defined as a microstructure consisting of about 75-85% ferrite phase with the remainder being a mixture of the martensite and lower amounts of other phases such as bainite and retained austenite (Rashid, 1981). As illustrates Figure 3.1, it can be observed that the microstructure of this DP600 steel is particularly comprised by harden island-shaped martensite inclusions randomly distributed (M, bright contrast), and a soft ferrite matrix (α-Fe, dark contrast).

Moreover, the as-received material was characterised by:

- An industrially processed, cold-rolled sheet
- Specimen thickness: 1.5 mm
- Specimen shape and dimensions:
    - Ball-on-disc tests: DP600 steel was machined into discs with an outer diameter of 120 mm Ball-on-plate tests: DP600 steel was cut into plate specimens with dimensions of 20x30 mm^2

DP600 steel specimens presented a Vickers Hardness of 230 ± 5 $HV_{1\ kgf}$, measured by a NanoTest 550 Micro Materials Ltd. nanoindenter, and a superficial average roughness

of 0.386 µm (R_a). Metallographic specimens were prepared according to standard procedures. They were mounted in an epoxy resin, ground down through successive grades of SiC paper to 2000 grade, degreased with alkaline cleaner and rinsed in tap water followed by deionized water, and finally polished with diamond paste of 3 and 1 µm.

For scanning electron microscopy (SEM) images of cross-sectional DP600 steel worn surfaces and subsurface layers, the specimens were etched with 2% Nital solution for 15 s, given that Nital preferentially etches ferrite and outlines their grain boundaries leaving martensite undissolved.

3.1.2. Corundum

The corundum (Al_2O_3) is a very versatile ceramic material. Its properties make it particularly suitable for applications where temperature or hardness is a critical parameter. Due to its high melting point (2050ºC (Schmitz, 2006)), corundum is for example used as refractory linings for high-temperature furnaces and reactors. Whilst, as a consequence of its extreme hardness (9 in Mohs hardness scale, ~2060 HV (Cardarelli, 2008)), it can be employed as an abrasive. Moreover, corundum has a relatively facility to adapt to different uses and environments.

In the present work, high purity (99.9%) corundum balls from Goodfellow were selected as counterbody due to its high wear resistance and its chemical inertness.

The standard product features are (Goodfellow Group, 2008):

- Diameter: 3.0 mm
- Tolerance: ± 2.5 µm
- Sphericity: 0.625 µm
- Condition: Polished -surface roughness of 12.83 nm (R_a) approximately
- Grade: Precision sphere; Grade 25

3.2 Experimental Methodology

3.2.1 Ball-On-Disc Test Method

One of the most chosen test methods for determining the friction and wear during sliding is the pin-on-disc configuration. Particularly, the geometry employed in the present work was the ball-on-disc Bruker CETR-UMT2 system (Figure 3.2). This test was conducted according to ASTM G99-95 standard.

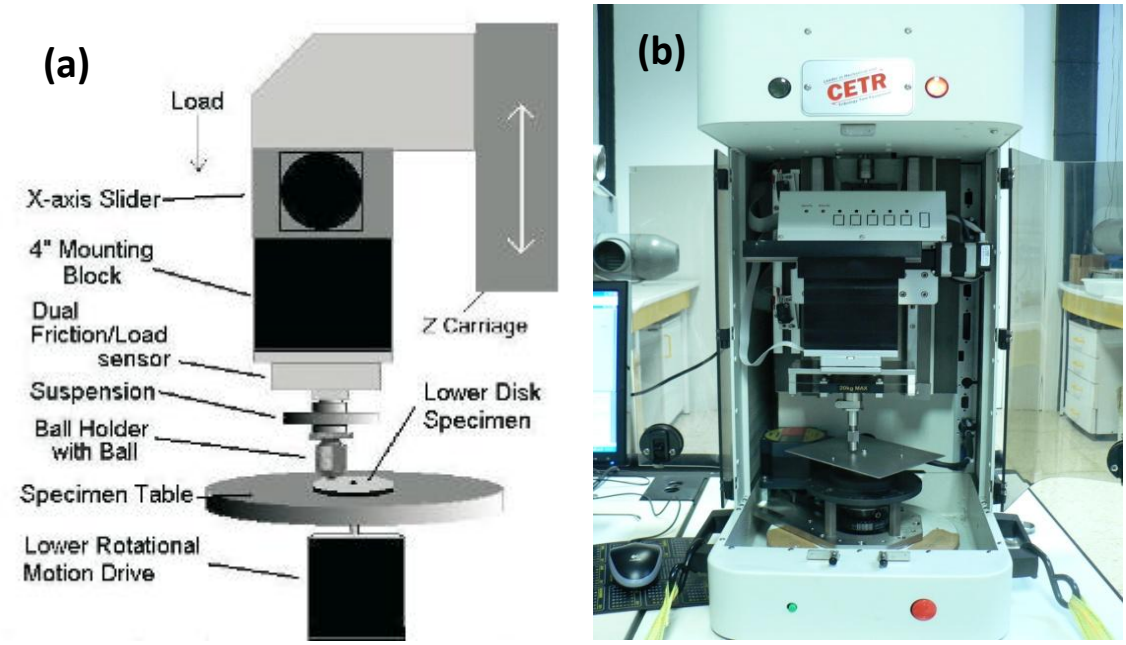

Figure 3.2 (a) Schematic image of a Bruker CETR-UMT2 tribometer ball-on-disc modulus (Bruker, 2006a) (b) Laboratory set-up of a Bruker CETR-UMT2 tribometer with the ball-on-disc modulus.

In this test system, a fixed ball-shaped body is loaded on top of the rotating disc -lower specimen- and slides under a specific set of conditions. The ball –upper specimen- is connected to a Z-axis carriage which, in turn, applies a vertically downward load on the disc using an accurate force/load sensor to maintain a constant load (Bruker, 2006a). The model force –or load cell- used, namely DFH-2 Dual Friction/Load Sensor, precisely ranges from 0.2 to 20 N. The lower rotational motion drive motor can spin between 0.001 and 1000 rpm.

This set-up characterisation normally facilitates the third body interaction since it limits the ejection of the debris from the contact area in comparison to other configuration where the disc is loaded on top of the pin/ball.

During testing, the ball-on-disc tests were performed in both unidirectional (clockwise) and bidirectional (combined clock- and counterclockwise) motion.

The ASTM G99-95 standard does not designate the test parameters, such as load, rotation speed or test duration. Therefore, all the wear tests were carried out at the following test conditions of load and test duration:

- Contact load: 2 N
- Total slided distance: 2000 m.

All test were performed under ambient conditions without lubrication, at Room Temperature of (23±3) ºC and a Relative Humidity of 30-50 %.

3.2.1.1 Unidirectional Sliding

In order to independently study the effect of linear sliding speed, and/or rotation -or contact- frequency on the wear rate for the discs, a thoroughly design of the experimental parameters was used. Notice that the sliding speed (linear speed), *v*, at a given contact or rotation frequency (angular speed), *f*, varies by adjusting the wear track diameter, *D*, in the case of ball-on-disc sliding tests (see Equation 1.6 in Section 1.2.5).

Whereby, a series of ball-on-disc wear tests was conducted at a given constant sliding speed but at different rotation speeds by modifying the wear track diameter to adjust the Equation 1.6. In addition, a series of ball-on-disc wear tests was carried out at a fixed rotation speed but at different sliding speeds, once again modifying the wear track diameter.

Therefore, these parameters were varied within the following intervals:

- Linear sliding speed: between 0.1 and 3.75 m/s
- Track diameter: between 12 and 75 mm
- Contact frequency: between 0.6 and 16 Hz

3.2.1.2 Bidirectional Sliding

Bidirectional motion was compared in this research work to unidirectional motion by taking into account the cyclic number, CN (Tang et al., 2011a). Such CN indicates how often the rotation direction of the disc is reversed. The unidirectional sliding is thus

represented by CN=0. Conversely, for bidirectional wear tests, namely CN≠0, the rotating direction is continuously varied after a fixed nuber of rotations as follows: CN=2, 5, 10, 20, 50. In other words, CN=i (being i>0) corresponds to i cycles which, in turn, are related to i x 2 times of reversing the wear path during the total rotation number, namely 2000 cycles. For instance, CN=20 represents 20 cycles corresponding to 20 x 2=40 times the rotation direction changes during the 2000 total rotation number.

As aforementioned, a precise design of the experimental parameters was studied. Hence, in this case the test conditions were varied as follows:

- Linear sliding speed: between 0.5 and 1.25 m/s
- Track diameter: between 31.8 and 91 mm
- Contact frequency: between 3.5 and 8.5 Hz

3.2.2 Ball-On-Plate Test Method

According to the ASTM G133-95:2002 standard, and using a Bruker CETR-UMT2 microtibometer (Figure 3.3), the lower specimen was a piece of sheet material, also known as plate or flat, which moves back and forth due to a linear reciprocating motion drive motor (Bruker, 2006b). Whilst, the upper specimen was a ball-shaped body which is loaded on top of the plate.

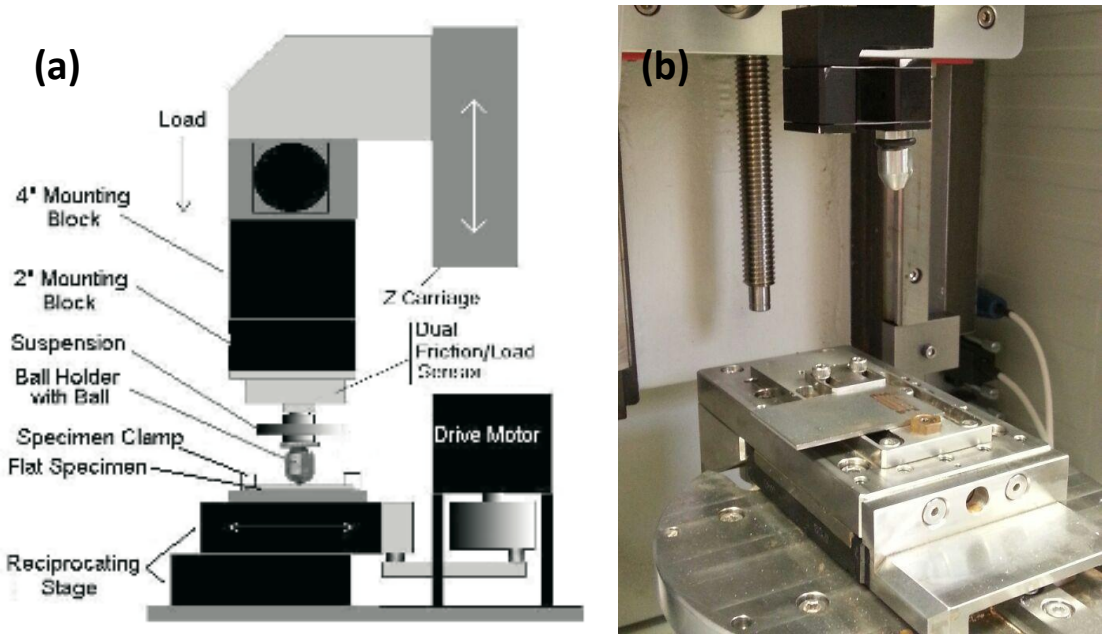

Figure 3.3 (a) Schematic Bruker CETR-UMT2 tribometer ball-on-plate modulus (Bruker, 2006b) (b) Laboratory set-up of a Bruker CETR-UMT2 tribometer with the ball-on-plate modulus.

As occurs in the previous wear test method explained (see Section 3.2.1), a vertically downward contact load was applied on the plate specimen which, in turn, is horizontally mounted. Moreover, the ASTM G133-95 standard, does not specify the test conditions (e.g. load, oscillatory frequency, test duration ...). Therefore, the selected test parameters chosen in this test method were:

- Contact load: 2 N
- Total slided distance: 2000 m.

All test were performed under ambient conditions without lubrication, at Room Temperature (23±3) ºC and a Relative Humidity of 30-50 %.

3.2.2.1 Linear Reciprocating Sliding

In the case of the linear reciprocating sliding, the sliding speed (linear speed), v, at a given contact frequency, f, varies by adjusting the stroke length, s. These three operational parameters are related as follows:

$$v = f \cdot s \tag{3.1}$$

Therefore, a series of ball-on-plate wear tests was conducted at a given constant sliding speed, but at different contact frequencies by modifying the stroke length in order to adjust the Equation 3.1. In addition, a series of ball-on-plate wear tests was carried out at a given fixed contact frequency but at different sliding speeds, modifying once again the stroke length.

The experimental data for these particular tests were varied as follows:

- Linear sliding speed: between 0.01 and 0.25 m/s
- Stroke length: between 8.06 and 15.65 mm
- Contact frequency: between 1 and 16 Hz

3.3 Data Analysis Methodology

3.3.1 Optical Confocal Profilometer

The 3D optical profiler instrument is typically used to characterise the surface of a specimen by accurately measuring and evaluating all the detailed features such as roughness, finish, texture, step-height, and warping, as well as its profile, dimension, volume, and area.

This microscope system takes image slices in multiple X-Y scans per Z plane. In other words, after each scan in the X-Y plane, a Z movement is made to get all the information. Consequently, it provides 3D plots and also 2D profiles by maintaining high resolution at all magnifications.

The specimen worn surface was studied by the PLμ 3200 Sensofar in order to calculate its volume wear loss. The PLμ 3200 Sensofar optical profilometer directly links to an advanced analysis software based upon Digital Surf's Mountains Technology®, namely SensoMAP. This software applies dimensional and surface state imaging, analysis and metrology solutions. Moreover, it automatically reports the analysis of 3D and 2D measurements from the selected area.

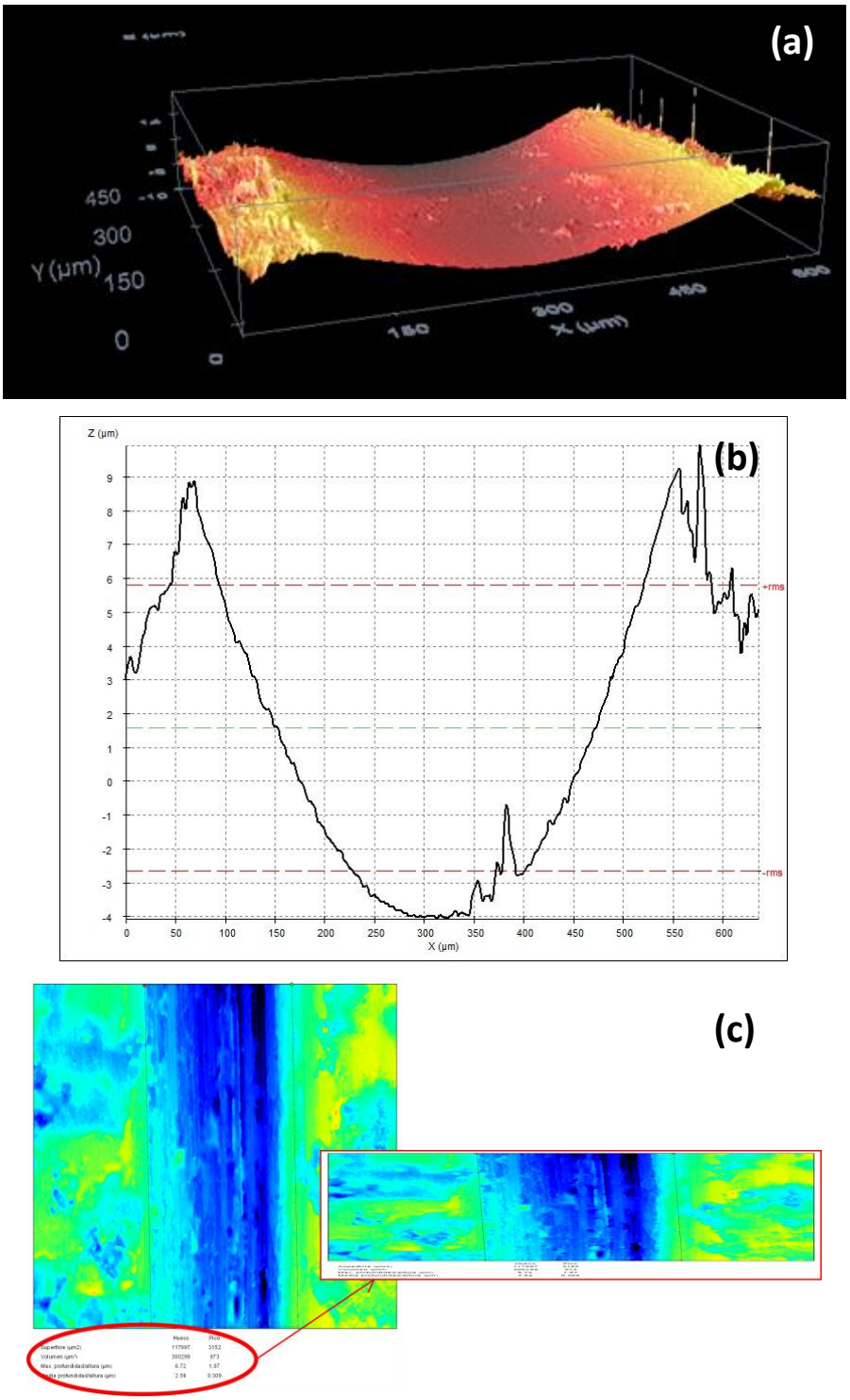

Figure 3.4 (a) 3D plot of a representative wear track in the DP600 steel by PLμ 3200 Sensofar, (b) 2D profile taken from a particular section of the previous 3D plot, (c) SensoMAP analysis associated to the same wear track observed.

The steps followed during the worn surface analysis can be schematically observed in Figure 3.4, and are listed below:

1. An accurate 3D plot of the selected surface was taken (Figure 3.4 (a)).
2. The 2D profile derived from the previous image allows one to measure the width of the wear track (Figure 3.4 (b)).
3. SensoMAP provides standard functional analysis by means of specific tools for wear analysis. Thus, the area/volume loss can be calculated (Figure 3.4 (c)).

The acquired data were processed in Excel-compatible text files to obtain the total volume loss and wear rate as follows:

- Volume wear loss (mm^3): Calculated from the width values (derived from the 2D profile) measured at ten different locations along the wear track, together with the area and volume experimental data provided by SensoMAP measurements.
- Wear rate ($mm^3/N \cdot m$): Obtained by dividing the volume wear loss per unit load and the sliding distance.

3.3.2 Scanning Electron Microscopy With Energy Dispersive X-Ray Spectrocopy

The worn surfaces, the collected debris, and the cross-section specimens were examined by field emission gun scanning electron microscopy (FEG-SEM, Hitachi S-4800) equipped with energy dispersive X-ray spectroscopy (EDS) facilities. The images were taken at 15.0 kV. The working distance was set at 15.0 mm approximately. Based on the item of interest, the magnifications used were:

- 300x for worn surfaces
- 2000x and 4000x for cross-sections
- 1000x, 4000x, 8000x, and 20000x for debris

Moreover, INCA software (linked to EDS facilities) was used to study the variations in chemical composition. In general, EDS analyses the energy spectrum in order to

determine the abundance of specific elements. Moreover, it can be used to find the chemical composition of materials down to a spot size of a few microns.

3.3.3 X-Ray Diffraction

This analysis technique was particularly used to determine the stoichiometric composition –phase identification- of the debris. Any compound found in the specimen produces a characteristic diffraction pattern. In each diffractogram, it can be distinguished different peaks which correspond to a particular phase or component (Callister, 2007).

X-Ray diffraction (XRD) analyses were performed using a Bruker AXS D8 diffractometer, with Co-Kα monochromatic radiation, with a wavelength of λ= 1.789 Å. Match!2, a software based on indexing and matching pattern, was run to resolve the phase or component from the peak position.

3.3.4 Berkovich Hardness Test

The hardness measurements were carried out by a NanoTest 550 Micro Materials Ltd. nanoindenter, using a Berkovich diamond tip. Tests were made at an average indentation depth of 840 nm by performing a 4x4 indentation pattern beneath each wear track. The local hardness (HV) results were estimated from the loading and unloading curves using the standard Oliver-Pharr methodology (Oliver and Pharr, 2004).

3.4 Experimental Outline

A simplified scheme of the materials and the test procedure utilised during this research work is shown in Figure 3.5.

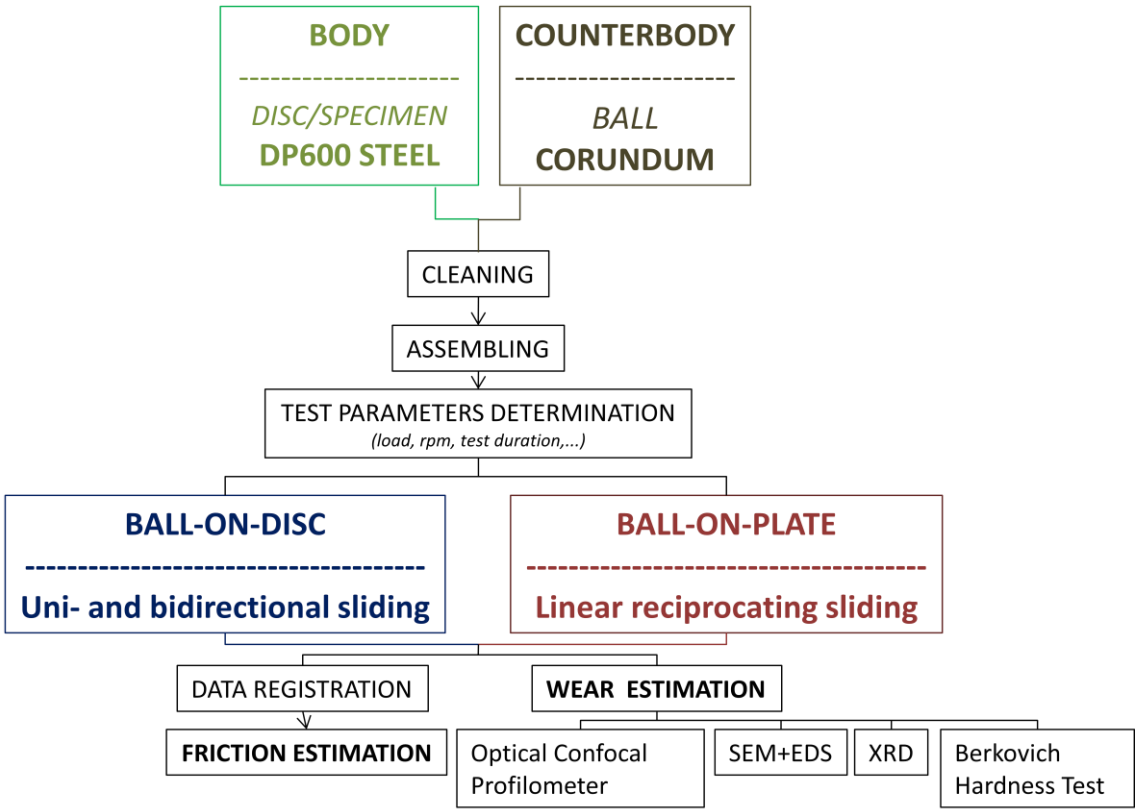

Figure 3.5 Schematic drawing corresponding to the process followed during this research work.

Specimen cleaning

All the specimens –body and counterbody- were perfectly degreased with suitable solvents and dried by blowing cold air in order to prevent any contaminants in their surface.

Specimen assembling

Previously to wear testing, it is necessary to ensure that the specimens are facing their right way. Consequently, the lower specimen -the body or disc- was perpendicularly mounted (± 1º) to the tribometer resolution axis (Z-axis) (see Figures 3.2 and 3.3). The body was immobilised by tightening on the specimen platform. Then, the upper specimen, i.e. the counterbody, was inserted and affixed to the ball holder to avoid sliding during testing.

Wear test parameters set up

The test is ready to run once the specimens are perfectly assembled, the required parameters (contact load, rotation frequency (rpm), and test duration) are loaded, and the programme displays a positive feedback window before testing.

Debris collection

After testing, wear debris –clearly visible to the naked eye- was carefully collected (Figure 3.6). This debris was subsequently examined by scanning electron microscopy and analysed by X-ray diffraction to identify its composition and phases, its wear processes, and, thus, its fundamental mechanisms.

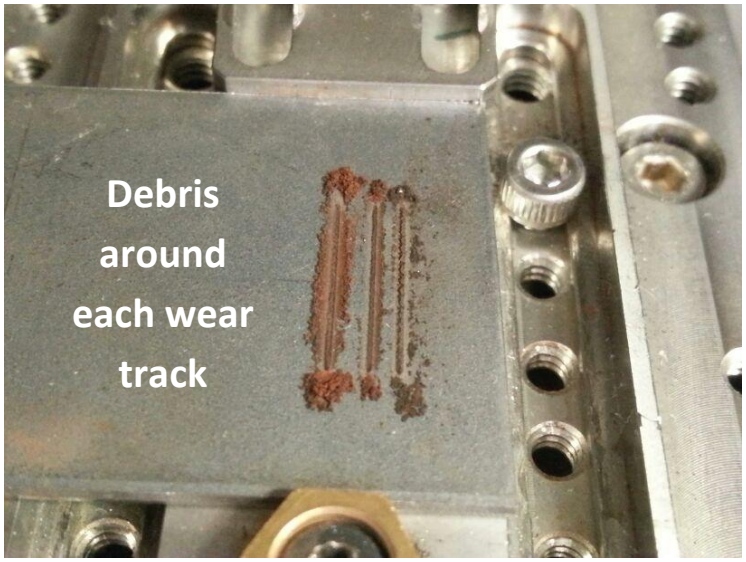

Figure 3.6 Macrograph illustrating an example of debris location after testing a DP600 steel specimen sliding against a corundum ball during a series of ball-on-plate wear tests.

Wear and friction estimation

The volume wear loss was calculated using the PLμ 3200 Sensofar optical profilometer, as explained in Section 3.3.1. Then, the wear rate was obtained by dividing the volume wear loss per unit load and the sliding distance.

Visual examinations of the counterbody surfaces after the wear tests completion indicated that the wear of these counterbodies can be considered negligible.

The data files generated with COF infomation during testing can be displayed on the screen into curve-shaped data. Moreover, data can be exported to ASCII format for further processing.

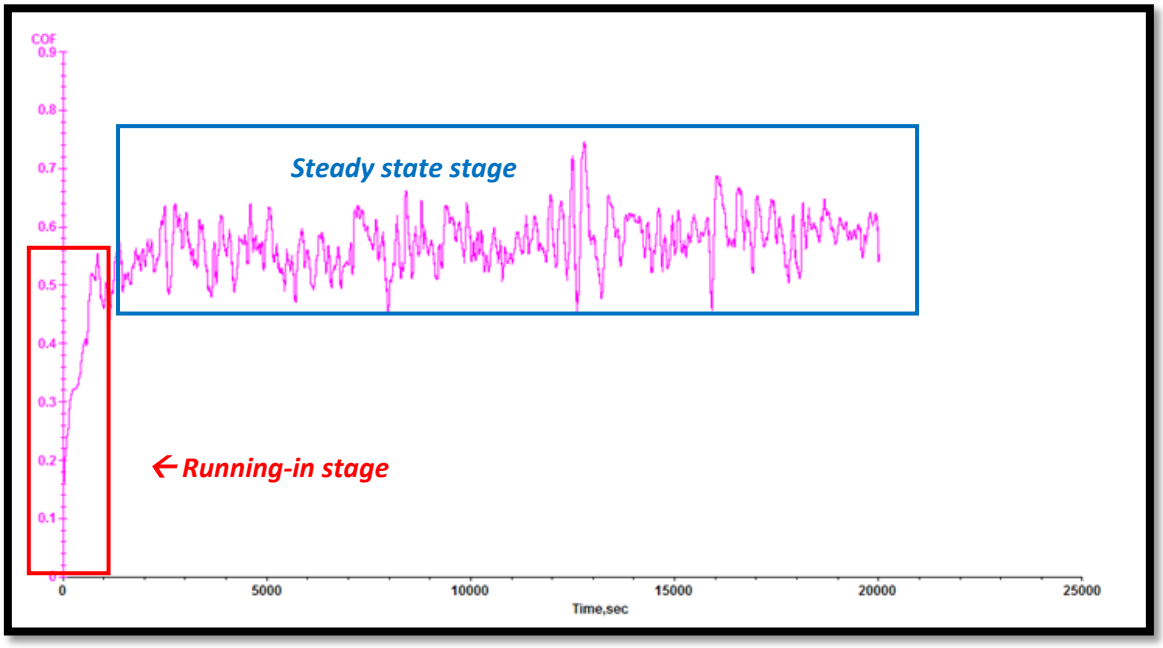

Figure 3.7 COF curve displaying the two distinct wear stages –running-in and steady state- as a function of the test duration –time in seconds.

In general, two distinct wear stages are able to be easily distinguished in all the COF curves examined, as representatively shown in Figure 3.7. Initially, a very short and steep running-in stage (normally less than 5% of the total sliding time) was observed. In this case, the COF rapidly increases up to reach a constant value. The second stage was characterised by the particular COF evolution which hardly varies, and is known as steady state stage.

The COF results presented in this research work were representative of the steady state stage. The effect of the running-in on the wear rate has not been thus taken into account. Moreover, any point related to both the COF and wear rate values was the result of triple tests carried out under identical conditions. Each testing condition showed excellent reproducibility, with less than 10% of variation.

4

Friction and Wear Behaviour of DP600 Steel in Discontinuous Sliding Contact Conditions as a Function of Sliding Speed and Contact Frequency

This chapter introduces the study of friction and wear rate behaviour of DP600 steel discs as a function of sliding speed, and contact frequency under unidirectional ball-on-disc dry sliding conditions. The analysis was conducted by means of a novel approach of sliding ball-on-disc wear tests, namely Garcia-Ramil-Celis model (Garcia et al., 2003), where the disc material is investigated.

Tests were performed under unidirectional ball-on-disc tests. In order to independently study the effect of linear sliding speed, and contact frequency on the wear rate for the DP600 discs sliding against corundum balls, a series of ball-on-disc wear tests was carried out at a given constant sliding speed but at different rotation speeds by modifying the wear track diameter to adjust the Equation 1.6 addressed in Section 1.2.5, and viceversa. In this sense, the sliding speed was varied between 0.1 and 3.75 m/s and the track diameter ranged within an interval from 12 to 75 mm. Thus the contact frequency studied in the present work varied between 0.6 and 16 Hz.

4.1 Worn Surfaces and Wear Debris

SEM images corresponding to the wear tracks formed on the DP600 disc during the dry sliding wear tests at a contact frequency of 1.20 Hz and a sliding speed of 0.1 m/s, and at a contact frequency of 16 Hz and a sliding speed of 0.9 m/s, as the representative

behaviour of the results obtained at low and high contact frequencies/sliding speeds respectively, are shown in Figure 4.1 (a)-(b). Wear tracks are characterised by surface deformation in form of smooth longitudinal grooves running parallel to the sliding direction. SEM images also reveal that the wear mechanism is mainly oxidative in both cases, although at 16 Hz and 0.9 m/s, larger oxidised areas along the wear track are observed.

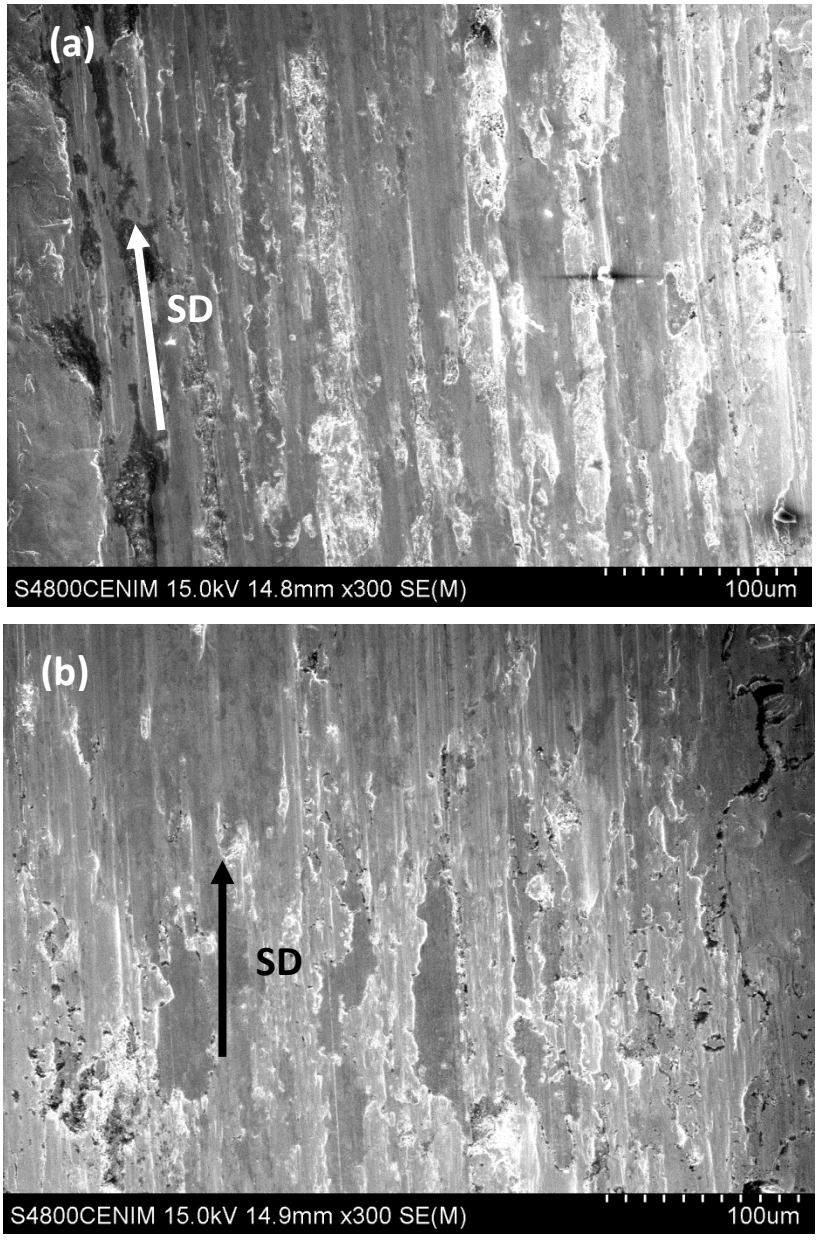

Figure 4.1 SEM images of wear tracks morphology on the disc after sliding tests performed at (a) 1.20 Hz, 0.1 m/s, 13.26 mm of radius; (b) 16 Hz, 0.9 m/s, 8.95 mm of radius.

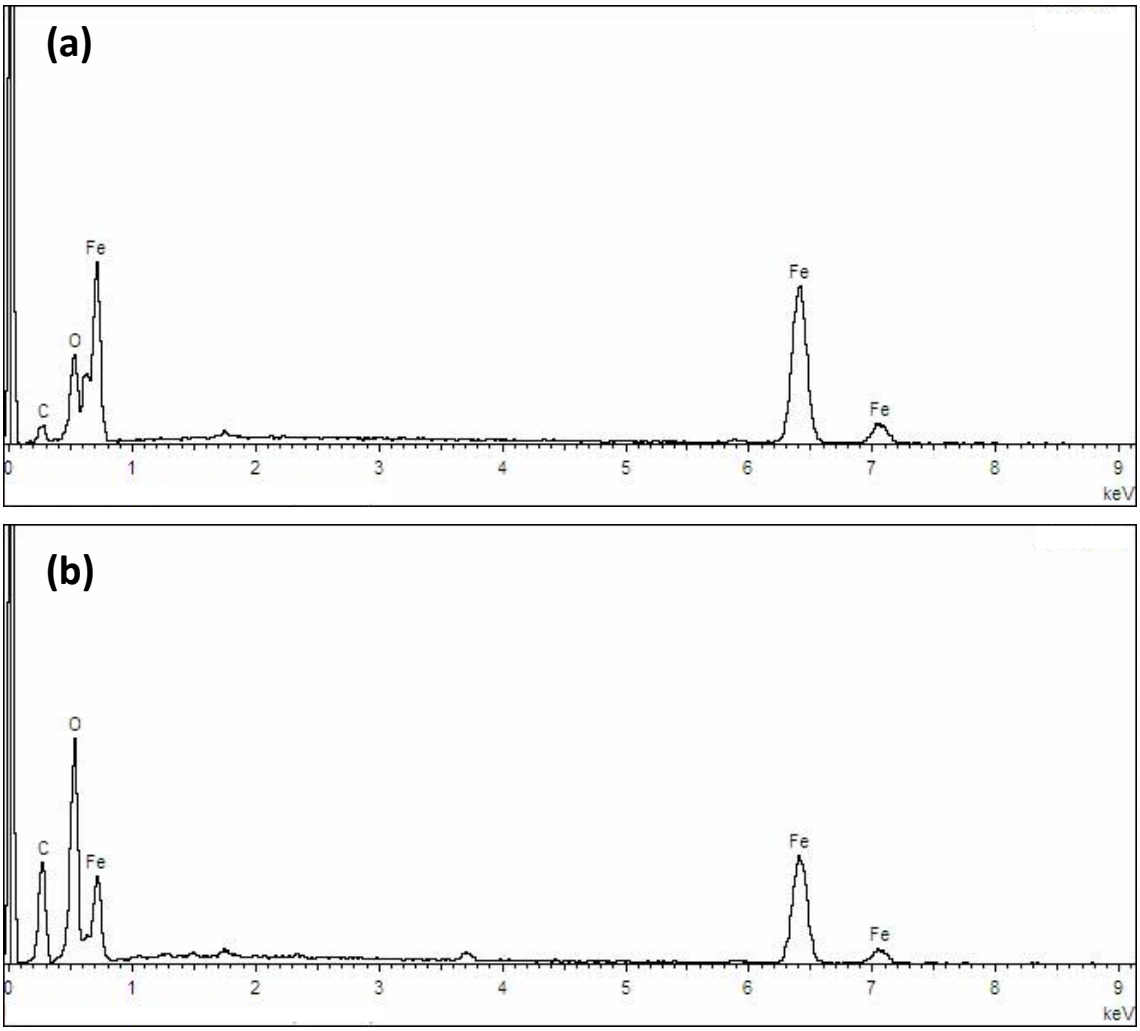

Figure 4.2 EDS spectra of wear tracks on the disc after sliding tests performed at (a) 1.20 Hz, 0.1 m/s, 13.26 mm of radius; (b) 16 Hz, 0.9 m/s, 8.95 mm of radius.

The EDS spectra of the worn surfaces along the tracks at these two contact frequencies are plotted in Figure 4.2 (a), i.e. 1.20 Hz and 0.1 m/s, and Figure 4.2 (b), i.e. 16 Hz and 0.9 m/s. Both spectra show the presence of Fe, O and C species, indicating thus that the DP600 worn surfaces have been oxidised during the dry sliding wear process.

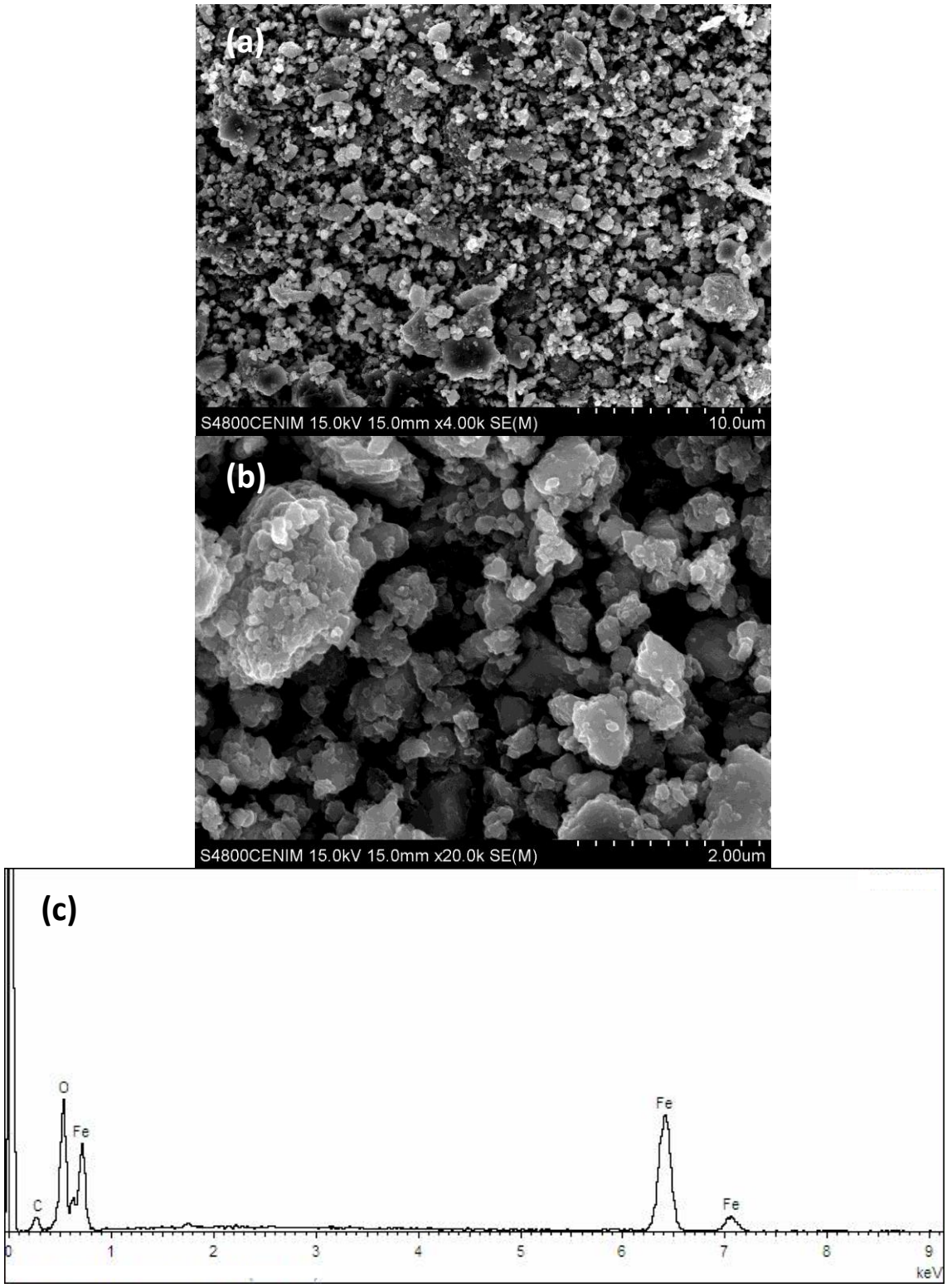

Figure 4.3 (a)-(b) SEM images and (c) EDS spectrum taken from debris collected after sliding tests performed at 1.20 Hz, 0.1 m/s, 13.26 mm of radius.

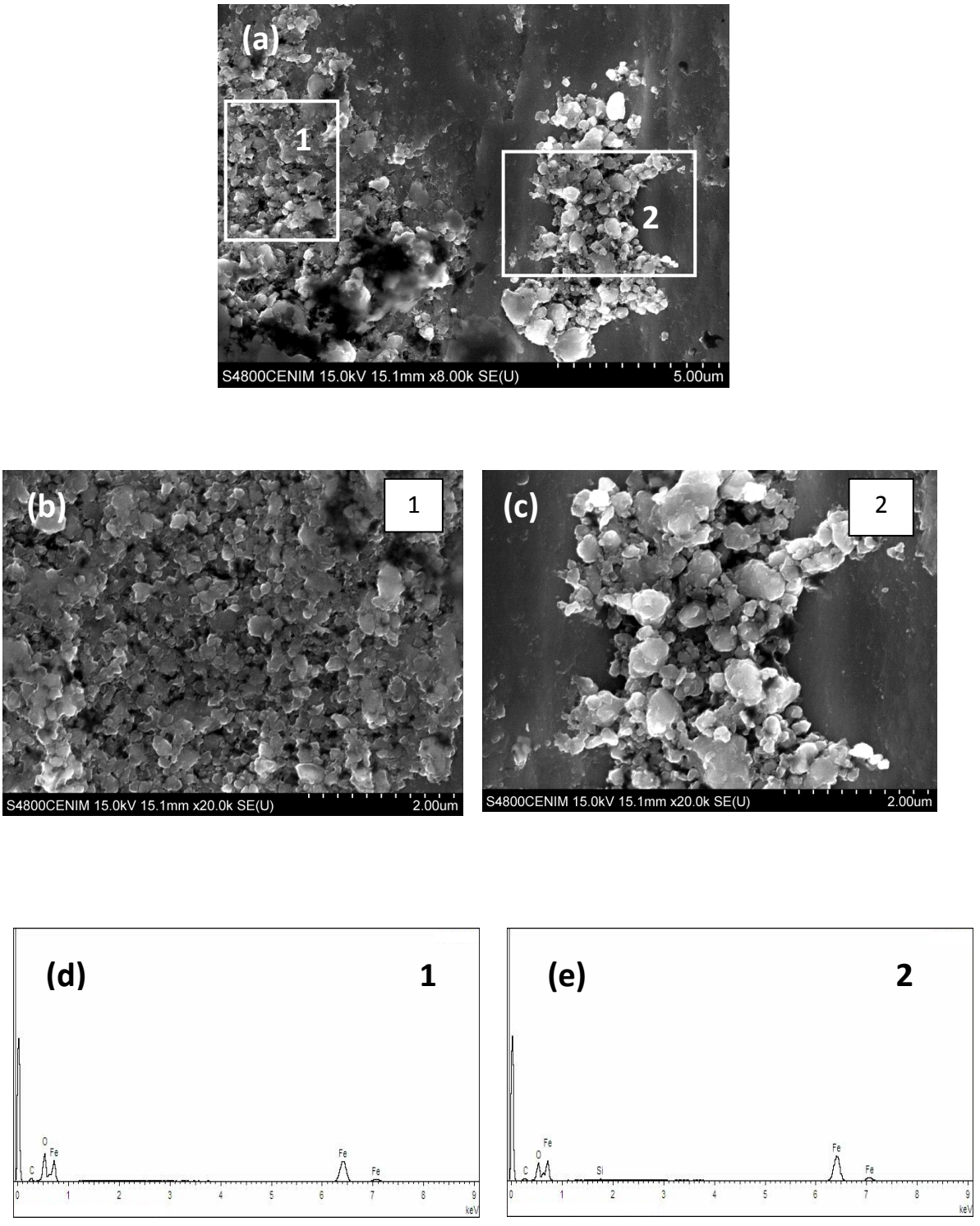

Figure 4.4 (a)-(c) SEM images and (d)-(e) EDS spectra taken from debris collected after sliding tests performed at 16 Hz, 0.9 m/s, 8.95 mm of radius.

Higher magnifications of the scanning electron micrographs, in Figures 4.3 and 4.4, show the wear debris produced at these contact frequencies and sliding speeds, 1.20 Hz and 0.1 m/s, and 16 Hz and 0.9 m/s, and their respective EDS spectra. At the lowest contact frequency, Figure 4.3 (a)-(b), the wear particles seem to be predominantly comprised by irregular fine particles of equiaxed shape of approximately 0.2 - 4 μm, size. The EDS spectrum (Figure 4.3 (c)) of this debris consists of Fe, O and C species, showing the presence of oxidised compounds.

The debris collected at 16 Hz and 0.9 m/s, Figure 4.4 (a)-(c), shows a similar appearance, fine equiaxed particles. Nevertheless, the difference in size with regard to the debris collected at low contact frequencies is clearly observed. The size of the debris particles varies from 0.1 to 1 μm.

EDS analysis corresponding to the fine equiaxed wear debris produced at high contact frequency (i.e.16 Hz) shows similar composition to those produced at low contact frequency (Figure 4.4 (d)-(e)). Sliding wear at 16 Hz and 0.9 m/s produces wear oxidised debris, with the presence of Fe, O and C species.

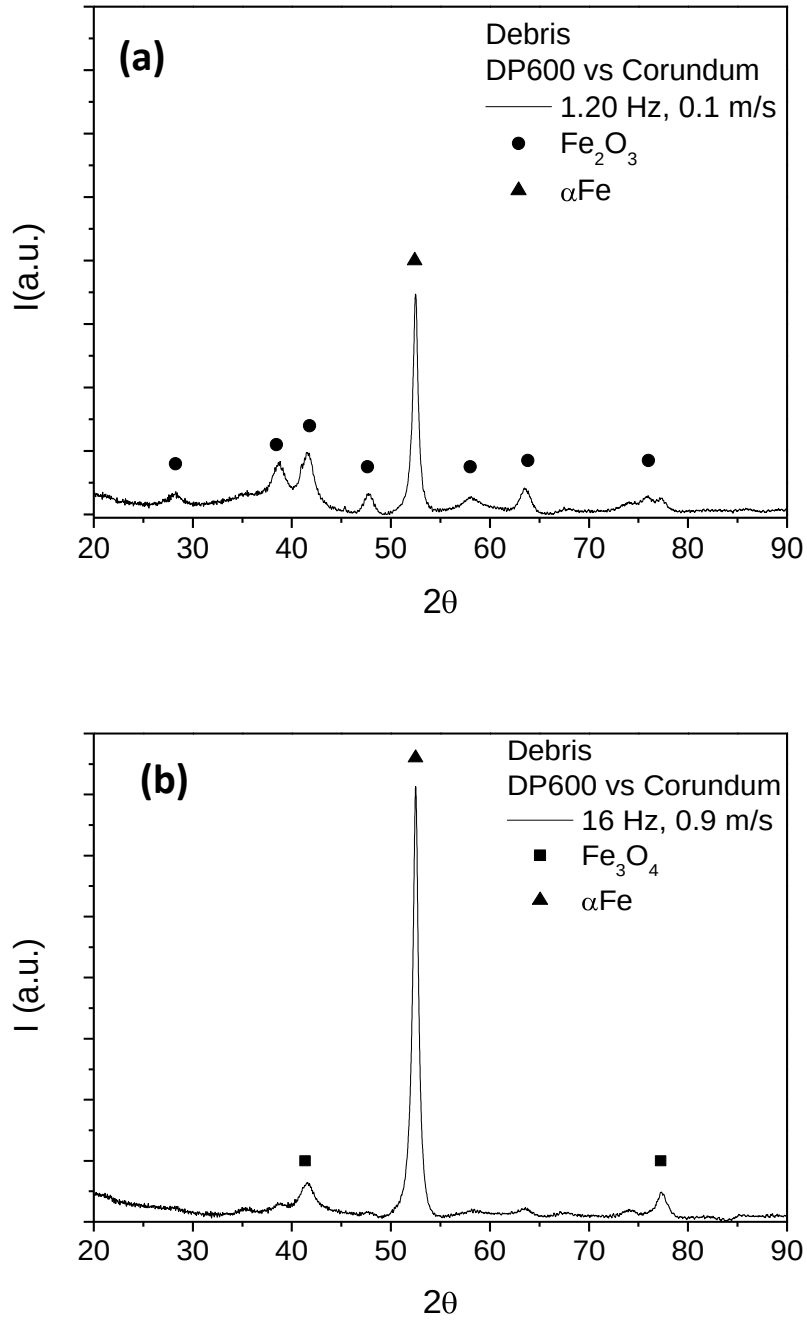

Figure 4.5 XRD diffractograms of debris generated after sliding tests performed at (a) 1.20 Hz, 0.1 m/s, 13.26 mm of radius and (b) 16 Hz, 0.9 m/s, 8.95 mm of radius.

The oxidative wear mechanism involved in these dry sliding wear tests is further confirmed by the XRD diffractograms. Figure 4.5 shows the XRD diffractograms of the collected debris generated at low and high contact frequencies, respectively. At 1.20 Hz (Figure 4.5 (a)), the XRD diffractogram reveals two phases, namely hematite (Fe_2O_3)

and alpha-iron (α-Fe), whereas at 16 Hz XRD analysis determines that the main wear debris constituents are magnetite (Fe_3O_4) and α-Fe, (Figure 4.5 (b)).

The nature of the iron oxide formed at both low and high contact frequencies can be explained according to the basis of the sliding temperature. Several authors (Quinn et al., 1980; Sullivan et al., 1980),-based on the static oxidation experiments, reported that the type of oxidised wear debris retrieved from dry sliding wear tests on low alloy steels were directly related to the temperature. According to the authors, for experiments conducted without external heating, the predominant oxide at temperatures below 450 ºC is Fe_2O_3; at temperatures ranging from 450ºC to 600 ºC, it is Fe_3O_4; whereas, at temperatures greater than 600ºC, FeO is the predominant oxide in the debris.

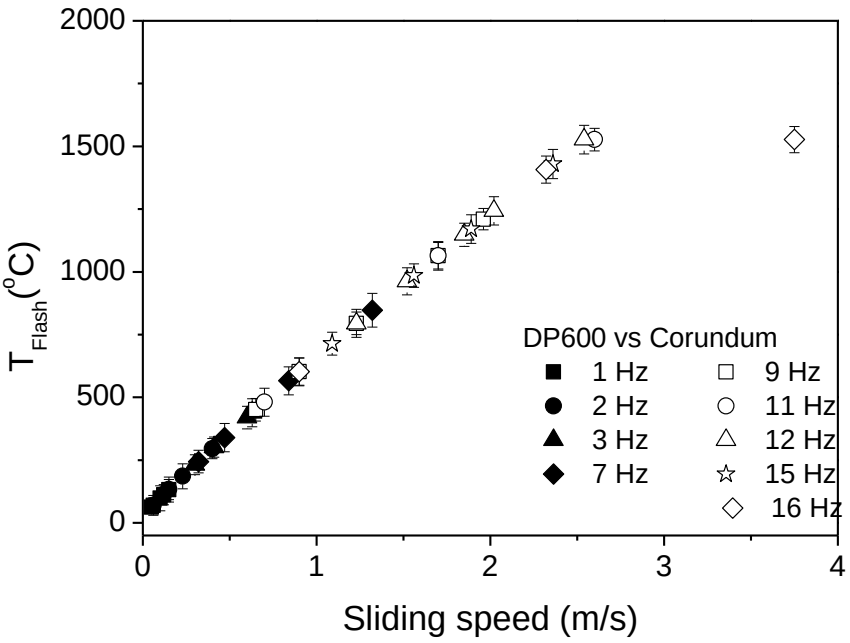

Figure 4.6 Theoretical estimation of flash temperature values measured on the discs.

A theoretical estimation of the flash temperature, T_f, for the different sliding speeds studied (Figure 4.6) has been calculated according to the equation given by Lim and Ashby (1987), defined as:

$$T_f = T_b \left(1 - \left(\frac{F}{N}\right)^{1/2}\right) + T_o \left(\frac{F}{N}\right)^{1/2} + \frac{\mu T_C^* \beta}{2} \left(\frac{F}{N}\right)^{1/2} v \qquad (4.1)$$

where $F$and v stand for normalised load and sliding speed, respectively; T_C^* is the effective equivalent temperature for metal (650 K approximately, based on calculations

made in Appendix 4 (Lima and Ashby, 1987)), β the dimensionless parameter for bulk heating (general order of 1), μ the coefficient of friction and N is the total number of contacting asperities. Here, T_b denotes the bulk temperature which, in turn, is obtained by the following expression:

$$T_b = T_o + \frac{\mu T^* \beta}{2 + \beta \ \pi v \ 8^{\ 1\ 2}} F v \tag{4.2}$$

where T_o is the sink temperature for bulk heating (in the present case, 298 K).

According to Lim and Ashby (1987), the normalised load on the sliding interface, F, and the normalised sliding speed, v, are defined in terms of:

$$F = \frac{F}{A_n H_o} \tag{4.3}$$

$$v = \frac{v r_o}{a} \tag{4.4}$$

In these formulations F is the normal load at the interface, A_n the nominal area of contact ($7.1 \cdot 10^{-6}$ m^2, approximately), H_o the hardness value of the dual phase steel, v the sliding speed, r_o the radius of the ball (1.5 mm) and a is the thermal diffusivity of the metal (about $1.09 \cdot 10^{-5}$ m^2/s).

Requiring, in addition, that N is expressed as:

$$N = \left(\frac{r_o}{r_a}\right)^{2} F \ 1 - F \ + 1 \tag{4.5}$$

where r_a the radius of an asperity (with a value about 10^{-5} m (Lim and Ashby, 1987).

The flash temperatures obtained at low contact frequencies (e.g. 1.20 Hz/0.1 m/s), and high contact frequencies (e.g. 16 Hz/0.9 m/s)) are thus in agreement with those described in literature (Quinn et al., 1980; Sullivan et al., 1980), i.e. below 450ºC, and between 450ºC and 600ºC, respectively. And the range of the temperatures obtained for the experimental conditions are, therefore, also in agreement with the type of oxides present in the wear debris.

4.2 Effect of Contact Frequency and Sliding Speed on Coefficient of Friction

The influence of the rotation speed on the wear behaviour of the DP600 steel disc was studied by performing wear tests at several sliding speeds keeping constant the contact frequency by the adjustment of adequate wear track diameters. The influence was then determined by calculating the wear rate of the dual-phase steel discs and the dynamic COF.

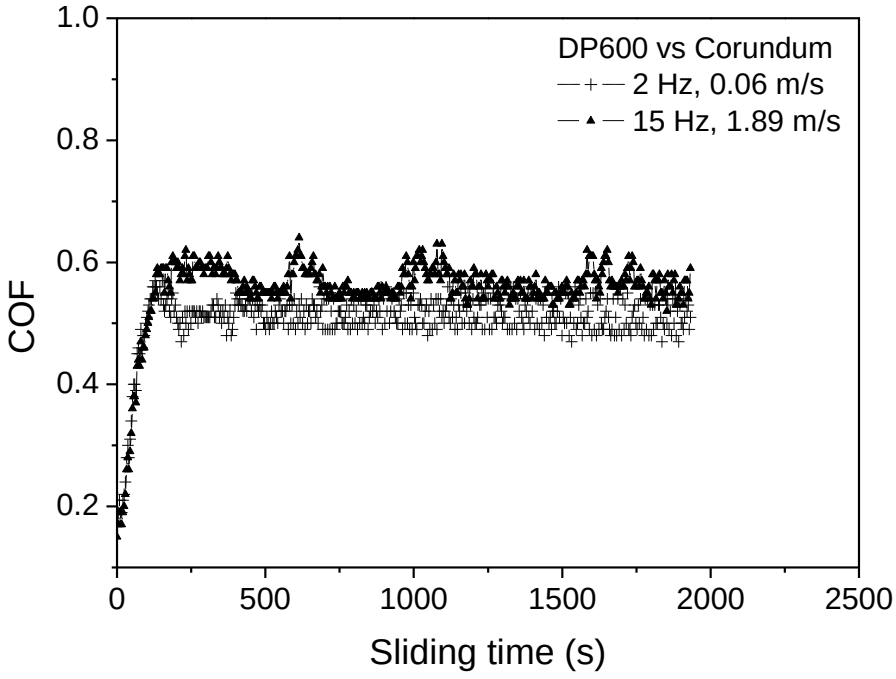

Figure 4.7 Evolution of coefficient of friction as a function of sliding time.

Two distinct wear stages can be easily distinguished in all the COF curves examined. Initially, a very short (less than 5% of the total sliding time) and steep running-in stage is observed, where the COF rapidly increases up to reach a constant value. This second stage where the COF hardly varies corresponds to steady state stage (Figure 4.7). The results presented in the following discussion are representative of the steady state stage, thus the effect of the running-in on the wear rate has not been taken into account.

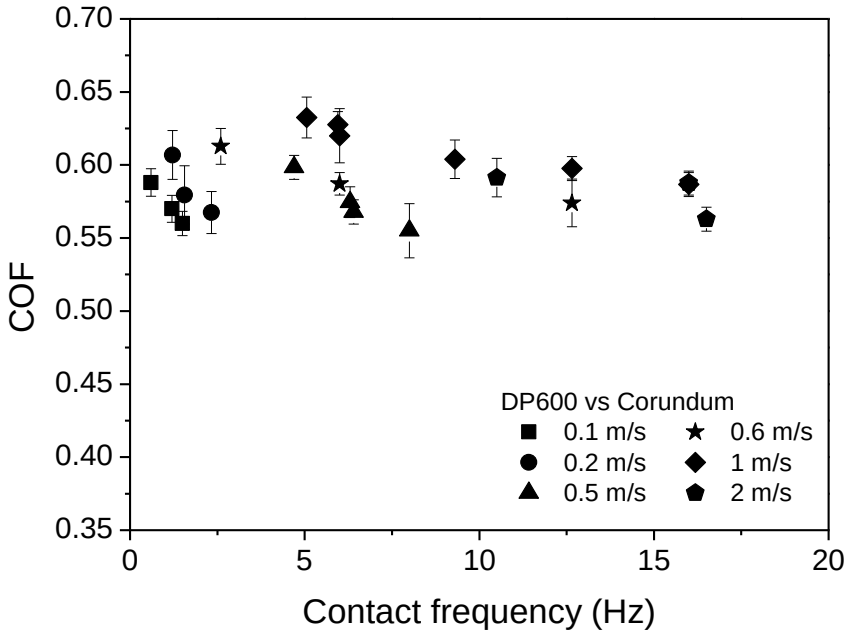

Figure 4.8 Coefficient of friction recorded between DP600 steel discs sliding against corundum balls as a function of contact frequency at six fixed sliding speeds.

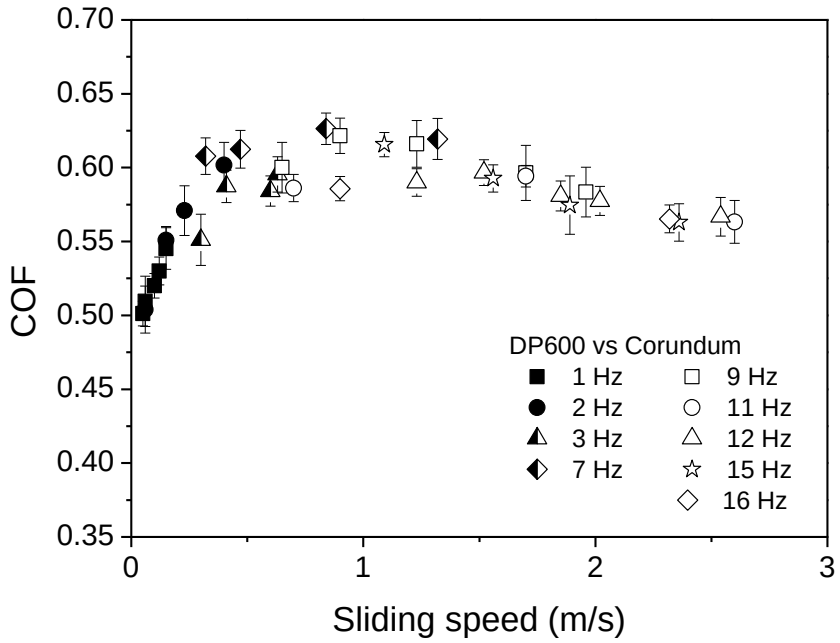

Figure 4.9 Coefficient of friction recorded between DP600 steel discs sliding against corundum balls as a function of sliding speed at nine fixed contact frequencies.

The dependence of the COF as a function of the contact frequency performed at six fixed sliding speeds, between 0.1 and 2 m/s, is presented in Figure 4.8. It can be noticed that the COF decreases as the contact frequency increases for each given constant sliding speed, e.g. a noticeable change occurs at 0.6 m/s, where the COF values vary from 0.61 to 0.51.

On the other hand, an overview of the COF behaviour as a function of the sliding speed, at nine fixed contact frequencies, between 1 and 16 Hz, is given in Figure 4.9. A clear correlation of the COF with the sliding speed can be detected. Initially, comparing the data sets for the fixed contact frequencies from 1 to 7 Hz, a steep increase in the COF concurrently with the sliding speed takes place. The COF values significantly vary between 0.4 and 0.62. Whilst from the fixed contact frequency of 7 Hz onwards, a distinct dependence emerges. In this case, the COF slightly decreases with the sliding speed. Moreover, even for data obtained at each given constant contact frequency, a strong dependence on the COF with the sliding speed is observed. The lower the fixed contact frequency, the higher the variation in the COF with the sliding speed is exhibited. For instance, at 1 Hz, the COF values range from 0.40 to 0.54, or also at 2 Hz, where the COF values vary between 0.50 and 0.60. Conversely, the higher the steady contact frequency, the lower the variation in the COF with the sliding speed.

4.3 Effect of Contact Frequency and Sliding Speed on Wear Rate

In an attempt to clarify the possible combined role of contact frequency and sliding speed on the DP600 steel, the wear rate of the discs tested at six fixed sliding speeds is presented in Figure 4.10, and at nine steady contact frequencies in Figure 4.11.

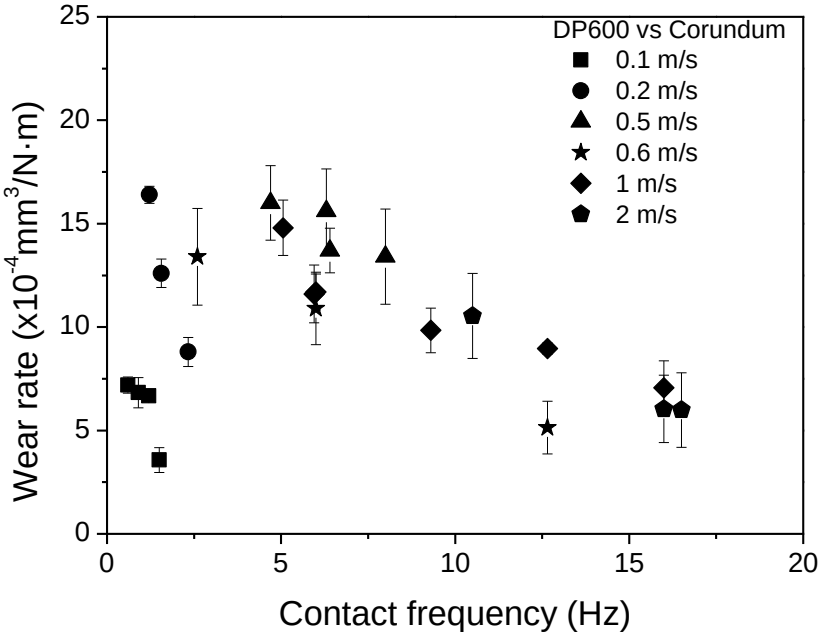

Figure 4.10 Wear rate (per total sliding distance) of DP600 steel discs sliding against corundum balls as a function of contact frequency at six fixed sliding speeds.

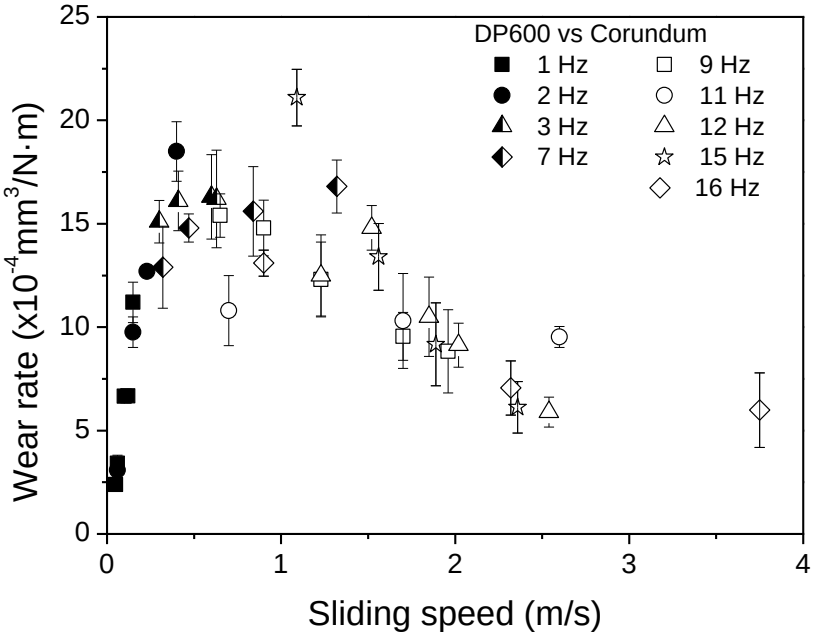

Figure 4.11 Wear rate (per total sliding distance) of DP600 steel discs sliding against corundum balls as a function of sliding speed at nine fixed contact frequencies.

Figure 4.10 shows that relationship between the wear rate and contact frequency for each data set obtained at a fixed sliding speed is inversely proportional. The decrease in wear rate is less abrupt as the given sliding speed grows. Wear rate ranges from $7.2 \cdot 10^{-4}$ to $4.11 \cdot 10^{-4}$ $mm^3/N \cdot m$ at 0.1 m/s, and from $10.55 \cdot 10^{-4}$ to $5.99 \cdot 10^{-4}$ $mm^3/N \cdot m$ at 2 m/s.

Conversely, the dependence of the wear rate on the sliding speed at nine fixed contact frequencies, Figure 4.11, shows a more complex behaviour. Initially, for fixed contact frequencies comprised from 1 to 7 Hz, the wear rate shows a strong dependence with the sliding speed. The wear rate exhibits an abrupt increase with the sliding speed for the contact frequencies ranging from 1 to 2 Hz, and then from 3 to 7 Hz, this dependence starts to attenuate with the sliding speed. These results indicate that, for contact frequencies below 7 Hz, the wear rate depends on the sliding speed, although they do definitely not follow an inverse reciprocal relationship as it might be expected from Quinn's model for oxidative wear (Quinn 1983, 1994, 1998).

However, at contact frequencies above 7 Hz, the wear rate behaves differently with increasing sliding speed. The wear rate gradually decreases as the sliding speed increases. In this case, the data displayed at steady contact frequencies higher than 7 Hz exhibits the expected behaviour from the Quinn's model.

It can also be observed that the wear rate values measured remain below $21.1 \cdot 10^{-4}$ $mm^3/N \cdot m$. In particular, at the low contact frequency range, e.g. 1Hz, the wear rate increases from $2.39 \cdot 10^{-4}$ to $11.2 \cdot 10^{-4}$ $mm^3/N \cdot m$. Whilst at 16 Hz, the highest contact frequency tested, the wear rate diminishes from $13.1 \cdot 10^{-4}$ to $5.99 \cdot 10^{-4}$ $mm^3/N \cdot m$.

As aforementioned, the Equation 1.8 directly relates the sliding speed and the contact frequency by adjusting the wear track diameter, i.e. the length of the wear track, $\pi \cdot D$. Therefore, a given total sliding length leads to a different number of cycles in function of the wear track diameter. In other words, for a given sliding distance the ball passes a different number of times over each point on the track depending on the wear track diameter. Consequently, one might think that the number of cycles or number of interactions between the ball and each point of the wear track can be a possible parameter which determines the wear rate along the total sliding distance. At this point, it may be thus interesting to calculate the wear rate as the wear volume loss per unit contact load and per number of cycles, in order to clarify that effect.

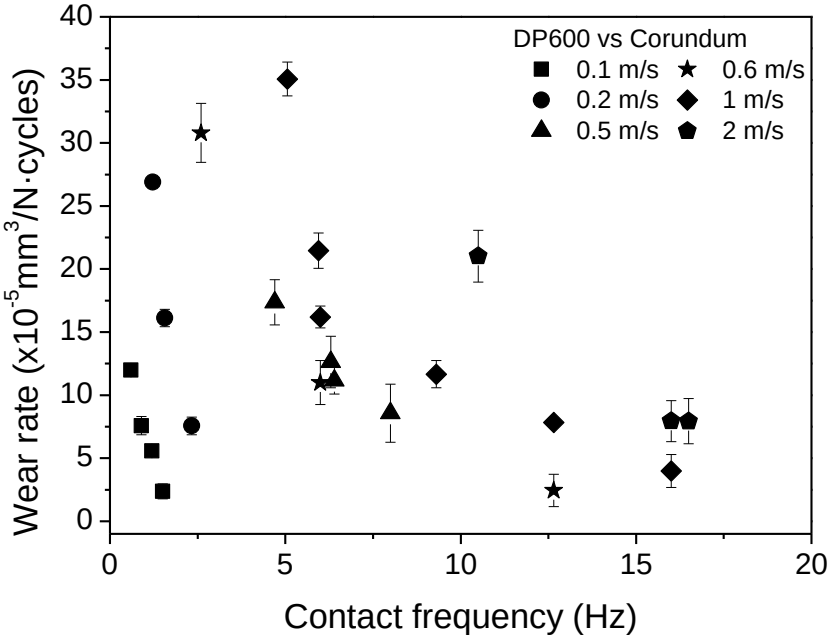

Figure 4.12 Wear rate (per number of cycles) of DP600 steel discs sliding against corundum balls as a function of contact frequency at six fixed sliding speeds.

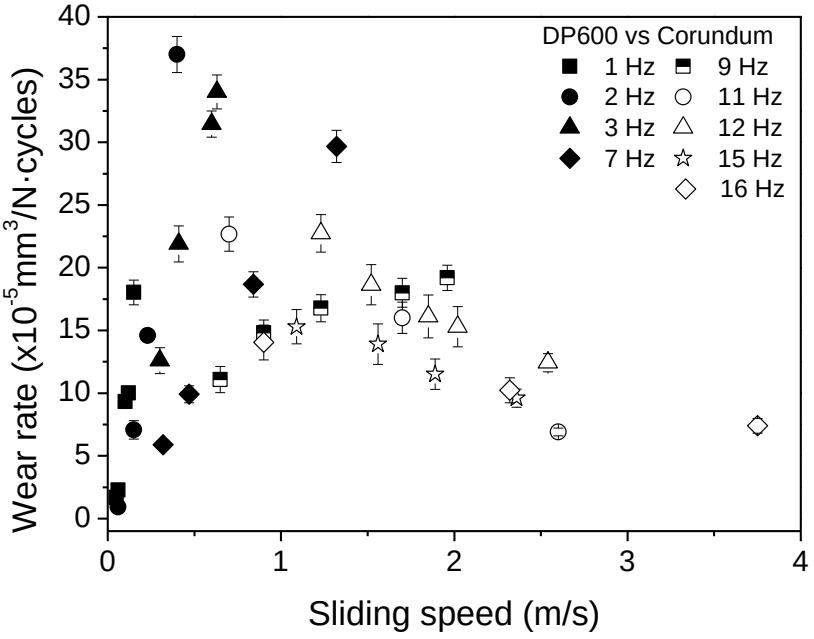

Figure 4.13 Wear rate (per number of cycles) of DP600 steel discs sliding against corundum balls as a function of sliding speed at nine fixed contact frequencies.

The newly defined wear rate is thus represented as a function of the contact frequency (Figure 4.12) and also as the sliding speed (Figure 4.13). Noticed is the similar wear behaviour, regardless of the wear rate definition, i.e. expressed per total sliding distance (Figures 4.10 and 4.11) or per number of cycles (Figures 4.12 and 4.13).

It can be observed in Figure 4.12 that the wear rate tested at six fixed sliding speeds decreases as the contact frequency increases. This diminishing is gradually smoother as the given sliding speed grows, as occurs in Figure 4.10. The wear rate evolution as the sliding speed increases at nine fixed contact frequencies is presented in Figure 4.13. Likewise as observed in Figure 4.11, the wear behaviour is more complex. Firstly, the wear rate steeply increases when the fixed contact frequencies vary between 1 and 7 Hz. Then at 9 Hz the wear rate attenuates its evolution with the sliding speed. Finally, at contact frequencies above 9 Hz, the wear rate gradually decreases with increasing the sliding speed.

Therefore, the wear rate seems to depend on the contact frequency and on the sliding speed. However, it does not rely on the number of cycles, i.e. the wear track diameter.

4.4 Validity of the Garcia-Ramil-Celis Model for Discontinuous Sliding Contact Events on DP600 Steel

In the present work, the wear rate values obtained differ from those found in the literature due to the fact that in most of the work published, the rotation speed was chosen as a constant when performing tests at different sliding speeds. In these cases, a change in the sliding speed also causes variation in the contact frequency. As a result, it is then not possible to distinguish the effect of sliding speed and contact frequency on the wear rate of the disc made of the material under study.

As was previously observed, the results presented in Figure 4.11 do not follow a consistent inverse reciprocal relationship between the wear rate and the sliding speed in the entire range for the fixed contact frequencies given, as is expected from Quinn's mild oxidation wear model (see Equation 1.5 in Section 1.2.4), since below 7 Hz the wear rate increases with increasing sliding speed.

Moreover, the effect of the contact frequency on the wear rate, experimentally determined in the present work (Figure 4.10), is hardly explained via Quinn's model when it is applied to the disc.

This model was developed in order to describe the wear of a pin, which is in continuous sliding contact with a disc. However, as can be seen in the literature, this model has been widely applied indistinctively for the counterbody –the pin or ball-, in continuous contact, or the specimen -the disc- which are in discontinuous sliding contact with the ball.

In order to overcome this limitation, Garcia et al. (2003) proposed a modification to Quinn's model to explain the wear behaviour for discontinuous sliding contact events. This new model is thus applicable to the wear of the discs in pin/ball-on-disc wear tests.

It should be noticed here that either Quinn's or Garcia's model have been developed assuming oxidative wear of single-phase materials. Tyagi et al. (2003) proposed an extension of Quinn's model for materials with two phases, studying specifically dual-phase steels and considering several possibilities about the kinetics of the oxidation, the critical thicknesses of the oxide layers and the probabilities of their removal. The authors concluded that the two phases, ferrite and martensite, usually have the same oxidation behaviour and also similar critical thicknesses for oxidative wear. Consequently, Quinn's model and its subsequent modifications for oxidative wear, e.g. Garcia et al. (2003), are assumed to be also applied for two phase materials.

The expression for the volumetric wear loss of a disc material, *W*, in Garcia-Ramil-Celis model is shown in Section 1.2.5, Equation 1.8.

Moreover, the authors stated a simplification of the equation for disc surface flash temperature, T_f, in discontinuous contact with a pin or ball, by computing the heat transmission equation (see Equation 1.7 in Section 1.2.5).

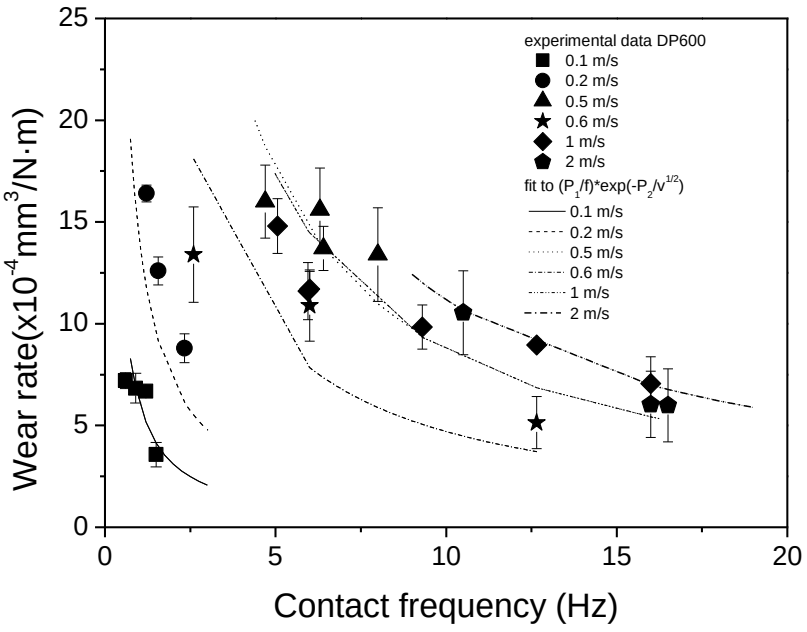

Figure 4.14 Experimental data displayed in Figure 4.10 fitted by Eqs. 1.7 and 1.8.

Figure 4.14 shows the obtained data from Figure 4.10, i.e. wear rate as a function of the contact frequency, simulated with Equation 1.8 and, also using the Equation 1.7 for T_f. A suitable fit is given for the wear rate of the DP600 steel disc material. This fit relies on two parameters, which are kept fixed for the sliding speeds, namely:

$$P_1 = \frac{A_c}{\xi^2 \rho^2} \frac{1}{H} , \qquad P_2 = \frac{Q}{R\tau} \tag{4.6}$$

The P_1 and P_2 parameter values chosen for the fitting process were those found which best describe the experimental data, generating a curve closely resembled to them. Using these values, an iterative procedure started. Similar P_1 and P_2 values were obtained for all the fixed sliding speed range tested. Therefore, P1 y P2, can be considered as a constant.

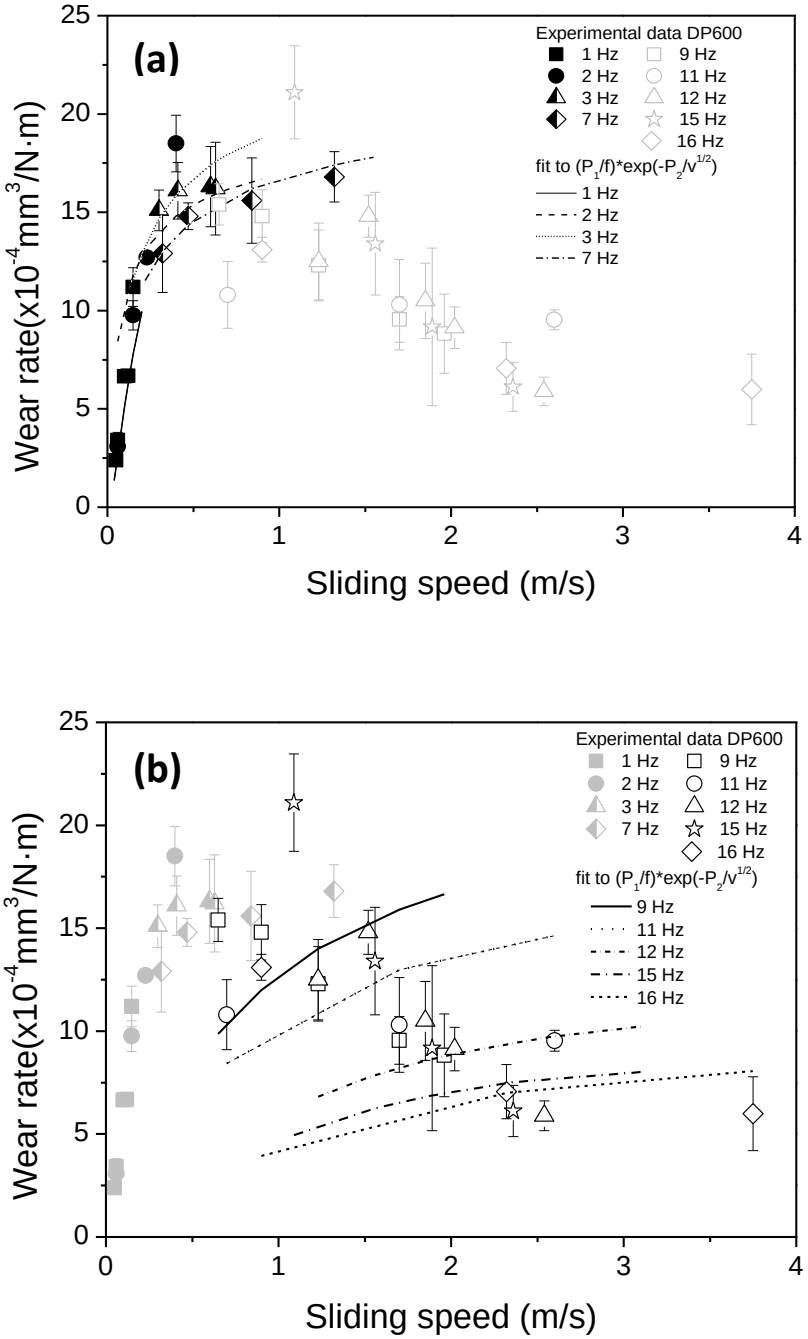

Figure 4.15 Experimental data presented in Figure 4.11 fitted by Eqs. 1.7 and 1.8: (a) 1Hz-7 Hz, (b) 9 Hz-16 Hz; based on fitting parameters derived from the fitting in Figure 4.14.

Subsequently, the two constant values obtained for P_1 and P_2 from fitting the data in Figure 4.14 were also used to simulate the experimental data displayed in Figure 4.11, for each of the contact frequencies. In this sense, Figure 4.15 presents the assessed predicted data and the experimental values (Figure 4.11) for the wear rate of the disc material as a function of the sliding speed. Initially, below 7 Hz (Figure 4.15 (a)), the predicted data fit the experimental data properly. From 7 Hz onwards (Figure 4.15 (b)), these theoretical data visibly mismatch with the experimental data.

The wear rate values exhibited as a function of the sliding speed for fixed contact frequencies above 7 Hz are expected to be in better concordance with the wear behaviour exposed in Quinn's model, due to the inversely reciprocal wear behaviour of the DP600 steel disc material shown in Figure 4.11. Therefore, a new fitting procedure was carried out, using Equation 1.5 (see Section 1.2.4), i.e. Quinn's model expression for volumetric wear loss, and a different expression for the flash temperature.

Based on Cowan and Winer (1992) work, the flash temperature expression for a pin/ball in elastic contact sliding against a disc leads to as follows:

$$T_f = 0.13\mu \left(\frac{1}{k}\right)^{1/3} \left(\frac{E}{r_o}\right)^{1/3} F^{2/3} v \qquad 4.7$$

where μ is the coefficient of friction, k the thermal conductivity, E the Young's modulus, r_o the pin/ball radius, F the load applied, and v the sliding speed.

The flash temperature, therefore, is directly dependent on the sliding speed. This expression was specifically proposed for permanent contact conditions, typically prevailed on pins/balls for pin/ball-on-disc wear tests, respectively.

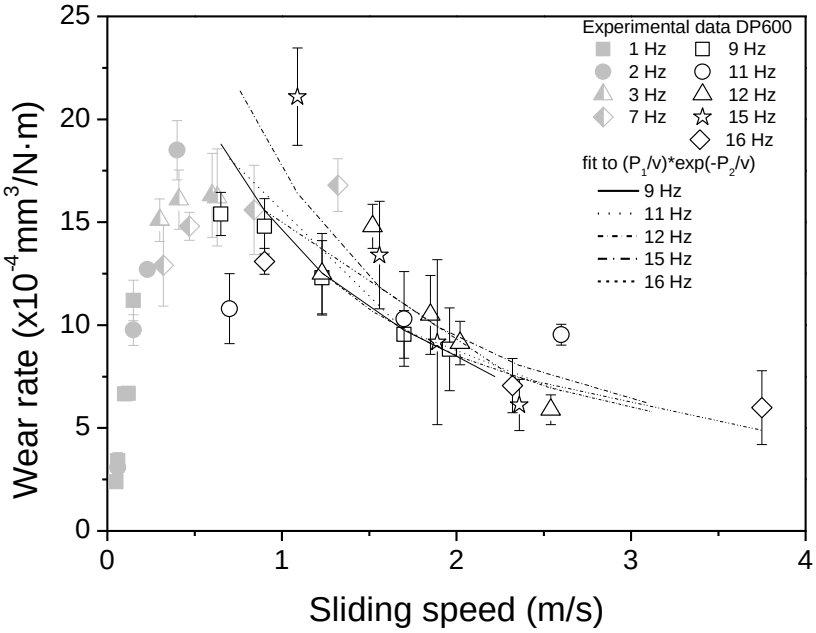

Figure 4.16 Experimental data presented in Figure 4.11 fitted by Eqs. 1.5 and 4.7; from 9 Hz to16 Hz.

Figure 4.16 thus presents the wear rate values shown in Figure 4.11, but only focused on the fixed contact frequencies range from 9 to 16 Hz, whose experimental data are on this occasion fitted by Equations 1.5 and 4.7. It can be noticed that the simulated data, estimated via Quinn's model, fit the experimental data properly and better than using the Garcia-Ramil-Celis model.

The Arrhenius activity factor, A_c, and the activation energy value, Q, have to be treated as adjustable parameters, chosen to fit data wear rate (Lim and Ashby, 1987). The Arrhenius constant, can be calculated from the fit parameter P_1, assuming a certain critical thickness for the oxides obtained, ξ; the hardness, H, and the density, ρ, of these oxides; and from the debris diameter (Garcia et al., 2003). On the other hand, the activation energy values can be obtained from the fit parameter P_2. In the present work, either the wear mechanism behaviour or the type of debris generated on the DP600 steel disc material make the Arrhenius activity factor difficult to calculate. Moreover, the uncertainties about τ (see Equation 1.7 in Section 1.2.5) complicate the estimation of the activation energy factor.

4.5 Other Materials

Different tribopairs, i.e. several material systems, have been studied in previous works (Garcia et al., 2003; Navas et al., 2006). They analysed the role of the contact frequency as an operational wear parameter in ball-on-disc dry sliding wear tests, when the disc material is investigated. Garcia et al. (2003) firstly reported the wear rate of PVD TiN-coated discs. Then, Navas et al. (2006) addressed the wear behaviour in AISI 1045 carbon steel discs. Both studies were conducted against corundum balls.

A semi-logarithmic plot gathers the published wear rate data (Ruiz-Andres et al., 2015b; Garcia et al., 2003; Navas et al. 2006) as a function of the contact frequency (Figure 4.17) and sliding speed (Figure 4.18).

In Figure 4.17, the results show a clear inversely proportional dependence between the wear rate and contact frequency, regardless of the disc material tested. Nevertheless, it should be noticed that the experimental data corresponding to TiN-coated discs behaves slightly different from the steel discs, i.e. DP600 and AISI1045. TiN-coated discs present a gradual and soft drop with increasing the contact frequency. Whilst, the inversely proportional relationship between the wear rate and contact frequency for DP600 and AISI 1045 discs depends on each data set obtained at a fixed sliding speed is inversely proportional. In other words, for both steel discs the decrease in wear rate is less abrupt as the given sliding speed grows.

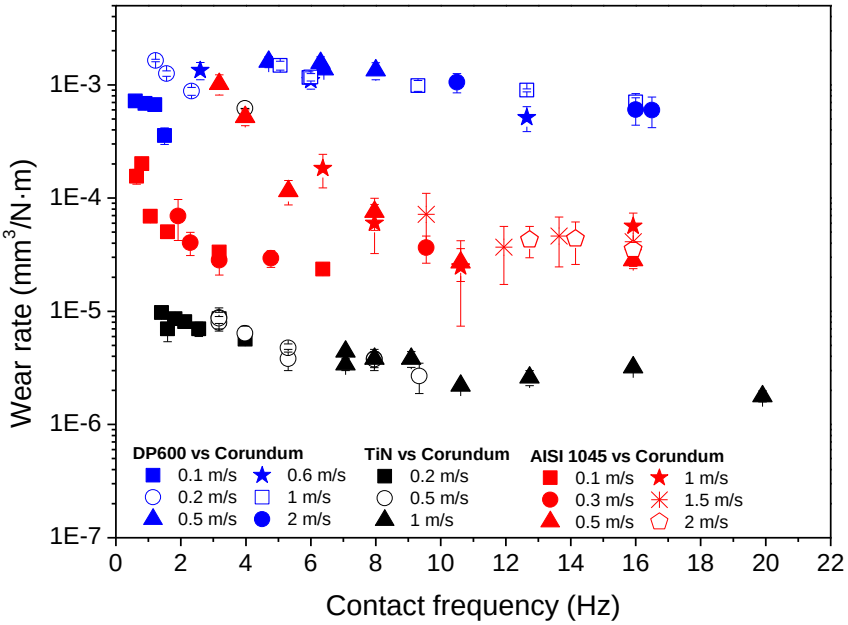

Figure 4.17 Composite plot of published wear rate data as a function of the contact frequency, and tested at different constant sliding speeds; DP600 steel discs vs Corundum balls (Ruiz-Andres et al., 2015b), TiN discs vs Corundum balls (Garcia et al., 2003), and AISI 1045 steel discs vs Corundum balls (Navas et al., 2006).

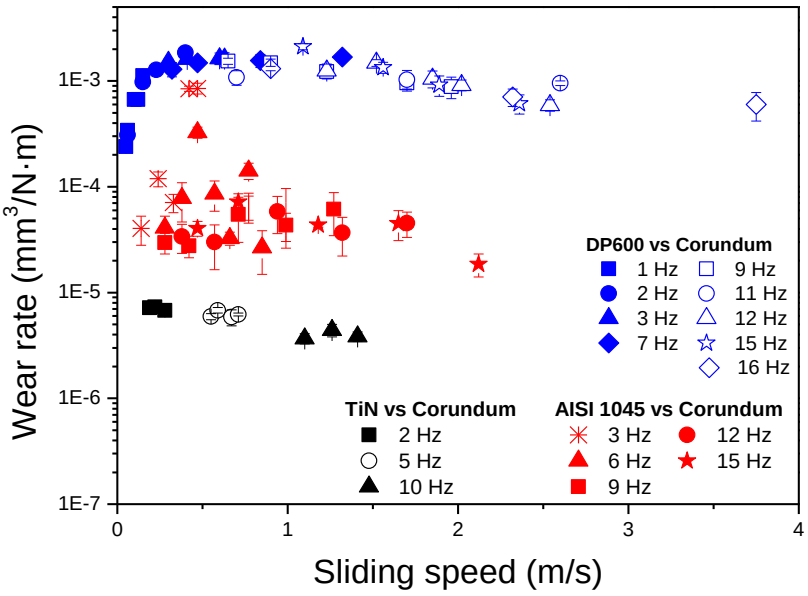

Figure 4.18 Composite plot of published wear rate as a function of the sliding speed, and tested at different constant contact frequencies; DP600 steel discs vs Corundum (Ruiz-Andres et al., 2015b), TiN-coated discs vs Corundum (Garcia et al., 2003), and AISI 1045 carbon steel discs (Navas et al., 2006).

Conversely, the wear behaviour as a function of sliding speed noticeably differs depending on the material tested (Figure 4.18). For DP600 steel discs, the wear rate initially increases with the sliding speed. Subsequently, at contact frequencies of 7 Hz, the wear rate behaves differently with increasing sliding speed. The wear rate gradually decreases as the sliding speed increases. Regarding AISI 1045 carbon steel discs, it can be observed that the wear rate a priori does not follow any relationship with the sliding speed. However, a more accurate survey of these results leads one to notice that at highest constant contact frequency tested, i.e. 15 Hz, the wear rate tends to decrease. Whilst, the wear rate of TiN-coated discs does not follow a clear tendency with the sliding speed.

4.6 Discussion

The prior results suggest that the contact frequency of the counterbody with a given part of the wear track on the disc seems indeed to be a key parameter affecting the COF and the wear rate.

In the present work, under sliding wear conditions, DP600 steel exhibits a mild oxidation wear, showing a change in the nature of the oxide grown during sliding as a function of sliding speed and contact frequency. The two main types of oxidised debris collected are Fe_2O_3 and Fe_3O_4. This variation in the iron oxide form is attributed to a significant change in the temperature (Hurricks, 1972, 1974). The oxide Fe_2O_3 retrieved is the expected oxide found when a low temperature below 450ºC is reached. Whilst, Fe_3O4 is an oxide usually found when the temperature range reached during sliding is between 450ºC and 600ºC (Quinn et al., 1980; Tyagi et al., 2002, 2004; Sullivan et al., 1980; Sullivan and Athwal, 1983). Kayaba et al. (1981) similarly supported these results by associating a reduction in the COF and the wear rate with increasing the temperature with the variation in the iron oxide from Fe_2O_3 to Fe_3O_4. Several authors (Clark et al., 1967; Foley et al., 1963) assumed that the diminishing in the COF and the wear rate at elevated temperatures is related to the formation of Fe_3O_4 which is thought to behave as a better solid lubricant than Fe_2O_3 due to its ability to adhere more strongly to the surface.

The demonstrated role of the contact frequency when studying the wear behaviour for a disc leads to the idea that the influence of the sliding speed on the type oxide grown is probably overshadowed by the contact frequency effect, due to its effect on the friction energy, and thus on the local contact temperature.

At this point it should be recalled that, as it is well-known in unidirectional pin-on-disc or ball-on-disc wear tests, the heat originated by friction contact at the pin/ball asperities is continuously generated due to these asperities are assumed to always be in contact with the disc asperities during the test. On the contrary, the frictional heat at the disc surface is only generated per rotation, i.e. during the time in contact time between the asperities from the disc and the counterbody. This frictional heat is generated at any point of the disc along the pin/ball trajectory and can be simulated as a square wave function (Garcia et al., 2003), where the frictional heat, q, per unit of nominal contact area, A_n, per second is defined as follows (Ahsby et al., 1991):

$$q = \frac{\mu F v}{A_r} \tag{4.8}$$

μ being the coefficient of friction, F the normal load, v the sliding speed, and A_r the real contact area.

When the pin/ball slides against the disc, the friction turns into heat at their interfaces, and also tends to flow through both bodies, in varying ways, depending on their thermal properties. The resulting rise in temperature make then modify the mechanical and metallurgical properties of the sliding surfaces, and it makes them oxidise, thus influencing the wear rate (Lim and Ashby, 1987).

It should be noticed that the literature is somewhat ambiguous on the application of Quinn's mild oxidation wear model in the case of unidirectional pin or ball-on-disc sliding wear tests. The contact conditions prevailing at the pin or ball surface, and at the disc surface are indeed different. At a macroscopic level, the pin or ball surface is in permanent contact with the disc during the sliding. Conversely, each segment of the wear track on the disc is only loaded for a limited time in between successive contact events. Therefore, the wear rate for a given material is thus different, depending on whether the material acts as disc or pin/ball material (Garcia et al., 2003).

Likewise, in Garcia-Ramil-Celis model, the elapsed time in between successive contact events is more important than the contact time duration for these events. Furthermore, the time required to reach the critical oxide thickness depends on the contact frequency, which is expressed as the inverse of the elapsed time in between two contacts at a given point.

The disagreement between the experimental and the fitting performed using Garcia-Ramil-Celis model above 7 Hz (Figure 4.15 (b)) may be related to the apparent contact frequency at a specific point of the wear track on the DP600 steel disc. In this work, therefore, it is assumed that the frictional heat at the disc surface is only generated during the contact time in between the asperities from the disc and the pin/ball, following a square wave function and depending on an inverse reciprocal relationship between the elapsed time and the contact frequency.

As the contact frequency increases, the elapsed time in between two successive frictional heat inputs notably decreases to such an extent, that the square wave function which describes the heat generated by friction, tends to convert into a type of constant linear function.

On account of this, by increasing the contact frequency, the elapsed time decreases during the contact intervals between the ball and a certain point of the disc. As the test

runs, a certain temperature, defined by a compromise between the constant energy input and the heat diffusion, is reached. As a result each point of the disc starts to heat up under a condition that becomes close to a continuous contact similar to the condition observed by the ball. At this point, the wear rate behaviour is more similar to the predicted behaviour in the Quinn's model for continuous sliding contact events of two bodies in frictional sliding movement, which is clearly observed in Figure 16, where the experimental data fit correctly with the theoretical data simulated via Quinn's model.

According to the wear rate comparison made amongst the published results for DP600, AISI 1045 and TiN-coated, it is reasonable to assume that the contact frequency must be considered as an operational wear parameter, regardless of the material tested. However, based on the material, the wear rate might be practically unaffected by the sliding speed. For both steel discs, it can be observed that there is a threshold value for contact frequency –different depending on the material disc- at which the wear rate stops to slide under discontinuous contact conditions with the sliding speed, and start to behave as a pin/ball in continuous sliding contact conditions. In other words, at a certain contact frequency the wear rate stops to increase with the sliding speed, and decreases.

4.7 Concluding Remarks

After studying the friction and wear behaviour of DP600 in unidirectional ball-on-disc test for discontinuous sliding contact conditions as a function of sliding speed and contact frequency, the following conclusion haven been established:

- The wear rate of DP600 steel discs relies not only on the sliding speed of the ball on the disc, but also on the contact frequency.
- The wear mechanism of the DP600 is mild oxidation wear. The nature of the iron oxide debris is a function of the sliding speed and the contact frequency. At low contact frequencies the predominant oxide is Fe_2O_3, while at high contact frequencies the oxide formed is mainly Fe_3O_4.
- The COF diminishes with the contact frequency and behaves distinctly with the sliding speed. Initially, the COF increases with the increase of the sliding speed, and then the COF decreases gradually with the increase of the sliding speed.
- The wear behaviour is complex. For the contact frequencies below 7 Hz, the wear mechanism suitably fit Garcia-Ramil-Celis model as a consequence of the

discontinuous sliding contacts. On the other hand, for contact frequencies above 7 Hz, the wear mechanism is visibly in concordance with Quinn's model.

- The contact frequency should be considered as an independent parameter, together with the contact load and the sliding speed, when wear features for materials that are subjected to discontinuous sliding contacts are tested and/or described.
- In pin/ball-on-disc wear tests, the pin/ball and the disc have to be considered differently. Consequently, this necessary distinction between the bodies of the tribological pair –pin/ball and disc- should always take into account whether the contact conditions are continuous and discontinuous due to the ball is in continuous contact with the disc, but conversely each given point of the disc wear track is in discontinuous contact with the ball.
- It is reasonable to assume that the contact frequency must be considered as an operational wear parameter, regardless of the material tested. However, based on the material, the wear rate might be practically unaffected by the sliding.

5

Analysis of the Contact Frequency on Reciprocating Sliding Wear Tests using the Energy Wear Approach

This chapter analyses the role of the contact frequency for DP600 steel specimens when wear tests are performed under reciprocating sliding using for the first time the energy wear approach.

For that, a set of bidirectional ball-on-plate tests were performed at a given constant sliding speed but at different contact frequencies by modifying the stroke length; and viceversa. In this sense, the sliding speed was varied between 0.01 and 0.25 m/s and the stroke length was ranged within an interval from 8.06 to 15.63 mm. Thus the contact frequency studied in the present work varied between 1 and 16 Hz.

5.1 Worn Surfaces and Wear Debris Characterisation

Considerable damage is produced on the DP600 steel plate specimens as shown in the SEM images corresponding to the wear tracks in Figure 5.1(a)-(b). These wear tracks correspond to tests performed at two representative combinations of low and high sliding speed and contact frequency respectively, namely 0.02 m/s / 2 Hz and 0.22 m/s / 16 Hz, which scan the entire range of values in all the experimental tests.

Visible surface deformation in the form of very smooth longitudinal grooves oriented in the back and forth sliding direction (SD), as well as apparently large oxidised plateau covering most of the area along the wear track is indicated in Figure 5.1(a). At the higher contact frequency and sliding speed (Figure 5.1(b)), the wear track damage is also characterised by smooth grooves which lay parallel to SD, and by some oxide scales extended through the surface. The main wear mechanism for DP600 steel at both contact frequencies and sliding speeds is thus oxidative wear due to the presence of oxide scales easily perceivable along the wear track.

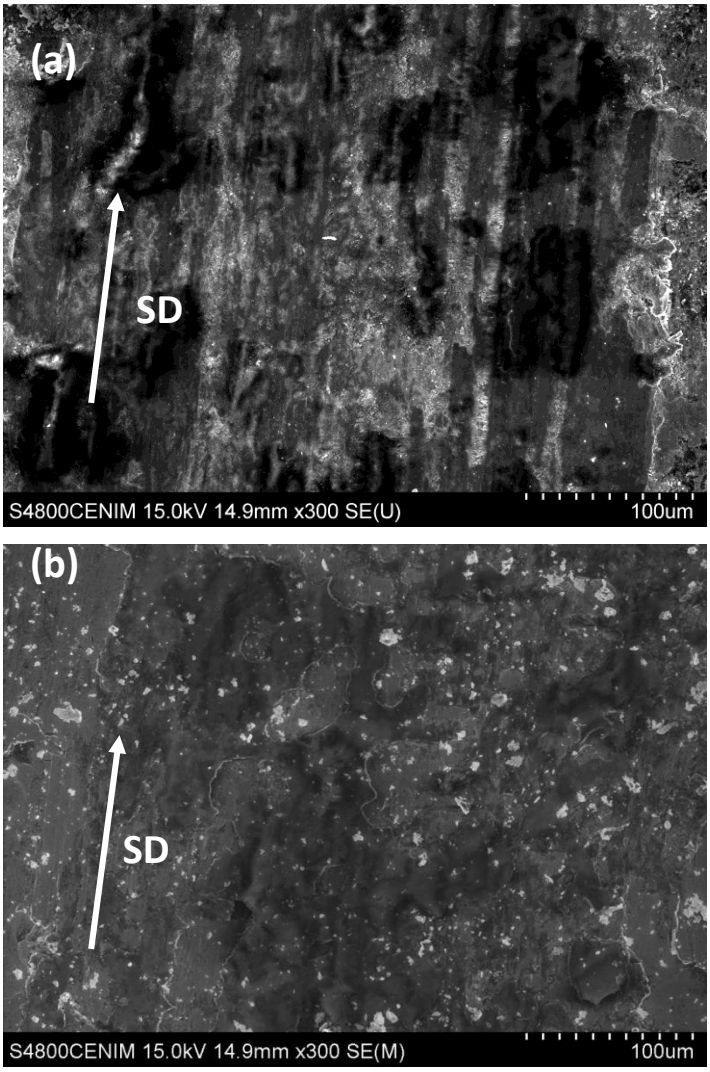

Figure 5.1 SEM images of wear tracks morphology on the DP600 steel plate specimen after sliding tests performed at a contact frequency of (a) 2 Hz and 0.02 m/s, and (b) 16 Hz and 0.22 m/s.

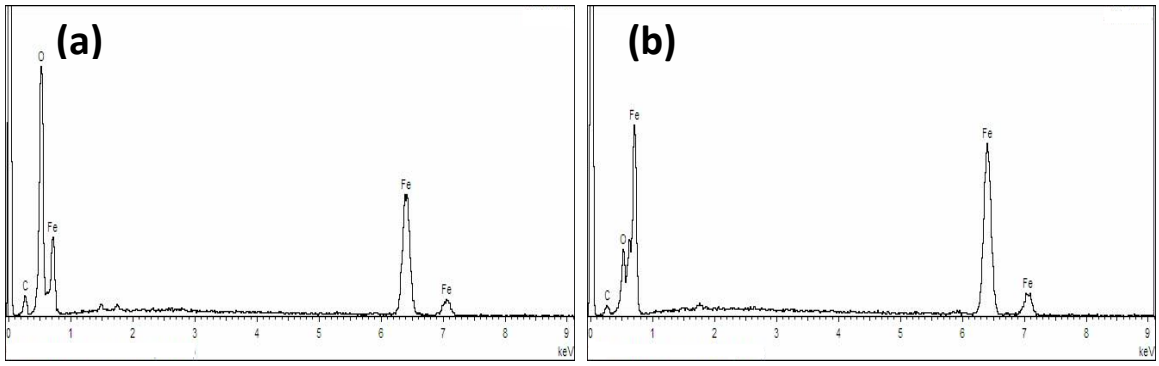

Figure 5.2 EDS spectra of the wear tracks on the DP600 steel plate specimen after sliding tests performed at a contact frequency of (a) 2 Hz and 0.02 m/s, and (b) 16 Hz and 0.22 m/s.

This predominant wear mechanism is confirmed from the EDS analyses. The EDS spectra of the worn areas shown in figure 1 are presented in Figue 5.2(a), 2 Hz and 0.02 m/s, and Figure 5.2(b), 16 Hz and 0.22 m/s. Both EDS analyses show the presence Fe, O and C species, indicating that the DP600 worn surfaces are thus oxidised after testing under these wear test conditions. However, differences in the oxygen content in both worn surfaces are perceivable. The amount of oxygen found along the wear track is higher at the lowest set of contact frequency and sliding speed analysed, whereas the oxidised areas thoroughly cover the track.

The wear debris retrieved during the reciprocating sliding has been also analysed. This debris was mainly collected from the outer edges of the wear track as in tests at 2 Hz and 0.02 m/s, but also appeared inside and along the wear path at 16 Hz and 0.22 m/s.

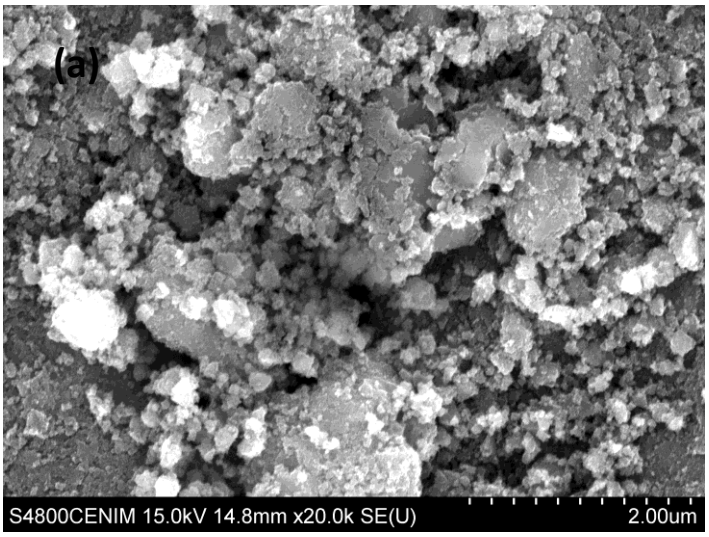

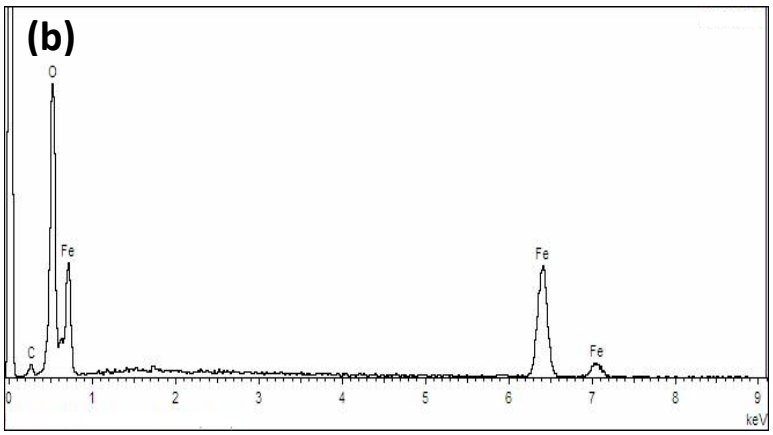

Figure 5.3 (a) SEM image and (c) EDS spectrum taken from debris collected after sliding tests performed at a contact frequency of 2 Hz and 0.02 m/s.

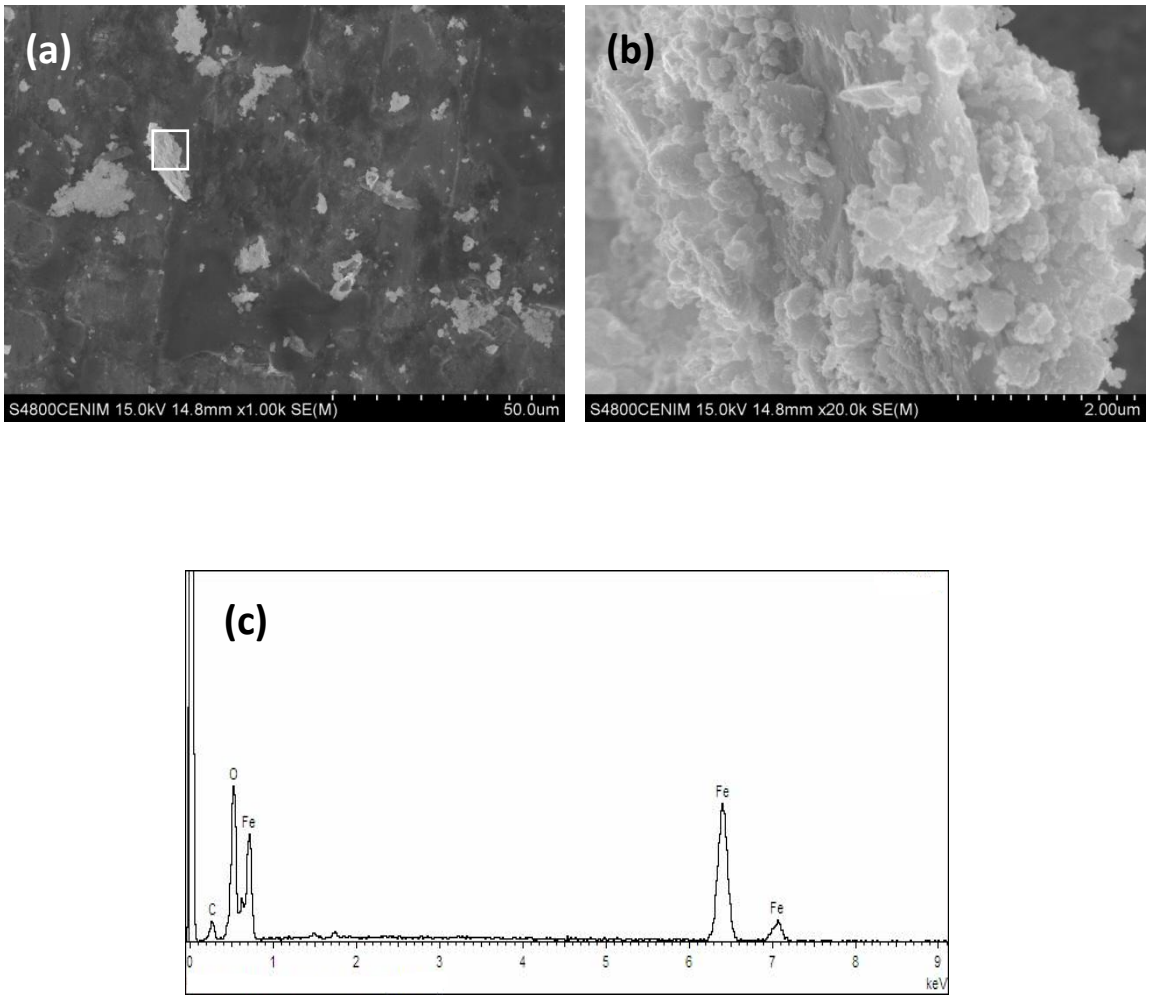

Figure 5.4 (a)-(b) SEM images and (c) EDS spectrum taken from debris collected after sliding tests performed at a contact frequency of 16 Hz and 0.22 m/s.

SEM images corresponding to the wear debris collected from these two different wear processes and their respective EDS spectra are displayed in Figures 5.3 and 5.4, respectively. The debris retrieved at 2 Hz and 0.02 m/s, Figure 5.3 (a), reveals irregular fine equiaxed-shaped fragmented particles which sizes vary approximately between 0.1 and 1.7 μm. The EDS spectrum of this debris (Figure 5.3 (b)) consists of Fe, O and C species, indicating the presence of oxidised compounds.

The examination of the wear particles at 16 Hz and 0.22 m/s (Figure 5.4 (a)) shows that the debris appearance is defined by irregular shaped particles of larger sizes. Higher magnifications (Figure 5.4 (b)) of the agglomerate inner structure reveal a compound of very fine particles (Zimitrowicz, 2005). These aggregates normally consist of milled debris and newly formed friction phases. The wear particles vary from 3 to 22 μm approximately. The EDS analysis also exhibits Fe, O and C species, which means that the presence of oxidised compounds is found.

In all these cases, therefore, the wear particles collected are iron oxides. However, it is clear the difference of oxygen content after testing at low and high contact frequencies and sliding speeds. The lower the contact frequency, the higher the oxygen content on the worn surfaces.

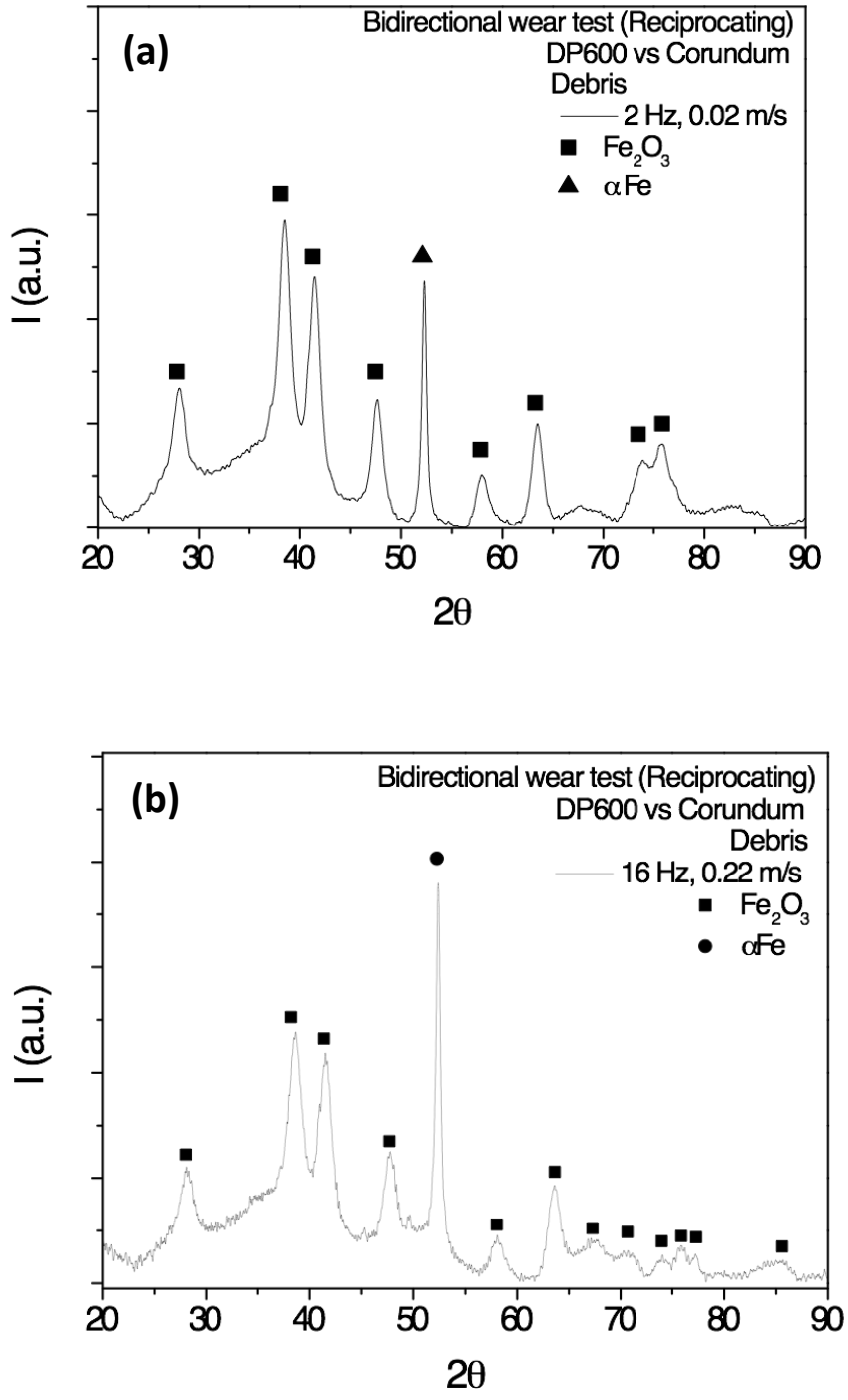

Figure 5.5 XRD diffractograms of debris generated after sliding tests performed at a contact frequency of (a) 2 Hz and 0.02 m/s, and (b) 16 Hz and 0.22 m/s.

Moreover, the XRD diffractograms (Figures 5.5 (a)-(b)) indicate that hematite (Fe_2O_3) and ferrite (αFe) are observed after testing at both contact frequency levels, i.e. 2 Hz and 0.02 m/s, and 16 Hz and 0.22 m/s. These results confirm, therefore, that oxidative wear is the main wear mechanism involved in these dry sliding wear tests.

Based on several works (Quinn et al., 1980; Sullivan et al., 1980), the nature of the iron oxide observed after dry sliding wear tests might be explained according to the basis of the sliding temperature. On low alloy steels, the type of oxidised wear debris collected after sliding were directly related to this temperature. The oxide which is mostly prevailed at temperatures below 450 ºC is Fe_2O_3. In a temperature range between 450 ºC and 600 ºC, Fe_3O_4 is mainly formed, whereas FeO is the predominant wear debris for temperatures greater than 600 ºC.

It is known that the frictional heating reached in the contact area facilitates atmospheric oxidation on the sliding surface when dry sliding wear at relatively low loads takes place. In this sense, due to the relatively low load, the range of sliding speeds, and contact frequencies applied in this work, it is reasonable to assume, in the present work, that the temperature reached at the contacts does not exceed 450ºC, which is in good agreement with those experimental results (Quinn et al., 1980; Sullivan et al., 1980; Tyagi et al., 2002, 2004; Sullivan and Athwal, 1983).

5.2 Effect of Contact Frequency and Sliding Speed on Coefficient of Friction

Some representative COF registration curves, resulting from reciprocating sliding tests between DP600 steel plate specimens and corundum balls, are plotted in Figure 5.6 as a function of the sliding time. Each curve represents the average of three performed wear tests. Two different wear stages, i.e. an early running-in stage followed by a state stage, can be easily distinguished.

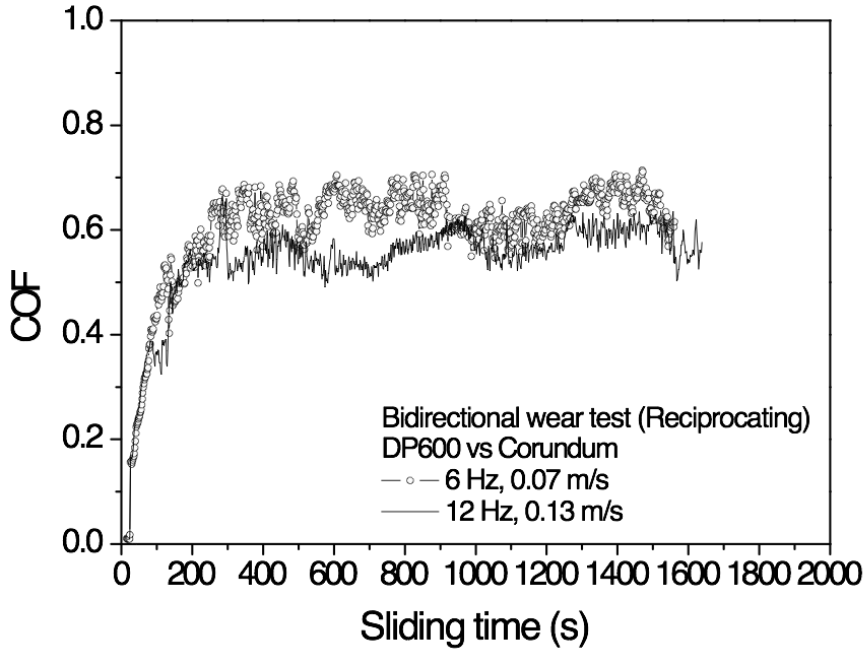

Figure 5.6 Representative coefficient of friction curves recorded between DP600 steel plate specimens sliding against corundum balls as a function of the sliding time.

During initial sliding contact, the friction level is high due to very restricted ball-on-plate contact areas (Bonny et al., 2010). The uncertainties that usually appear in the COF curves can be related to the continuous changes in the sliding contact surface, particularly during the running-in period. In fact, the initial friction contact is basically caused by considerable strong interactions between asperities.

As sliding proceeds, the roughness is smaller due to the initial asperities are worn down. Therefore, the interlocking friction component also decreases and the fluctuations in the friction curves diminish, indicating that an equilibrium stage has been reached (Bonny et al., 2010).

It should be here noticed that in the running-in stage a sharp increase (less than 5% of the sliding time) is observed. In the following discussion, the running-in effect on the COF determination is not taken into account. Therefore, the COF values were calculated by summing up and averaging the values for the steady state friction period.

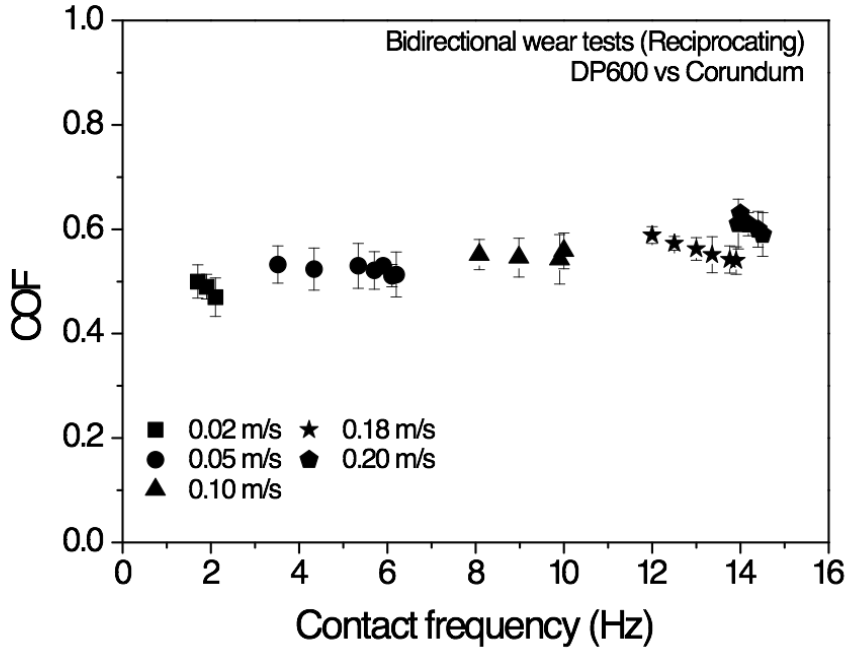

Figure 5.7 Coefficient of friction recorded between DP600 steel plate specimens sliding against corundum balls as a function of the contact frequency at five fixed sliding speeds.

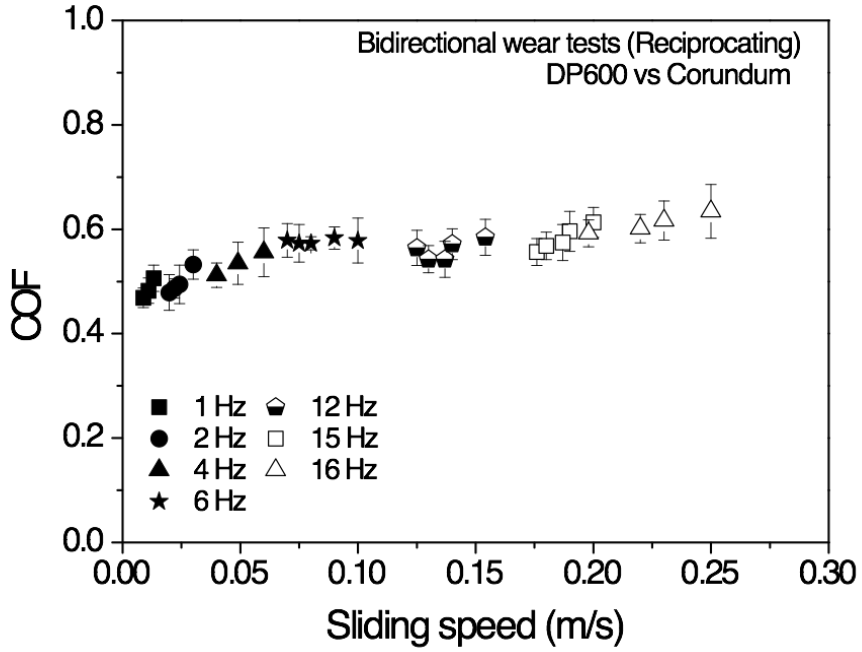

Figure 5.8 Coefficient of friction recorded between DP600 steel plate specimens sliding against corundum balls as a function of the sliding speed at seven fixed contact frequencies.

The COF behaviour, along with the contact frequency for a set of five fixed sliding speeds, between 0.02 and 0.20 m/s, is given in Figure 5.7. For each given sliding speed, the COF slightly decreases as the contact frequency increases. This diminution is more significant at the highest fixed sliding speeds tested, i.e at 0.18 m/s, the COF values is reduced from from 0.59 to 0.54 when contact frequency increases from 12 to 13.9 Hz.

Moreover, Figue 5.8 shows the COF as a function of the sliding speed, at seven fixed contact frequencies between 1 and 16 Hz. It is found that the COF mildly increases with increased sliding speed for each fixed contact frequency. This might be a probable response of the wear particles entrapped between the bodies during sliding. Specifically, the COF values exhibit a smaller variation -from 0.57 to 0.58- during the test at 6 Hz compared to the COF values at 15 Hz, which increases from 0.56 to 0.61.

5.3 Effect of Contact Frequency and Sliding Speed on Wear Rate

As known in ball-on-plate tests, the three operational parameters, namely sliding speed, contact frequency, and stroke length are linked as indicated in Equation 3.1 (see Section 3.2.2.1). Two of these parameters are independent, and the other is thus not significant in the wear rate study.

In an attempt to clarify the possible combined role of contact frequency and sliding speed on the DP600 steel plate specimens, the contact frequency was chosen as a constant when performing tests at different sliding speeds, and vice versa. By not taking this into account, a change in the sliding speed causes a variation in the contact frequency. Consequently, it is then not possible to distinguish the effect of the sliding speed and contact frequency on the wear rate for the plate specimen material.

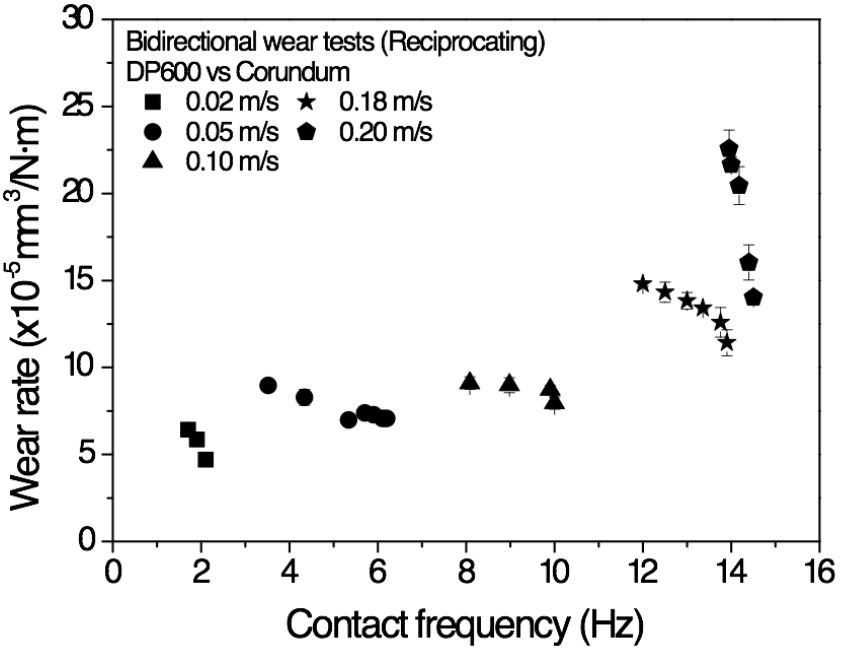

Figure 5.9 Wear rate of DP600 steel plate specimens sliding against corundum balls as a function of the contact frequency at five fixed sliding speeds.

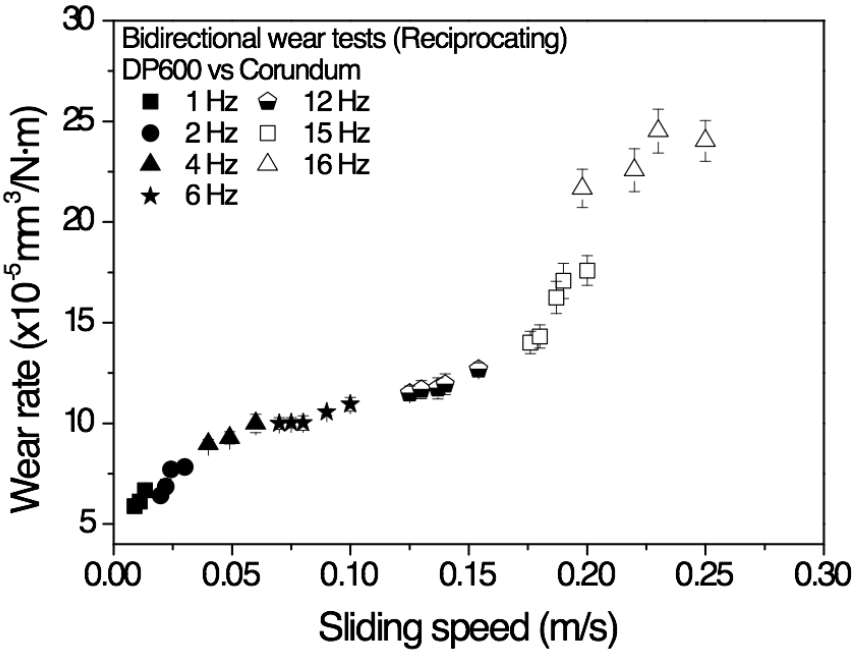

Figure 5.10 Wear rate of DP600 steel plate specimens sliding against corundum balls as a function of the sliding speed at seven fixed contact frequencies.

Figure 5.9 shows an inversely proportional relationship between the wear rate and the contact frequency which recurs for each single set of steady sliding speed data measured. It is also easily perceivable that the wear rate values are greater as the constant sliding speed values increase. At 0.02 m/s, the wear rate ranges from $6.42 \cdot 10^{-5}$ to $4.72 \cdot 10^{-5}$ $mm^3/N \cdot m$. Whilst, at 0.2 m/s the wear rate values vary between $2.17 \cdot 10^{-4}$ and $1.40 \cdot 10^{-4}$ $mm^3/N \cdot m$, noticeably higher results –in one order of magnitude- than the values obtained at 0.02m/s.

On the other hand, the dependence of the wear rate with the sliding speed at seven fixed contact frequencies is depicted in Figure 5.10. The higher the sliding speed, the higher the wear rate. However, the wear rate behaves slightly differently with regard to the fixed contact frequency tested.

Initially, for fixed contact frequencies from 1 to 6 Hz, the wear rate increases very steadily, concurrently with the sliding speed, varying between $5.89 \cdot 10^{-5}$ and $1.19 \cdot 10^{-4}$ $mm^3/N \cdot m$. At 12 Hz, a transition in the wear rate evolution is easily observed. At steady contact frequencies of 15 Hz or above, the gradually rising trend of wear rate as the

sliding speed increases changes drastically, the increase in the wear rate being much more abrupt. In this case, the wear rate varies from $1.40 \cdot 10^{-4}$ to $2.40 \cdot 10^{-4}$ $mm^3/N \cdot m$.

It can be observed that the wear rate depends on the sliding speed although it does definitely not follow an inverse reciprocal relationship as one might expect from Quinn's model for oxidative wear (Quinn, 1992, 1994, 1998) when the ball under continuous contact conditions is the body analysed.

Therefore, these results, corresponding to the contact frequency and sliding speed dependence with the wear rate, highlight the importance of taking into account the mode of contact conditions -continuous or discontinuous- in dry sliding wear tests.

As aforementioned, the Equation 3.1 (shown in Section 3.2.2.1) directly relates the sliding speed and the contact frequency by adjusting the stroke length, i.e. the length of the wear track, $f \cdot s$. Thus, a given total sliding length leads to a different number of cycles as a function of the stroke length. In other words, for a given sliding distance the ball passes a different number of times over each point on the track depending on the wear stroke length. Consequently, one might think that the number of cycles or number of interactions between the ball and each point of the wear track can be a possible parameter which determines the wear rate along the total sliding distance. In order to clarify that effect, it may be thus interesting to calculate the wear rate as the wear volume loss per unit contact load and per number of cycles.

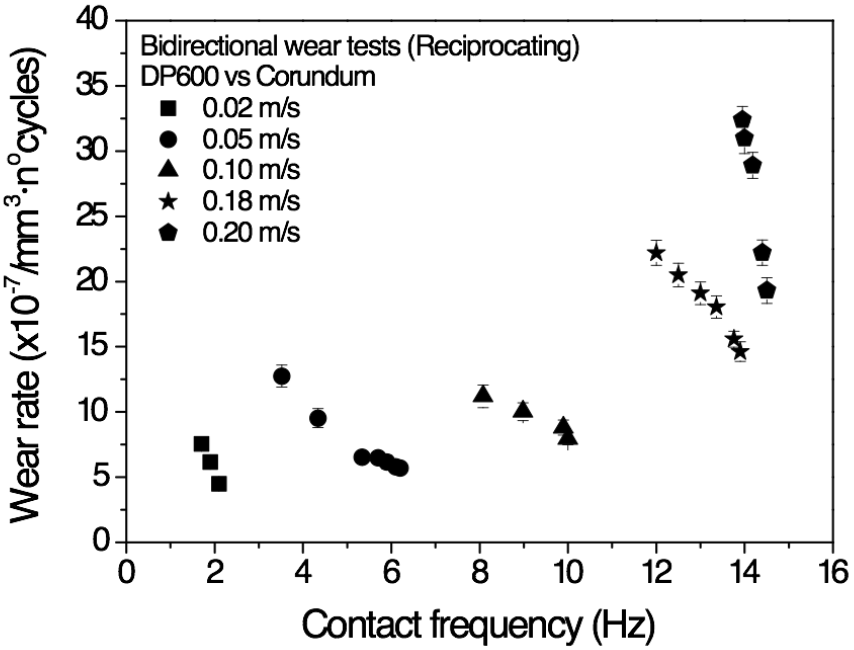

Figure 5.11 Representation of wear rate of DP600 steel plates, measured as the volume wear loss per unit load and number of cycles, sliding against corundum balls as a function of the contact frequency at five fixed sliding speeds.

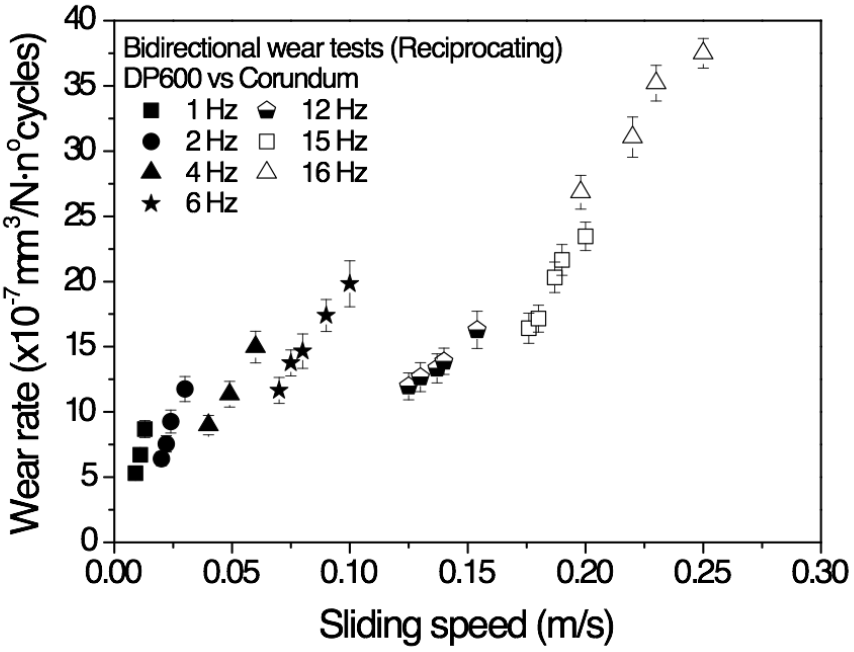

Figure 5.12 Representation of wear rate of DP600 steel plates, measured as the volume wear loss per unit load and number of cycles, sliding against corundum balls as a function of the sliding speed at seven fixed contact frequencies.

Therefore, the wear rate measured as the volume wear loss per unit load and number of cycles is presented in Figure 5.11. The wear rate behaviour as a function of the contact frequency exhibits similar trends to the values in Figure.5.9. At each fixed sliding speed tested, the wear rate diminishes with the contact frequency. Likewise, Figure 5.12 gathers the wear rate values plotted as a function of the sliding speed and conducted at fixed contact frequencies. The wear rate, as occurs in Figure 5.10, also increases with increasing the sliding speed.

Consequently, the wear rate appears to depend on the contact frequency and the sliding speed. However, it does not rely on the number of cycles, i.e. on the wear stroke length.

5.4 Discussion

The dominant wear mechanism which mainly takes place in the tests performed is the oxidative wear. The worn surfaces of the DP600 steel plate specimens are partially oxidised (Figures 5.1 and 5.2) within the entire range of contact frequency and sliding speed tested. In all these cases, Fe_2O_3 is only the wear particles detected in the debris

collected. However, certain differences related to size, the morphology and/or the ratio of iron to oxygen in the oxide have been found during these performed tests (Figures 3 and 4).

Oxidative wear proceeds by gradual material removal due to the growth and delamination of a surface oxide layer generated in the wear track as a result of mechanical, chemical, and thermal interaction between the tribocouple asperities (Williams, 2005).

The friction phenomenon is very sensitive to changes in sliding conditions (Kuwahara and Masumoto, 1980). Additionally, the friction dissipation actives the wear mechanisms due to the specific flow involving debris formation and debris ejection (Fouvry et al., 2007). The presence of debris implies modifications of the COF and the wear rate (Jiang et al., 1998). The COF evolution is reflected by the wear particles features such as their morphology, size, and also by their generated quantity and distribution.

In order to correlate the coefficient of friction in the wear analysis, the wear volume is compared with the accumulated friction work (Mohrbacher et al., 1995; Fouvry et al., 2003; Fouvry and Kapsa, 2001) which has been dissipated through the interface at the contact area.

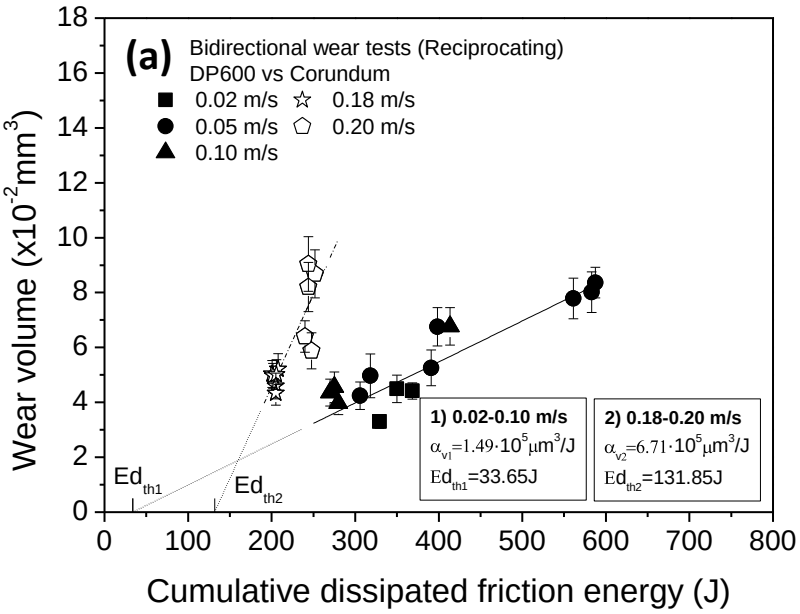

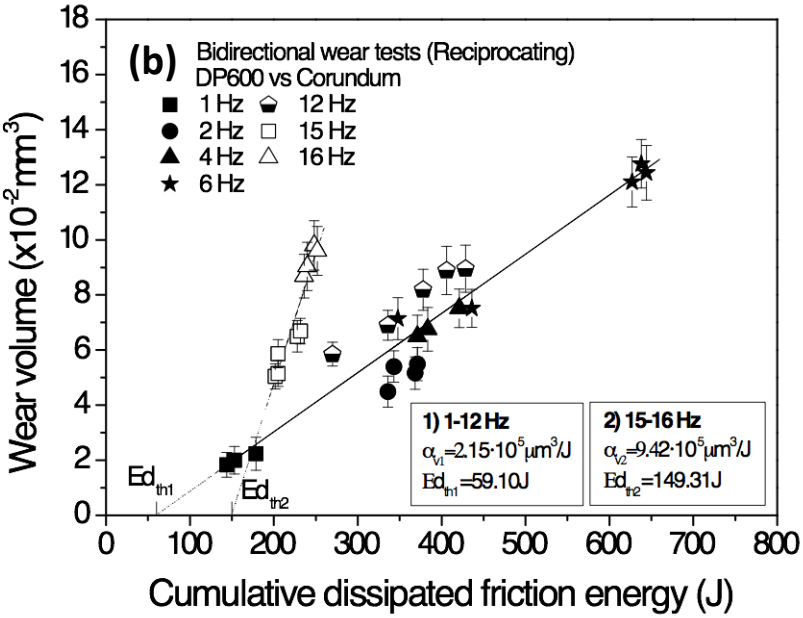

Figure 5.13 Volumetric wear of DP600 steel plate specimen plotted as a function of the cumulative dissipated friction energy. (a) At five fixed sliding speeds (0.02-0.2 m/s). (b) At seven fixed contact frequencies (1-16 Hz).

The wear volume loss evolution for the DP600 steel plate specimens is plotted as a function of the cumulative dissipated friction energy (Figure 5.13). This dissipated energy corresponds to the accumulated energy obtained as a result of the sum of the

reciprocating cycle area. The results are presented in Figure 5.13(a), tested at five fixed sliding speeds, and in Figure 5.13(b), at seven fixed contact frequencies.

In both cases, it is noticed visibly that under the chosen conditions the wear volume exhibits a linear relationship with the dissipated energy, in which two different energy wear coefficient, α_v, are easily appreciated. In other words, the wear volume can be reasonably fitted by two linear lines with distinct slopes as indicated in each case in Figure 5.13.

The results strongly rely on the operational parameters applied, i.e. the contact frequency and the sliding speed. The slope, α_v, corresponding to the tests performed at the fixed sliding speed between 0.02 and 0.10 m/s (solid line, Figure 5.13 (a)), is approximately $1.49 \cdot 10^5$ $\mu m^3/J$. This directly proportional factor is, in turn, around four and a half times lower than that factor calculated after the tests conducted at 0.18 and 0.20 m/s (dashed line), which is $6.71 \cdot 10^5$ $\mu m^3/J$.

This similarly occurs when the tests are carried out at fixed contact frequencies (Figure 5.13 (b)). The results plotted present linearity but they do not fit to the same trend. From tests conducted between 1 and 12 Hz (solid line), the α_v value obtained is approximately $2.15 \cdot 10^5$ $\mu m^3/J$. This slope is thus around four times lower than that calculated for contact frequencies of 15 Hz or above (dashed line), which is around $9.42 \cdot 10^5$ $\mu m^3/J$.

The changes in the wear volume (i.e. differing slopes, α_v) closely coincide with the variation observed in the wear rate plots measured as a function of the contact frequency (Figure 5.10), where the wear rate is an order of magnitude higher for tests at 0.18-0.20 m/s, and as a function of the sliding speed (Figure 5.11), with an increasingly steep wear rate from 15 Hz onwards.

These results, therefore, show once again that the wear for DP600 steel plate specimens under discontinuous contact conditions is a complex process which depends not only on the normal load applied and the sliding speed, but also on the contact frequency.

At this point, a molar analysis should be taken into account in order to extent the energy balance analysis of the wear behavior and consequently, to compare the results with other thermodynamical variables (Fouvry and Kapsa, 2001). The energy wear coefficient can be thus expressed in terms of molar energy wear (J/mol), as leads to as follows:

$$\varphi_{mol} = M/\alpha_v \rho \quad (5.1)$$

where M is the molar weight (around 56 g/mol) and ρ the density ($7.31 \cdot 10^{-3}$ g/mm3 approximately).

The α_v values previously calculated correspond to a molar energy of 51.4 MJ/mol for tests conducted from 0.02 to 0.10 m/s, and 11.4 MJ/mol, for tests at 0.18 and 0.20 m/s. Likewise, the α_v values correspond to tests measured between 1 and 12 Hz present a molar energy value of 35.6 MJ/mol. For tests conducted at 15-16Hz, the molar energy is 8.13 MJ/mol. These results confirm that a large quantity of energy needs to be dissipated to generate a relatively small quantity of wear.

The calculation of the activation energy, E_a, is very sensitive to the temperature reached during rubbing at the interface. However, different studies on steels have determined activation energies values as a function of specific temperature ranges. From 400 to 450ºC, where only Fe_2O_3 is formed, the activation energy is assumed to be 243 kJ/mol approximately (Molgaard and Srivastava, 1977). Therefore, it is pointed out that much more energy is dissipated at the interface contact than the energy necessary to activate the oxidation of the DP600 steel. Moreover, the energy ratio, φ_{mol}/E_a, indicates that less than 0.1% of the dissipated energy participates in the oxidation process.

It can be also observed that none of the linear approximations cross the origin and they present different shifts along the energy axis. This behavior normally occurs for metallic materials (Fouvry et al., 2003) and is related to the threshold dissipated energy, Ed_{th}. The Ed_{th} values (Figures 5.13(a) and (b)) indicate the required energy to activate the different processes involved in the wear processes, such as the mechanical and tribochemical transformation, third body approach (Sauger et al., 2000), and the thermal phenomena.

The varying linear relationships exhibited in Figure 5.13 (i.e. distinct α_v values) imply that the same wear mechanism is not operative during testing even though the wear track and the collected debris indicate a mild oxidative wear behaviour for the entire range of parameters studied.

As aforementioned, the oxidation process consumes a low quantity of the total energy which is dissipated in the interface. It is, therefore, reasonable to assume that the differences related to the size, morphology, and the ratio of iron to oxygen observed in

the oxidised debris play an important role in the wear damage. These differences may likely be, in turn, caused by the flash temperature rise at the interface, since it could contribute to a modification in the rheology or composition of the oxidised layer and thus, to the debris generated within the tribocouple.

It is assumed that the frictional heat at the disc surface is only generated during the contact time in between the asperities from the specimen and the ball during discontinuous sliding contact conditions (Garcia et al., 2003), by depending on an inverse reciprocal relationship between the elapsed time and the contact frequency.

5.5. Concluding Remarks

The conclusions drawn of the analysis of the contact frequency effect in DP600 steel specimens using the energy wear approach when specimens are subjected to reciprocating sliding wear tests are listed below:

- The COF and the wear rate of the DP600 steel plate specimens depend not only on the sliding speed of the ball on the plate specimen, but also on the contact frequency, in which each part of the wear track trajectory on the plate specimen comes into contact with the counterbody.
- The wear mechanism which takes place during sliding in bidirectional reciprocating wear tests is oxidative wear. Induced changes in the nature of the iron oxide as a function of the sliding speed and the contact frequency have not taken place. Only Fe_2O_3 is obtained after testing,which indicates that the tribosystem does not presumably exceed a temperature of 450ºC in the contact area.
- A peculiar influence of the contact frequency in ball-on-plate tests is exhibited when the plate specimen is studied. A visible inversely proportional relationship between the wear rate and the contact frequency for each set of steady sliding speed data measured is observed. This tendency recurs even for each fixed sliding speed tested.
- For fixed contact frequencies from 1 to 12 Hz, the wear rate increases very steadily concurrently with the sliding speed. At 15 Hz or above, the gradually rising trend of wear rate as the sliding speed increases changes drastically, being the increase in the wear rate much more abrupt.

- The wear rate behaviour -the wear volume as a function of the cumulative dissipated friction energy- shows a directly linear relationship with the dissipated energy. The results reveal that the oxidation process does not consume a considerable quantity of energy during testing. The heat generation at the interface is, however, concluded from the importance in characterising the wear behavior of the tribosystem as it could contribute to a modification in the rheology or composition of the oxidised layer and thus, to the debris generated within the tribocouple.
- The contact frequency for DP600 steel discs is an independent parameter together with the contact load and the sliding speed, when wear features for materials subjected to discontinuous sliding contacts are tested and/or described in bidirectional wear tests.

6

Influence of Sliding Direction Changes, Contact Frequency, and Bauschinger Effect on the Wear of DP600 Steel

In this chapter, the influence of sliding direction changes on wear behaviour for DP600 steel discs is discussed. Several authors (Tang et al., 2011a, 2011b; Harea et al., 2013; Wu et al., 1999) addressed that there is a remarkable difference in the wear rate on the pin/ball when the sliding direction varies. They also reported that this result is attributed to the Bauschinger effect (BE) that can take place during wear tests on the materials tested. However, to the author's best knowledge, no other works have reported on the responses of disc materials after a changeable wear sliding direction. For that reason, it is also interestintg to analyse how contact frequency (see Chapter 4 and 5), and others factors such as hardness affect the friction and wear rate of DP600 steel discs in those changeable sliding direction wear tests.

These wear tests were conducted under both unidirectional and bidirectional motion by taking into account the cyclic number, CN, proposed by Tang et al. (2011a). Such CN indicates how often the rotation direction of the disc is reversed. The unidirectional sliding is thus represented by CN=0. For bidirectional wear tests, i.e. CN≠0, the rotating direction was continuously varied after a fixed number of rotations as follows: CN=2, 5, 10, 20, 50. In order to indenpendently study the effect of linear sliding speed, and contact frequency on the wear rate for the DP600 discs sliding against corundum balls, a series of ball-on-disc wear tests was conducted at a given constant sliding speed, but at different rotation speeds, by modifying the wear track diameter to adjust the Equation 1.6 (see Section 1.2.5), and viceversa. In this sense, the sliding speed was varied

between 0.5 and 1.25 m/s. The contact frequency studied in the present work varied between 3.5 and 8.5 Hz.

6.1 Effect of the Cyclic Number on Coefficient of Friction

The COF dependence on the CN for the DP600 steel discs at a fixed contact frequency of 4.50 Hz, within a sliding speed range between 0.5 and 1.25 m/s is shown in Figure 6.1. For each sliding speed, the friction under unidirectional sliding (CN=0) is slightly higher than the friction obtained under bidirectional wear conditions (CN≠0).

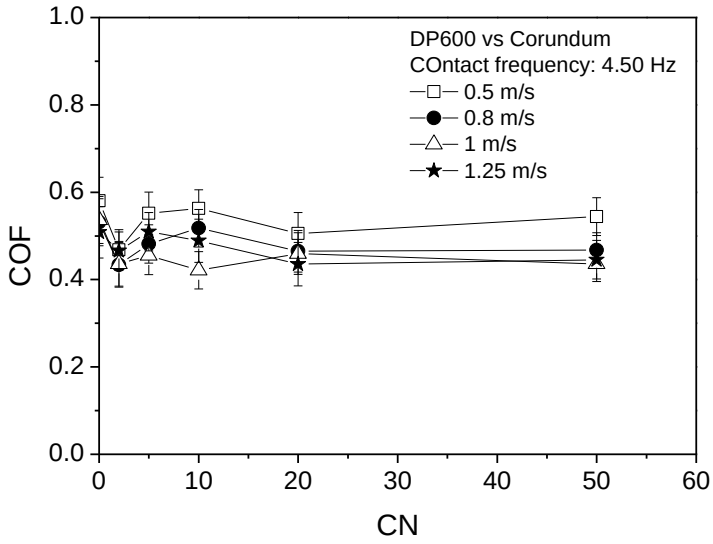

Figure 6.1 COF dependence on CN for tests measured at a fixed contact frequency value of 4.50 Hz within a sliding speed range of 0.5-1.25 m/s.

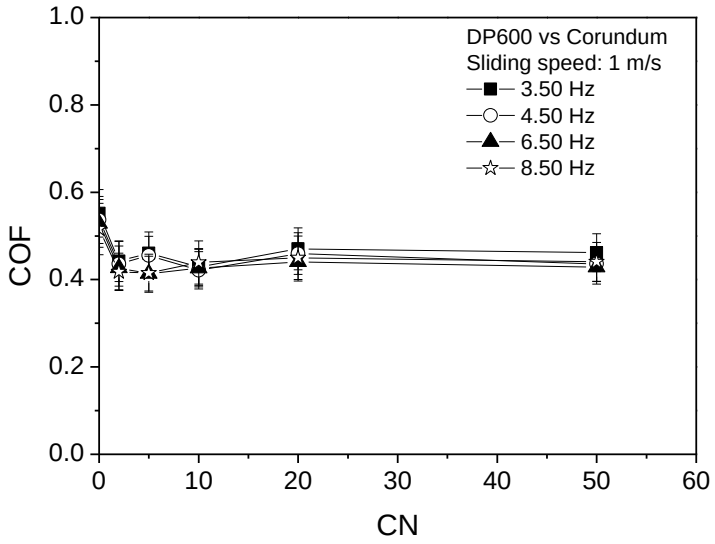

Figure 6.2 COF dependence on CN for tests measured at a constant sliding speed value of 1 m/s within a contact frequency range of 3.5-8.5 Hz.

On the other hand, the COF behaviour as a function of the CN measured at a fixed sliding speed of 1 m/s, within a contact frequency interval which varies from 3.50 to 8.50 Hz, is gathered in Figure 6.2. Once again, it can be observed that the friction is higher for tests performed at CN=0 than tests in CN ≠0 wear configuration. During testing in bidirectional sliding, the COF remains almost invariable regardless of the CN and contact frequency. The COF values average 0.53 approximately in tests conducted at CN=0. For CN≠0 wear tests, the COF varies from 0.47 to 0.41.

6.2 Effect of the Cyclic Number on Wear Rate

The wear rate evolution with the CN for DP600 steel discs, at 4.50 Hz and in a sliding speed interval of 0.5-1.25 m/s is presented in Figure 6.3. It can be easily observed that the material loss at CN=0 is higher than that after sliding at CN ≠0. The wear rate abruptly decreases until CN reaches a value around CN=5. The wear rate therefore tends to decrease gradually. It similarly occurs for each sliding speed analysed. For the lowest sliding speed analysed (i.e. 0.5 m/s), the wear rate values ranges between $7.65 \cdot 10^{-4}$ $mm^3/N \cdot m$ (CN=0) and $1.82 \cdot 10^{-4}$ $mm^3/N \cdot m$ (CN=50). In the case of the highest sliding speed tested (1.25 m/s), for instance, the wear rate varies from $17.2 \cdot 10^{-4}$ $mm^3/N \cdot m$ (CN=0) to $4.53 \cdot 10^{-4}$ $mm^3/N \cdot m$ (CN=50). In addition, it is possible to

distinguish from Figure 6.3 that the higher the sliding speed tested the higher the material loss, regardless of the CN.

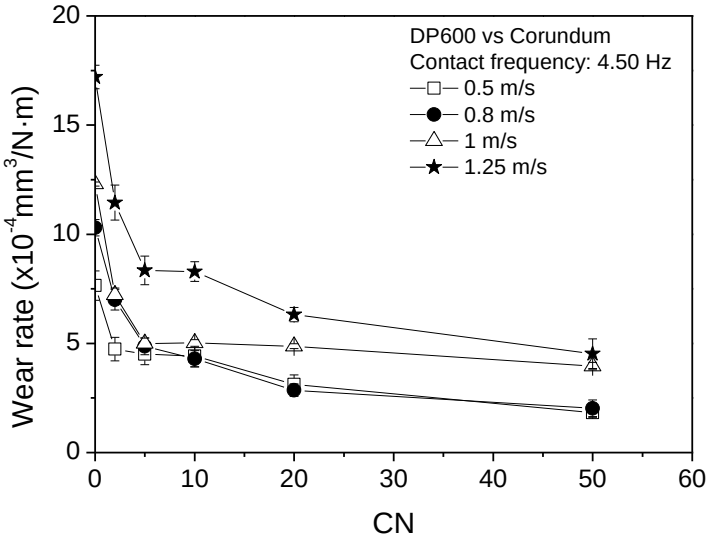

Figure 6.3 Wear rate as a function of CN for tests measured at a fixed contact frequency value of 4.50 Hz within a sliding speed range of 0.5-1.25 m/s.

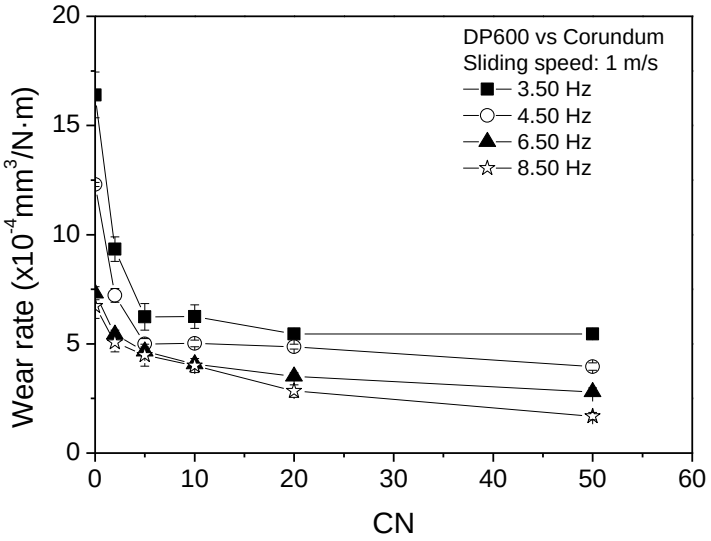

Figure 6.4 Wear rate versus CN for tests measured at a constant sliding speed value of 1 m/s within a contact frequency range of 3.5-8.5 Hz.

Conversely, Figure 6.4 shows the wear rate as a function of the CN measured after testing at 1 m/s and by applying a contact frequency range between 3.50 and 8.50 Hz. In this case, the results obtained at CN=0 are also substantially higher than the results for

tests carried out at CN ≠0. In general, the wear rate steeply decreases as the CN increases, and becomes relatively stable from CN=5 onwards. At low contact frequencies, e.g. 3.50 Hz, the difference between the wear damage measured at CN=0 and CN=50 vary from $16.4 \cdot 10^{-4}$ to $5.45 \cdot 10^{-4}$ $mm^3/N \cdot m$. For tests conducted at 8.50 Hz, wear rate drops from $6.73 \cdot 10^{-4}$ to $1.69 \cdot 10^{-4}$ $mm^3/N \cdot m$. It can be also noticed that the higher the contact frequency the lower the wear rate.

6.3 Effect of the Cyclic Number on Hardness

Figure 6.5 plots the hardness behaviour of the DP600 steel cross-sectional worn surfaces as a function of CN for a representative curve measured at a wear process featured by 1 m/s and 4.50 Hz. After an initial rise, which takes place from CN=0 to CN=5, the hardness of the worn surface decreases as CN increases. Furthermore, from CN=5 onwards, a softening of the strain-hardening effect in the DP600 steel is increasingly apparent with the increase of the wear direction reversal passes. Despite the significant diminishing in hardness as the sliding direction is reversed, the DP600 steel worn surfaces are still harder than the original surface alloy, i.e. 230 HV.

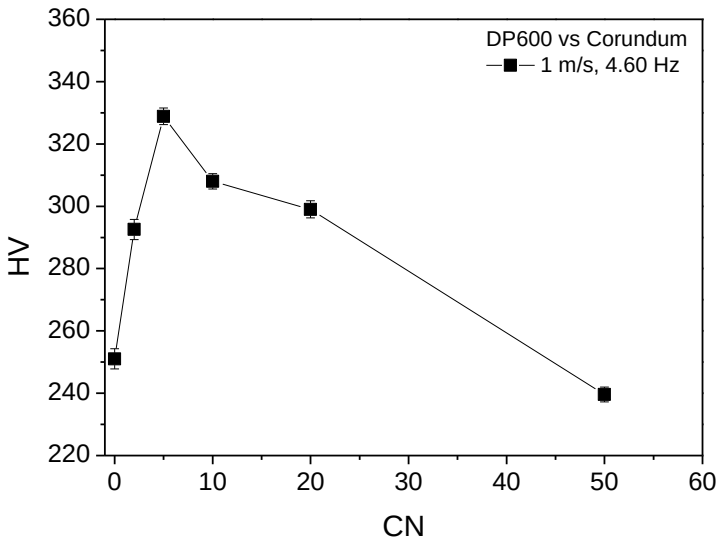

Figure 6.5 Hardness effect on CN for wear caused in tests at 4.5 Hz and 1 m/s.

6.4 Worn Surfaces Characterisation

SEM images and their EDS microanalysis of the DP600 steel discs sliding against corundum balls at 1 m/s and 4.50 Hz are displayed in Figures 6.6 and 6.7, respectively, after testing at CN=0, CN=5, and CN=50. The worn surface corresponding to CN=0 (Figure 6.6(a)) exhibits clearly defined grooves parallel to the sliding direction (SD), wear particles aggregates, and also larger oxidised scales along the wear track. In Figure 6.6 (b), for tests performed at CN=5, these same features are also identified but they appeared to be weaker. Wear damage under bidirectional motion is, then, characterised by the formation of smoother worn surfaces and also by oxidised areas which cover partially the wear track. A completely distinct image is, however, shown in Figure 6.6 (c) for wear tests after CN=50. In this case, the compacted oxide layer (O) almost covers the entire surface of the wear track, whereas significant areas of exposed metal (M) are also visible. The material removed might be related to severe plastic deformation which, in turn, leads to a breaking and fragmentation of the oxide film. The cracks are primarily found on the boundaries of the fragments.

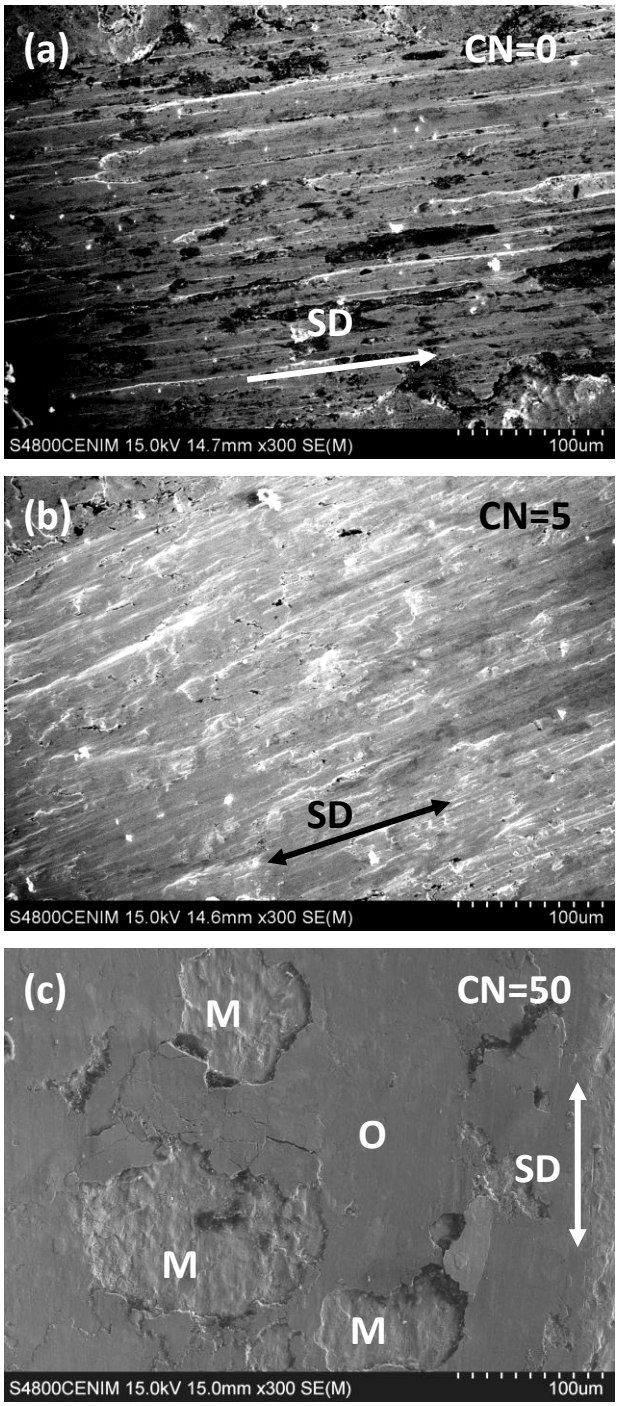

Figure 6.6 SEM images of wear tracks morphology on the disc after sliding tests performed at 4.5 Hz and 1 m/s for (a) CN=0, (b) CN=5, and (c) CN=50.

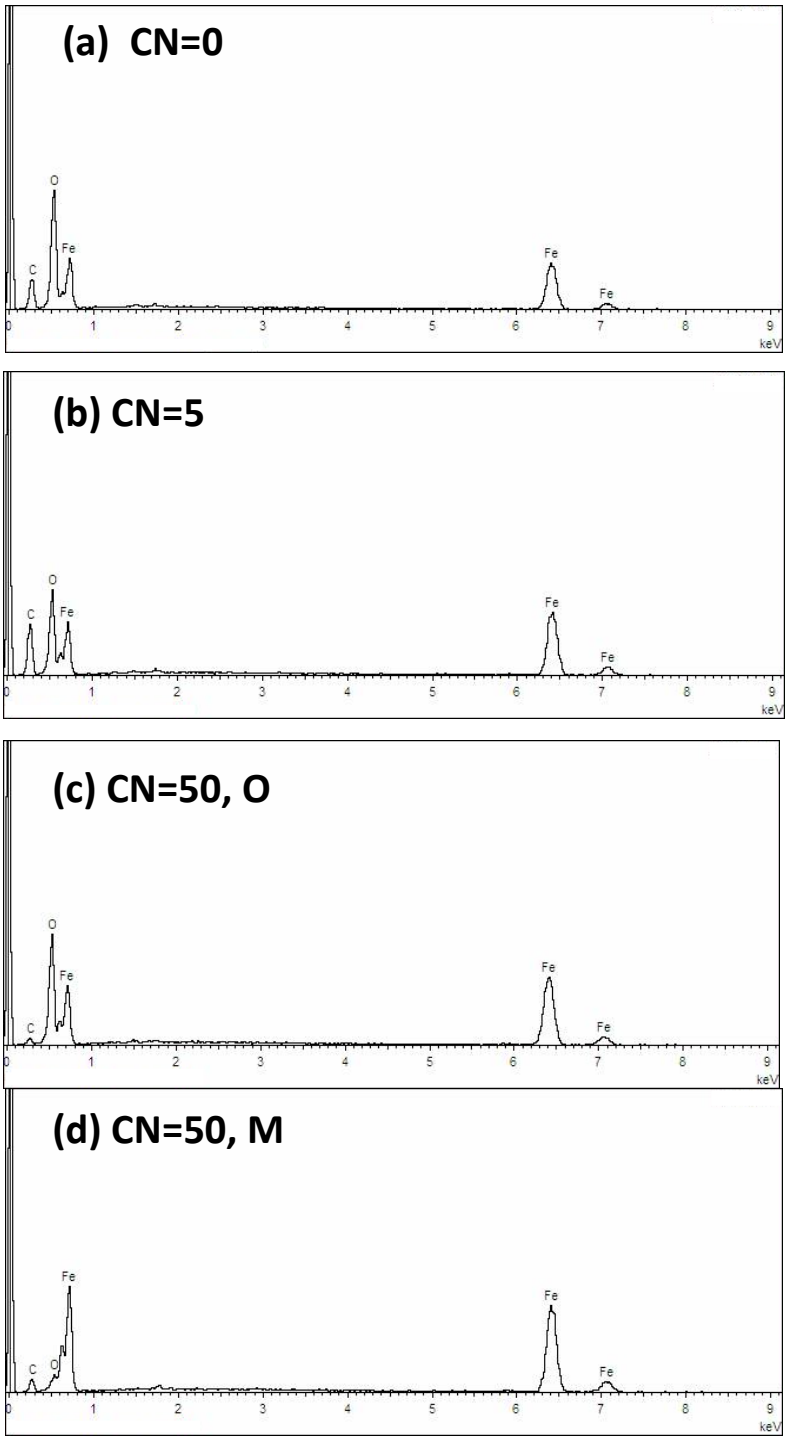

Figure 6.7 EDS spectra of wear tracks on the disc after sliding tests performed at 4.5 Hz and 1 m/s for (a) CN=0, (b) CN=5, (c) CN=50 (O), and (d) CN=50 (M) .

The EDS analysis of the worn surface after testing under unidirectional wear motion, CN=0, reveals the presence of Fe, O, and C species indicating that the surface has been, at least, partially oxidised during the rubbing wear process (Figure 6.7(a)). The EDS spectra of the worn surfaces under bidirectional sliding configurations at CN=5 (Figure 6.7(b)) and at CN=50 (Figures 6.7(c) and (d)) confirm as well the presence of oxides on

those surfaces. At CN=50, EDS confirms that the oxide film (O) (Figure 6.7(c)) is richer in oxygen. In the exposed metallic areas (M) (Figure 6.7(d)), the presence in oxygen is minimal.

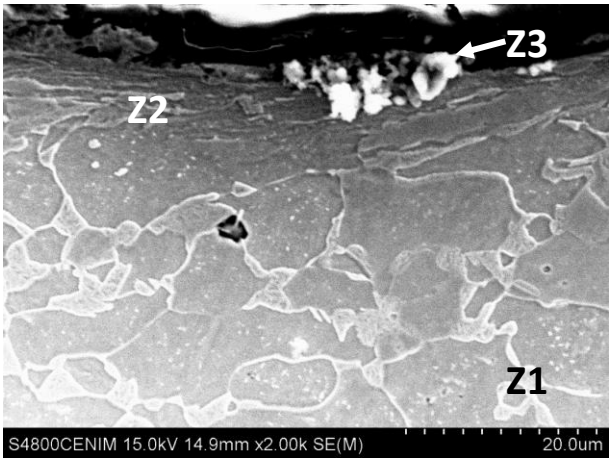

Figure 6.8 Representative SEM image of a cross-section of the DP600 steel worn surface.

In order to get further insight into the wear mechanisms responsible for the friction and wear phenomena, in the present work the subsurfaces of the worn surfaces have been examined. Figure 6.8 shows a representative micrograph of the cross-section of the DP600 steel worn surface. This SEM image displays three different zones easily distinguished (Wayne and Rice, 1983). Zone 1 (Z1), located furthest from the contact region, is identified by the non-deformed base material. As noticed, DP steels are characterised by a microstructure consisting of a soft ferrite phase (dark areas) with a hard second phase martensite (bright areas) randomly distributed as islands. Zone 2 (Z2) encompasses the nearest intermediate layers to the worn surface and is plastically deformed. This localised plastic strain might be resulting from the mismatch deformation between the soft ferritic matrix and the harder martensite phase (Wu-rong et al., 2011; Imandoust et al., 2014). Finally, zone 3 (Z3) depicts the wear track surface.

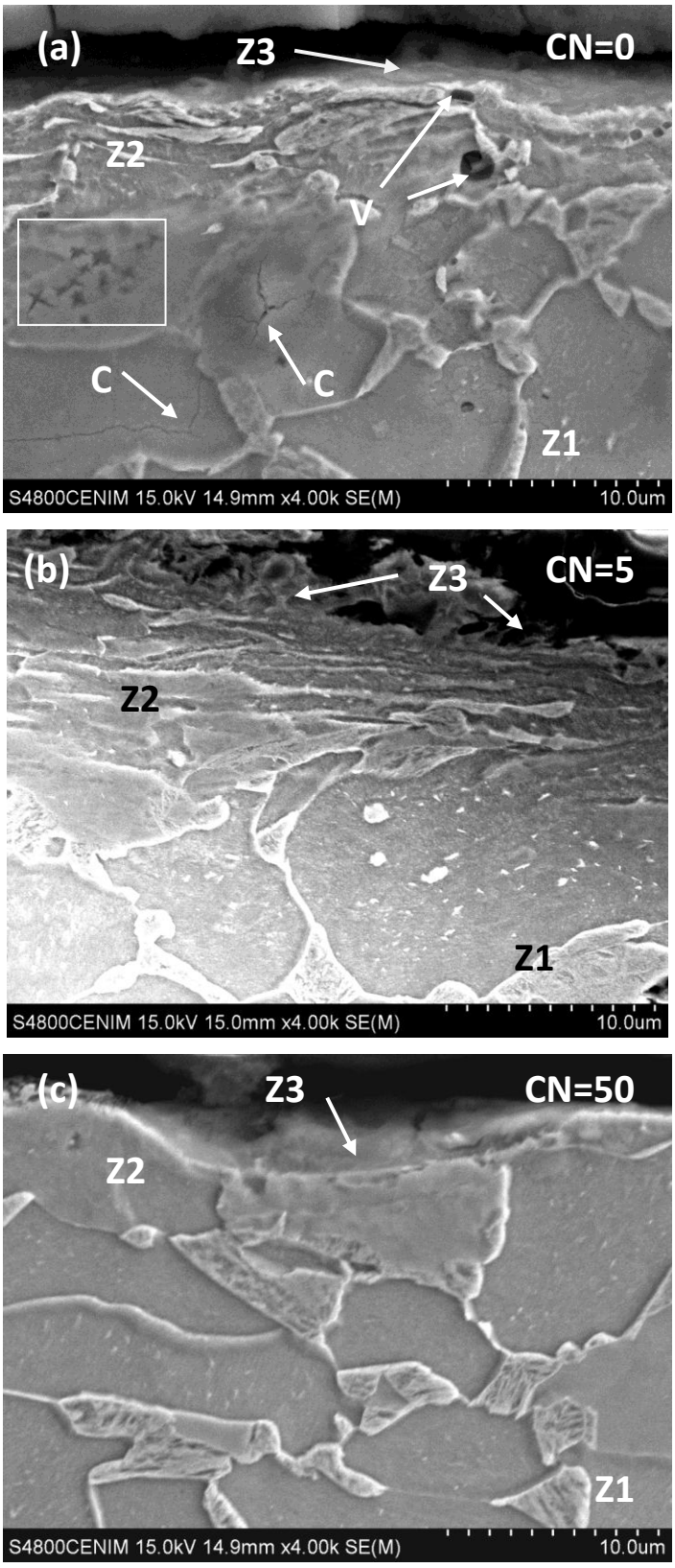

Figure 6.9. SEM images corresponding to the cross-section DP600 steel worn surfaces and subsurface layers tested at 1 m/s and 4.60 Hz for (a) CN=0, (b) CN=5, and (c) CN=50.

The microstructures of the cross-section of the worn surfaces and subsurface layers tested at 1 m/s and 4.60 Hz are shown in Figures 6.9 (a) and (c) for CN=0, 5 and 50, respectively. A significant plastic deformation in the outer subsurface layers is distinguished in Figure 6.9 (a). Cracks are also visible at several depths below the worn surface. Essentially, these fractures occur within the ferrite grains and they seem to come together into a main crack. Moreover, there is a visible area where a evident number of cross-shaped cracks are found. In Figure 6. 9 (b), clear plastic deformation of the first subsurface layers is also observed. However, no crack formation or presence of voids is detected as in Figure 6.9 (a) (C and V labels, respectively). As CN increases, the wear damage is less extended as shown in Figure 6.9 (c). Significant material loss and early stages of deformation are visible.

6.5 Effect of the Sliding Speed and Contact Frequency on the Wear Rate

Material loss is shown as a function of the contact frequency and the sliding speed in Figures 6.10 and 6.11, respectively. The wear rate decreases with the increase in contact frequency (Figure 6.10), whereas in Figure 6.11 it can be observed that the wear rate increases as the sliding speed increases. In both cases, it is visible that the wear resistance of DP600 steel is higher when CN increases, i.e. the material loss is more significant when tests are carried out under unidirectional motion.

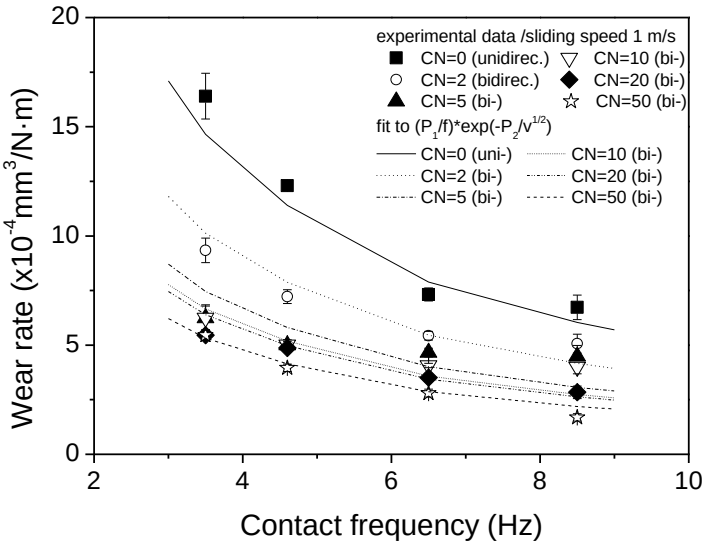

Figure 6.10 Experimental data for wear rate of DP600 steel discs versus contact frequency at a constant sliding speed value of 1 m/s during unidirectional (CN=0) and bidirectional (CN≠0) motion fitted according to Garcia-Ramil-Celis model.

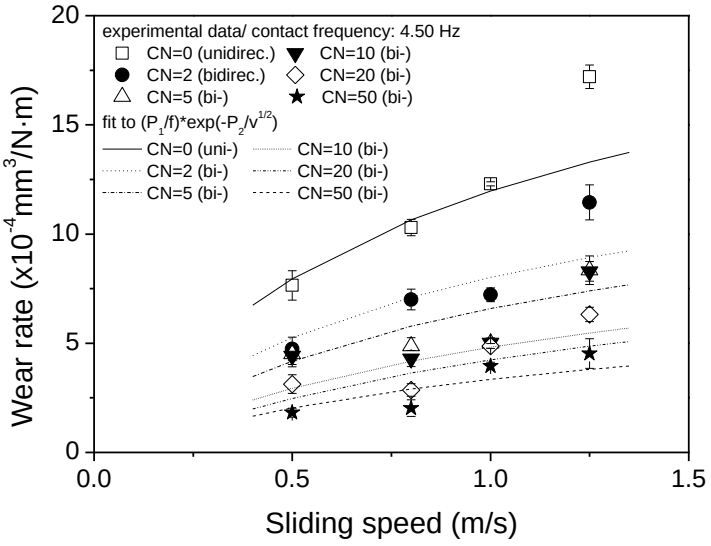

Figure 6.11 Experimental data for wear rate of DP600 steel discs versus sliding speed at a fixed contact frequency of 4.50 Hz during unidirectional (CN=0) and bidirectional (CN≠0) motion fitted according to Garcia-Ramil-Celis model.

Undoubtedly, the wear rate values as a function of the sliding speed (Figure 6.11) do not follow an inverse reciprocal relationship as is expected from Quinn's model for mild oxidative wear (Quinn, 1992, 1994, 1998).

As is known, Quinn developed the mild oxidative wear model to describe the wear of a pin, which is in continuous contact with a disc. Such a model has been widely applied indistinctively for the tribocouple. However, the disc is in discontinuous sliding contact with the pin.

Hence, Garcia et al. (2003) proposed a modification to Quinn's model in order to overcome this limitation and consequently, to explain the wear behaviour for discontinuous sliding contacts, by including contact frequency as parameter. The data shown in Figure 6.10 and 6.11 can be simulated using Garcia et al. (2003) expression for wear rate as a function of the contact frequency and sliding speed. Figure 6.10 plots an excellent fit for the wear rate of the DP600 steel discs vs. the contact frequency. Likewise, a suitable fit is obtained for the wear rate of the DP600 steel discs as a function of sliding speed (Figure 6.11). However, it can be observed that a clear dispersion at 1.25 m/s exists for each CN tested. Furthermore, this fit becomes better as the CN increases, i.e. CN>10.

6.6 Discussion

The friction and wear behaviour of the DP600 steel discs have been analysed during unidirectional and bidirectional sliding. The results show that the wear rate in unidirectional wear tests is higher than in those cases where the rotation direction is repeatedly reversed. These results agree with the wear behaviour of Zn-Cu alloys studied by Tang et al. (2011a, 2011b). However, they are opposite to the wear behaviour results shown by Wu et al. (1999) work on TiN coatings.

The visible decrease in wear rate values as CN increases could be attributed to the formation of an oxidative film of compacted debris observed at the higher CNs (Figure 6.6), which limits direct contact between the rubbing surfaces, since this film could behave as a lubricant.

However, the observed differences in the sub-surface deformation layer and material hardening after the distinct wear testing make it reasonable to assume that the improved

wear rate resistance in the bidirectional wear tests may be related not only to the formation of such oxide film. The material loss can be also influenced by complex strain-hardening effect in the DP600 steel (Figure 6.5) and involve a noticeable plastically deformation and wear damage (Figure 6.6 and 6.9).

Dual-phase steels contain high mobile dislocation densities at the interfaces between martensite and ferrite due to the dilatational strains imposed during transformation (Mediratta et al., 1985). Upon wear testing under unidirectional sliding, these mobile dislocations usually pile-up (or build-up) in the worn surface layer as a result of interactions between dislocations with the same sign, and as well as to the grain and inter-phases boundaries which block the dislocation movement (Tang et al., 2011b). Consequently, the worn surface increases its hardness.

If the wear direction (or stress) is continuously changed, the local dislocation accumulation might diminish due to the reversible movement of dislocation and their annihilation with others in opposite signs (Zhu et al., 2013). Therefore, a noticeable strain-hardening stagnation (Kim et al., 2012) takes place, known as the BE.

In the present work, the initial rise in hardness observed from CN=0 to 5 in Figure 6.5 could be related to the response of limited sliding direction changes which, in turn, reduce the local accumulation of dislocations, whereas the hardness still increases (Tang et al., 2011a, 2011b).

However, when the number of variations in the sliding path is high enough, i.e. above CN=5 (Figure 6.5), the BE and a permanent softening is noticed in the DP600 steel, since the density of local dislocations decreases accompanied a drop in the local stress build-up, and, thus, in hardness.

Examination of the SEM images (Figure 6.9), corresponding to the cross-section of the worn subsurface layers, reveals noticeable plastic flow and microcracks which occurred below the original surface when CN=0. The DP600 steel discs performed under unidirectional wear tests exhibit greater damage, such as plastic deformation, cracking and voids, than in bidirectional wear motion. This wear and fracture mode evolution could be directly related to the dramatic change exhibited in the slope of both wear rate versus CN curves, from CN=0 to 5 (Figures 6.3 and 6.4).

The combined role of contact frequency and sliding speed on the DP600 steel discs during testing in unidirectional and bidirectional sliding is therefore demonstrated. The effect of both parameters on the wear of the disc material is different, regardless of the sliding mode. The wear rate of the DP600 steel sliding against corundum balls exhibits an inversely proportional relationship with the contact frequency, whereas it is directly proportional with the sliding speed.

Such results for discontinuous contacts in sliding wear systems, combined with the wear path suitably, fit the Garcia-Ramil-Celis model (Garcia et al., 2003). This demonstrates that there is a clear differentiation between the contact frequency and the sliding speed effect. In addition, the observed scatter in the experimental data (Figures 6.10 and 6.11) could be considered the consequence of a hidden effect of the contact frequency on the wear rate (Ruiz-Andres et al., 2015b; Garcia et al., 2003; Navas et al., 2006).

The discrepancies of the present work regarding Wu et al. (1999) results might be caused due to the fact that those authors did not performed unidirectional and bidirectional wear tests at the same testing conditions, i.e. sliding speed and contact frequency, as in the present work. Consequently, such differences can be considered a result from the relationship between wear rate and sliding speed/contact frequency, which is quite far from the idea about the unidirectional or bidirectional wear test effect.

6.7 Concluding Remarks

A thorough study of the influence of sliding direction changes, contact frequency, and Bauschinger Effect on the wear of DP600 steel discs has led to the following conclusions:

- DP600 steel discs respond differently to unidirectional and bidirectional sliding wear against corundum balls. It is shown that unidirectional sliding, CN=0, results in more wear damage than in bidirectional motion, CN≠0.
- The strain-hardening rate for tests at CN ≤5 increases as a result of limited sliding direction changes which, in turn, reduce the local dislocations accumulation. Conversely, for tests performed at CN>5 the hardness decreases in the subsurface worn layer of the DP600 steel.

- The plastic deformation and fracture in the DP600 steel are more noticeable and severe in unidirectionally worn DP600 steel discs than in bidirectionally worn specimens.
- The Bauschinger Effect takes place during the bidirectional sliding processes. However, it is important to highlight that this Bauschinger Effect is only noticeable when the sliding direction is reversed for some limited times, i.e. CN>5, where the wear volume loss decreases and is accompanied by a weak strain-hardening effect.
- The Bauschinger Effect and permanent softening in the DP600 steel discs are directly affected not only by the sliding speed, but also by contact frequency. The wear rate of the DP600 steel discs exhibits an inversely proportional relationship with the contact frequency, whereas it is directly proportional with the sliding speed.

7

Conclusions

This thesis has been devoted to the study of the tribological behaviour of DP600 steel on uni- and bi-directional discontinuous sliding wear. The following conclusions have been established:

- The contact frequency is an independent parameter together with the contact load and the sliding speed. The contact frequency clearly affects the wear rate in discontinuous sliding wear conditions. Moreover, the contact frequency was shown to be a key factor determining the wear behaviour. However, the relationship between wear rate and contact frequency differs according the sliding wear test. In unidirectional ball-on-disc tests: At low contact frequencies analysed, the wear rate increases as the sliding speed increases. Whilst, at high contact frequencies, the wear rate decreases with the sliding speed. For bidirectional ball-on-plate tests: The wear rate increases with the sliding speed within the complete interval of contact frequencies measured. For ball-on-disc continuously reversed tests: The wear rate of the DP600 steel discs exhibits an inversely proportional relationship with the contact frequency, whereas it is directly proportional with the sliding speed.

- DP600 steel discs responded differently to unidirectional and bidirectional sliding wear against corundum balls. It was shown that unidirectional sliding results in more wear damage than in bidirectional motion.

- The COF is affected by the contact frequency, in which each part of the wear track trajectory on the DP600 steel specimens comes into contact with the

counterbody when wear features for DP600 subjected to discontinuous sliding contacts are tested and/or described in uni- and bi-directional wear tests.

- The wear mechanism induced in DP600 steel is mild oxidative wear. The nature of the iron oxide debris is a function of the sliding speed and the contact frequency. In unidirectional ball-on-disc tests: At low contact frequencies the predominant oxide is Fe_2O_3, while at high contact frequencies the oxide formed is mainly Fe_3O_4. For bidirectional ball-on-plate wear tests: Only Fe_2O_3 is obtained after testing,which indicates that the tribosystem does not presumably exceed a temperature of 450ºC in the contact area.

- The wear behaviour of DP600 steel specimens presented a directly linear relationship with the dissipated energy. This indicated that the oxidation process of DP600 steel did not consume a considerable quantity of energy during testing. The heat generation at the interface was, however, concluded from the importance in characterising the wear behaviour of the tribosystem as it could contribute to a modification in the rheology or composition of the oxidised layer and thus, to the debris generated within the tribocouple.

- The Bauschinger Effect and permanent softening in the DP600 steel discs took place during the bidirectional sliding processes. However, it was only perceived when the sliding direction was reversed for some limited times. Besides, the Bauschinger Effect was directly affected not only by the sliding speed, but also by contact frequency.

Conclusiones

Las principales conclusiones que se pueden extarer de esta tesis son:

- La frecuencia de contacto, junto con la carga aplicada y la velocidad de deslizamiento, es un parámetro operacional determinante y a tener en cuenta durante los ensayos de desgaste en condiciones de deslizamiento por contacto discontinuo, puesto que afecta significativamente el comportamiento frente al desgaste del acero DP600. Sin embargo, la tasa de desgaste evoluciona de distinto modo con la frecuencia en función de las geometrías de ensayo. En el caso de los ensayos unidireccionales de bola-sobre-disco, se observó que el desgaste varía drásticamente su comportamiento dependiendo de los valores de frecuencia de contacto aplicados. A valores bajos de frecuencia, el desgaste aumenta a medida que la velocidad de deslizamiento aumenta. En cambio, para valores altos de frecuencia, la tasa de desgaste disminuye considerablemente con el aumento de la velocidad. En cambio, en los ensayos bidireccionales de bola-sobre-plano, la tasa de desgaste aumenta al incrementar la velocidad de deslizamiento independientemente de las condiciones de ensayo. Finalmente, en los ensayos de bola-sobre-disco con sentido de rotación variable, los resultados evidencian una relación inversamente proporcional entre la tasa de desgaste y la frecuencia.

- Los discos de acero DP600 respondieron de diferente modo según fueron ensayados, es decir, si fueron ensayados bajo condiciones de desgaste unidireccional o bidireccional. Se observó un mayor daño en los discos al ser ensayados unidireccionalmente.

- La frecuencia de contacto influye en los valores del COF de las muestras de acero DP600. Esta influencia es significativa independientemente de que los ensayos se realicen de modo unidireccional o bidireccional.

- El mecanismo de desgaste inducido en los discos de acero DP600 fue, en todos los casos ensayados, oxidativo ligero. Se observó que la naturaleza de las partículas de desgaste generadas dependen tanto de la frecuencia como de la velocidad. Así pues, bajo condiciones de ensayos unidireccionales de bola-sobre-disco y frecuencias de contacto bajas, se observó que, en todas las partículas desgastadas recogidas, el óxido predominante es Fe_2O_3. Sin embargo, a altas frecuencias de contacto ensayadas, el óxido predominante, en las partículas de desgaste que se analizaron tras los ensayos, es Fe_3O_4. Cuando los ensayos se llevaron a cabo bajo condiciones bidireccionales en bola-sobre-plano, el óxido que se recogió, tras realizar todos ensayos, fue Fe_2O_3. Al haberse ensayado bajo un amplio intervalo de velocidades de deslizamiento y frecuencias de contacto, se concluyó que, en este tipo de ensayos, la temperatura en el area de contacto no superó en ningún caso los 450ºC.

- El comportamiento frente al desgaste del acero DP600 depende directamente de la energía disipada. Esto es indicativo de los procesos de oxidación producidos durante los ensayos no consumieron gran cantidad de energía. La generación de calor en el area de contacto caracteriza notablemente el comportamiento del desgaste del acero DP600, así como contribuye en los cambios que se pueden llegar a dar en la composición de las capas de óxido y, por ello, en las partículas de desgaste.

- Se infirió que, como consecuencia del modo de ensayo, los discos de acero DP600 evidencian un marcado efecto Bauschinger durante los ensayos bidireccionales cuando se controla el cambio del sentido en la rotación. Así mismo, el efecto Bauschinger se vió afectado por los parámetros de velocidad de deslizamiento y de frecuencia de contacto

References

Abouei V, Saghafian H, Kheirandish S. Effect of microstructure on the oxidative wear behavior of plain carbon steel. Wear 2007a; 262:1225-1231.

Abouei V, Saghafian H, Kheirandish S. Dry Sliding Oxidative Wear in Plain Carbon Dual Phase Steel. Journal of Iron and Steel Research, Int 2007b; 14:43-48.

Abouei V, Saghafian H, Kheirandish S, Ranjbar K. An investigation of the wear behaviour of 0.2% C dual phase steels. Journal of Materials Processing Technology 2008; 203:107-112.

Archard J F. Contact and rubbing of flat surface. Journal of Applied Physics 1953; 2:981-988.

Archard J F, Hirst W. The wear of metals under unlubricated conditions. Proceedings of Royal Society A of London, 1956; 236: 397.

Archard J F. The temperature of rubbing surfaces. Wear 1958-1959; 2:438-455.

Archard J F. Friction between metal surfaces. Wear, 1986; 113: 3-16.

Ashby M F, Abulawi J, Kong H S. Temperature maps for frictional heating in dry sliding. Tribology Transactions 1991;34:577-587.

Axén N, Hormark S, Jacobson S. Friction and Wear Measurement Techniques. 2001 CRC Press LLC.

Basak A, Reddy D C, Kanth D V K. Computer modeling of wear resistance for plain carbon steels. Material Science Technology 1998;14:776-782.

Basu B and Kalin M. Tribology of Ceramics and Composites: Materials Science Perspective. The American Ceramic Society. Published by Wiley & Sons. Inc. Hoboken, New Jersey. 2011. ISBN: 981-02-1516-9.

Bayer R G. Mechanical Wear Prediction and Prevention. 1994. Marcel Dekker, Inc., NY.

Bayer R G. Fundamentals of Wear Failures. ASM Handbook. Vol.11. Failure Analysis and Prevention. Becker W T and Shipley R J (Volume Editors). ASM International Handbook Committee. 2002.

Bergman F, Hedenqvist P, Hogmark S. The influence of primary carbides and test parameters on abrasive and erosive wear of selected PM high speed steels. Tribology International 1997; 30(3): 183-191.

Bhushan B and Gupta B K. Handbook of Tribology, Materials, Coatings and Surface Treatments. McGraw Hill. 1991. ISBN: 0-07-005249-2.

Bhushan B. Micro/Nanotribology and its Applications. 1st Ed. Kluwer Academic Publishers, 1997.

Bhushan B. Modern tribology Handbook. Vol. 1. 2000. CRC Press LLC. ISBN: 9780849384035.

Bhushan B. Introduction to Tribology. Published by Wiley & Sons. Inc. Hoboken, New Jersey. 2002. p732.

Bhushan B. Principles and Applications of Tribology. 2nd Ed. Published by Wiley & Sons. Inc. Hoboken, New Jersey. 2013.

Birks N, Meier G H, Pettit F S. Introduction to the High-Temperature Oxidation of Metals. 2nd Ed. Cambridge University Press, NY. 2006.

Blau P J. An investigation of the unlubricated friction and wear break-in behavior of a dual-phase steel. Wear 1981;72:67-80.

Bonny K, Baets P De, Perez Y, Vleugels J, Lauwers B. Friction and wear characteristics of WC-Co cemented carbides in dry reciprocating sliding contact. Wear, 2010; 268: 1504-1517.

Bowden F P and Tabor D. The Friction and Lubrication of Solids. Part I. 5th Ed. Oxford University Press, 2001

Bruker; Application note: Pin-on-Disk sliding wear using the micro-tribometer mod. CETR-UMT 2, ASTM G99-95. 2006a.

Bruker; Application note: Non-rotating Pin-on-Flat test method. 2006b.

Burwell J T, and Strang C D. On the empirical law of adhesive wear. Journal of Applied Physics 1952; 23:18.

Callister W D. X Ray Diffraction: Determination of Crystal Structures. In: Material Science And Engineering. 7th Ed. USA. 2007. ISBN: 0471736961.

Campbell W E,. Boundary Lubrication, an Appraisal of Word Literature. ASME. 1969.

Caplan D, Cohen M. Effect of cold work on the oxidation of iron from 400-650ºC. Corrosion Science, 1966; 6: 321-335.

Cardarelli F. Materials Handbook: A Concise Desktop Reference. 2nd ed. Springer-Verlag London Ltd. 2008. ISBN: 978-1-84628-668-1.

Chang L C. The rolling/sliding wear performance of high silicon carbide-free bainitic steels. Wear 2005; 258:730-743.

Chen H, Wu P Q, Quaeyhaegens C, Xu K W, Stals L M, He J W, Celis J –P. Comparison of fretting wear of Cr-rich CrW and TiN coatings in air of different relative humidities. Wear 2002; 253(5-6): 527-532.

Chen R Y, Yuen W Y D. Review of the high-temperature oxidation of iron and carbon steels in air or oxygen. Oxidation of Metal 2003; 59: 433-468.

Clark W T, Pritchard C, Midgley J W. Mild wear of unlubricated hard steels in air and carbon dioxide. Proceedings of the Institu of Mechanical Engineering, Conference Proceedings 1967; 182: 97-105.

Cornell R M, Schwertmann U. The Iron Oxides. VCH Publishers, NY. 1996.

Cosemans P, zhu X, Celis J –P. Development of low friction wear-resistant coatings. Surface and Coatings Technology 2003; 174-175: 416-420.

Cowan R S, Winer W O. Frictional Heating Calculations. ASM Handbook Vol. 18. Friction, Lubrication, and Wear Technology. Blau P J (Volume Chairman). ASM International Handbook Committee. 1992.

Cui X, Zhang H, Wang S, Zhang L, Ko J. Design of lightweight multi-material automotive bodies using new material performance indices of thin-walled beams for the material selection with crashworthiness consideration. Materials & Design 2011;32: 815-821.

Czichos H. Tribology, A System Approach to the Science and Technology of Friction, Lubrication and Wear. Elsevier. 1978.

Davis J R (Ed.). Surface Engineering for Corrosion and Wear Resistance. ASM International. 2001.

Davoudi KM, Nicola L, Vlassak JJ. Bauschinger effect in thin metal films: Discrete dislocation dynamics study. Journal of Applied Physics 2014; 115: 013507-1-7.

Demir E, Raabe D. Mechanical and microstructural single-crystal Bauschinger effects: Observation of reversible plasticity in copper during bending. Acta Materalia 2010; 58:6055-6063.

D'Errico G E, Bugliosi S, Calzavarini R, Cuppini D. Wear of advanced ceramics for tool materials, Wear 1999; 225-229 (Part 1): 267-272.

Eddoumy F, Addiego F, Celis J –P, Buchheit O, Berradja A, Muller R, Toniazzo U, Ruch D. Reciprocating sliding of uniaxially-stretched ultra-high molecular weight polyethylene for medical device applications. Wear 2011; 273(1,3):50-61.

Eissenberg D M and Haynes H D. Motor-Current Signature Analysis. ASM Handbook Vol. 18. Friction, Lubrication, and Wear Technology. Blau J P (Volume Chairman) ASM International Handbook Committee. 1992.

Fehlner F P, Mott N F. Low temperature oxidation. Oxidation of metals, Vol 2. 1970, p. 56-99.

Foley RT, Peterson MB, Zapf C. Frictional characteristics of cobalt, nickel, and iron as influenced by their surface oxide films. ASLE Transactions 1963;6:29-39.

Fouvry S, Kapsa P. An energy description of hard coatings wear mechanisms. Surface and Coatings Technology 2001; 138: 141-148.

Fouvry S, Liskiewicz T, Kapsa P, Hannel S, Sauger E. An energy description of wear mechanisms and its applications to oscillating sliding contacts. Wear, 2003;255: 287-298.

Fouvry S, Paulin C, Liskiewicz T. Application of an energy wear approach to quantify fretting contact durability: Introduction of a wear energy capacity concept. Tribology International 2007; 40: 1428-1440.

Fromhold A T. Theory of Metal Oxidation. Vol. 1-Fundamentals. Elsevier, Amsterdam. 1992

Fromhold AT. Theory of Metal Oxidation.Vol 1. Fundamentals. Elsevier, Amsterdam. 1976.

Futamura Y, Miura M, Tsunezawa M. Characteristics of highly formable 590-980Mpa grade hot-dip galvannealed steel sheets for automobiles. Kobelco Technology Review 2011; 30:80-84.

Garcia I, Ramil A, Celis JP. A mild oxidation model valid for discontinuous contacts in sliding wear tests: role of contact frequency. Wear 2003;254:429-440.

Godet M. The third-body approach: A mechanical view of wear. Wear 1984;100: 437-452.

Goel A, Ray RK, Murty GS. Bauschinger effect in a dual-phase steel. Scripta Metallurgia 1983; 17:375-380.

Goodfellow Group. All the Materials for Scientific and Industrial Research and Manufacturing. Corundum balls. 2008.

Greenwood J A, Alliston-Greiner A F. Wear, 1992; 2:269-275

Han Q-h, Kang Y-l, Zhao X-m, LÜ C, Gao L-f. Microstructure and Properties of Mo Microalloyed Cold Rolled DP1000 Steels. Journal of Iron and Steel Research, Int 2011;18:52-58.

Harea E, Lapsker I, Laikhtman A, Rapoport L. Bauschinger's effect and dislocation structure under friction of LiF single crystals. Tribology Letters 2013; 52: 205-212.

Hirst W. Tribology Engineering, Vol. 26, No 3, 285-304. 1973.

Holm R. Electrical Contacts, Stockholm: H. Gerber, (1946).

Hulka K. Dual Phase and Trip Steels. ASM Metal Park Ohio; 2000, p. 1-4.

Huq M Z, Celis J -P, Expressing wear rate in sliding contacts based on dissipated energy, Wear, 252 (2002) 375-383.

Hurricks PL. Fretting wear of mild-steel from room temperature to 200ºC. Wear 1972;19:207—229.

Hurricks PL. Fretting wear of mild-steel from 200ºC to 500ºC. Wear 1974;30:189-212.

Hutchings I M. Tribology. Friction and Wear of Engineering Materials. Ed. Edward Arnold. 1992. ISBN: 0-340-56184-X.

Ibáñez J J, Mecánica de suelos en civilizaciones ancestrales: El caso de las pirámides egipcias. 2014. madridmasd.org.

Imandoust A, Zarei-Hanzaki A, Manesh H, Moemeni S, Changizian P. Effects of ferrite volume fraction on the tensile deformation characteristics of dual phase twinning induced plasticity steel. Materials & Design 2014; 53:99-105.

Iwai Y, Honde T, Yamada H, Matsubara T, Larsson M, Hogmark S. Evaluation of erosive wear resistance of TiN coatings by a slurry jet impact test. Wear 2006; 261(1):112-118.

Jiang J, Stott F H, Stack M M, The role of triboparticulates in dry sliding wear, Tribology International 31 (1998) 245-256.

Jiang J, Stack M M. Modelling sliding wear: From dry to wet environments. Wear 2006;261:954-965.

JIS. Methods of Wear Resistance Test for Metallic Coating. JIS H8503. 1989.

Johnson K L, Greenwood J A, Poon S Y. A simple theory of sperity contact in elastohydro-dynamic lubrication. Wear 1972; 19(1):91-108.

Jost H P. Tribology: How a word was coined 40 years ago. Tribology & Lubrication Technology 2006; 62(3):24-28.

Kato H, Eyre TS, Ralph B. Wear mechanism map of nitrided steel. Acta Metallurgica 1994; 42:1703-1713.

Kayaba T, Iwabuchi A. The fretting wear of 0.45% C steel and austenitic stainless steel from 20 to 650ºC in air. Wear 1981;74:229-245.

Kennedy D M, Hashmi M S J. Methods of wear testing for advanced surface coatings and bulk materials. Journal of Materials Processing Technology 1998; 77:246-253.

Kim JH, Kim D, Barlat F, Lee M-G. Crystal plasticity approach for predicting the Bauschinger effect in dual-phase steels. Materials Science and Engineering A 2012; 539:259-270.

Kivioja S, Kivivuori S, Salonen P. Tribology. 3rd Ed. Helsinki, Otatieto. 2001. 351s

Kondo Y, Koyama T, Sasaki S. Ionic liquids-New Aspects for the Future. Tribological Properties of Ionic Liquids. Jun-ichi Kadokava (Ed) 2013. ISBN:978-953-51-0937-2.

Kubaschewski O, Hopkins B E. Oxidation of Metals and Alloys. 2nd Ed. Butterworths, London. 1962.

Kuhlmann-Wilsdorf D. Demystifying flash temperature Part I. Analytical exoressions based on a simple model. Material Science and Engineering A 1987a; 93:107-117

Kuhlmann-Wilsdorf D. Demystifying flash temperature Part II. First-order approximation for plastic contact spots. Material Science and Engineering A 1987b; 93:119-133

Kuwahara K, Masumoto Il, Influence of wear particles on the friction and wear between copper disk and pin of various kinds of metal, Lubrication Engineering, 1980; 36 :362.

Lim S C and Ashby M F. Overview No.55: Wear-mechanism maps. Acta Metallurgica 1987; 35:1-24.

Lipson C. Machine Design. Vol. 41. 1969. 74-77

Liu Y, Ashtana R, Rohaygi P. A map for wear mechanisms in aluminium alloys. Journal of Material Science 1991;99-102.

Lockwood F E and Dalley R (Eds.) Lubricant Analysis. Friction, Lubrication and Wear Technology, Vol. 18. ASM Handbook. ASM International, 1992.

Ludema K. Scuffing, run-in and the function of surface films, particularly oxides. Review paper for interdisciplinary collaboration in tribology project, NASA-Lewis; 1981.

Marston H F, Bolt P H, Laprince G, Roder M, Klimo K, Niska, Jeol M. Challenges in the modelling of scale formation and decarburisation of high carbon, special and general steels. Ironmark. Steelmark. 2004; 31:57-65.

Martin H R. Vibration Analysis. ASM Handbook Vol.18. Friction, Lubrication, and Wear Technology. Blau P J (Volume Chairman). ASM International Handbook Committee. 1992.

Matsunga M, Ito Y, Kobayashi H. Wear test of bucket teeth. American Society of Mechanical Engineers. 1972; 15: 336-342.

Mediratta SR, Ramaswany, Rao PR. Influence of ferrite-martensite microstructural morphology on the low cycle fatigue of a dual-phase steel. International Journal Fatigue 1985; 7:107-116.

Mehrota P K (Ed). Mechanisms of Wear in Ceramic Materials. Wear of materials. American Society of Mechanical Engineers. 1983.

Meng Q, Li J, Zheng H. High-efficiency fast-heating annealing of a cold-rolled dual-phase steel. Materials & Design 2014;58:194-197.

Miller J M. "Slippery" work surfaces: Towards a performance definition and quantitative coefficient of friction criteria. Journal of Safety Research 1983; 14(4): 145-158.

Ming-tu MA, Du-xing C. Bauschinger effect and coercivity in dual-phase steels. Chinese Physics Letters 1984; 1:35-38.

Miyashi K and Chung Y-w. Surface Diagnostics in Tribology:Fundamental Principles and Applications. Word Scientific Publishing Co., Ptc., Ltd. 1993. ISBN: 981-02-1516-9.

Modi OP, Bashad BK, Jha AK, Dasgupta R, Yegneswaran AH. Low stress wear behaviour of 0.2 %C steel: Influence of microstructure. Tribology Letters 2003;15:249-255.

Mohrbacher H, Celis J -P, Roos J R. Laboratory testing of displacement and load induced fretting. Tribology International 1995; 28: 269-278.

Molgaard J, Srivastava V K. The activation energy of oxidation. Wear 1977; 41: 263.

Navas C, Garcia I, Ye X, de Damborenea J, Celis JP. Role of contact frequency on the wear rate of steel in discontinuous sliding contact conditions. Wear 2006;260:1096-1103.

Neupane R, Farhat Z. Wear mechanisms of nitinol under reciprocating sliding contact. Wear 2014; 315(1-2):25-30.

Oliver W C and Pharr G M. Measurement of hardness and elastic modulus by instrumented indentation: Advances in understanding and refinements to methodology. Journal of Material Research 2004; 19(1): 3-20.

Ozturk F, Toros S, Kilic S. Tensile and Spring-Back Behavior of DP600 Advanced High Strength Steel at Warm Temperatures. Jour of Iron and Steel Research, Int 2009;16: 41-46.

Persson B N J. Sliding Friction: Physical Principles and Applications. 2nd Ed. Springer, Heidelberg. 2000.

Persson B N J, Albohr O, Tartaglino U, Volokitin A I, Tosatti E. On the nature of surface roughness with application to contact mechanics, sealing, rubber friction and adhesion. Journal of Physics: Condensed Matter 2005; 17:R1.

Põdra P. FE Wear simulation of sliding contacts. Doctoral Thesis. Royal Institue of Technology, Stockholm, Sweden. 1997. ISSN: 1400-1179.

Pritchard S B and Trowsdale A J, Dual Phase Steel-High Strength Fasteners Without Heat Treatment Corus Construction and Industrial, U.K., 2002. 1-10.

Quinn TF. The Classifications, Laws, Mechanisms and Theories of Wear. Part VII of Fundamentals of Tribology. Editors N.P. Suh and N. Saka. The M.I.T; 1980a:477-492.

Quinn TFJ, Rowson DM, Sullivan JL. Application of the oxidational theory of mild wear to the sliding wear of low alloy steel. Wear 1980b;65:1-20.

Quinn TFJ. NASA Interdisciplinary Collaboration in Tribology. A Review of oxidational wear. 1983a.

Quinn TFJ. Review of oxidational wear: Part I: The origins of oxidational wear. Tribology International 1983b;16:257-271.

Quinn T F J. Oxidational wear modelling: I, Wear, 1992; 153: 179-200.

Quinn TFJ. Oxidational wear modelling: Part II. The general theory of oxidational wear. Wear 1994;175:199-208.

Quinn TFJ. Oxidational wear modelling Part III. The effects of speed and elevated temperatures. Wear 1998;216:262-275.

Quinn TFJ. The oxidational wear of low alloy steels. Tribology International 2002;35:691-715.

Ramazani A, Mukherjee K, Scwedt A, Goravanchi P, Prahl U, Bleck W. Quantification of the effect of transformation-induced geometrically necessary dislocations on the flow-curve modelling of dual-phase steels. International Journal of Plasticity 2013;43:128-152.

Rashid MS. Dual Phase Steels. Annual Review of Material Science 1981;11:245-266.

Reynier B, Phalippou C, Riberty P, Sornin J. Influence of a periodic latency on the impact/sliding wear damage of two PWR control rods and guide cards specimens. Wear 2005;259:1314-1323.

Rice R H, Gnecco E, King W P, Szoszkiewicz R. Heterogeneity of spiral wear patterns produced by local heating on amorphous polymers. Materials Chemistry and Physics 2013; 141(1):477-481.

Ruiz-Andres M, Conde A, De Damborenea J, Garcia I. Wear behaviour of aluminium alloys at slow sliding speeds. Tribolology Transactions 2015a DOI: 10.1080/10402004.2015.1027432

Ruiz-Andres M, Conde A, De Damborenea J, Garcia I. Friction and wear behaviour of dual phase steels in discontinuous sliding contact conditions as a function of sliding speed and contact frequency. Tribology International 2015b; 90: 32-42.

Ruscoe M J H (Ed). A Predictive Test for Coin Wear in Circulation. Wear of Materials. American Society of Mechanical Engineers. 1987.

Sauger E, Fouvry S, Ponsonnet L, Martin J M, Ph. Kapsa, L. Vincent, Tribologically transformed structure in fretting, Wear 2000, 245: 39-52.

Sawa M, Rigney DA. Sliding behavior of dual phase steels in vacuum and in air. Wear 1987;119:369-390.

Schmitz C. Handbook of Aluminium Recycling. Fundamentals: Mechanical Preparation, Metallurgical Processing, and Design. Ed. Vulkan-Vorlag GmbH. 2006. ISBN: 3-8027-2936-6.

Schumacher W J. Wear and galling can knock out equipment. Chemical Engineerign. 1977. 155-160.

Sowerby R, Uko DK, Tomita Y. A review of certain aspects of the Bauschinger effect in Metals. Materials Science and Engineering 1979; 41: 43-58.

Stott F H. The role of oxidation in the wear of alloy. Tribology International 1998; 31(1-3):61-71.

Stachowiak W and Batchelor W (Ed). Engineering Tribology. 2nd Ed. Butterworth Heinemann. 2001. ISBN: 0750673044.

Stephens J H (Ed). Kemper's Engineer's Yearbook 2002. CMP Information Ltd. 2001.

Sui X, Zhao X, Li X, Yao W, Wang Q, Ying H, Bi W. Proceedings of the Conference on Low Carbon Silicon-Niobium Dual Phase Steels Wires for Wear Resistant Screens. HSLA Steels: Processing, Properties and Applications. Beijing, China, Oct.28th-Nov.2nd,1990. The Minerals, Metals and Materials Society, 420, Commonwealth Dr., Warrendale, PA, USA. 1992. pp.483-488.

Sullivan JL, Quinn TFJ, Rowson DM. Developments in the oxidational theory of mild wear. Tribology International 1980;13:153-158.

Sullivan JL, Athwal SS. Mild wear of a low alloy steel at temperatures up to 500ºC. Tribology International 1983;16:123-131.

Sun S and Pugh M. Properties of thermomechanically processed dual-phase steels containing fibrous martensite. Material Science and Engineering A 2002;335:298-308.

Tabor D. Wear- A critical synoptic view. Proc Int Conference on Wear of Materials, St. Louis, Missouri, April 1977, ASME; 1978, p.1-10.

Tang C, Wang JM, Wen GW, Wang Y, Li DY. Bauschinger effect in wear of Cu-40Zn alloy and its variations with the wear condition. Wear 2011a; 271:1237-1243.

Tang C, Li DY, Wen W. A follow-up study on Bauschinger's effect in bidirectional wear of Cu-40%Zn against different types of counter-face. Tribology Letters 2011b; 43: 101-106.

Tyagi R, Nath SK, Ray S. Dry sliding friction and wear in plain carbon dual phase steel. Metallurgical and Materials Transactions A 2001;32:359-367.

Tyagi R, Nath SK, Ray S. Effect of Martensite Content on Friction and Oxidative Wear Behaviour of 0.42 Pct Carbon Dual-Phase. Metallurgical and Materials Transactions A 2002; 33: 3479-3488.

Tyagi R, Nath SK, Ray S. Modelling of dry sliding oxidation-modified wear in two phase materials. Wear 2003; 255:327-332.

Tyagi R, Nath SK, Ray S. Development of wear resistant medium carbon dual phase steels and their mechanical properties. Materials Science and Technology 2004; 20:645-652.

Tylczak J H and Oregon A. Abrasive Wear. ASM Handbook Vol. 18. Friction, Lubrication, and Wear Technology. Blau P J (Volume Chairman). ASM International Handbook Committee. 1992.

Troyer D. Soft Alignment has a Bearing on Lubrication. Excellence Machinery Lubrication. 2010.

Tu J P and Matsumura M. Interfacial reaction effects on erosion of aluminum matrix composites. Scripta Materalia, 1999; 40(6):645-650.

Wang D F and Kato K. Nano-scale fatigue wear of carbon nitride coating. Part II- Wear mechanisms. Journal of Tribology 2003; 125(2): 437-444.

Wang W, Li M, Zhao Y, Wei X. Study on stretch bendability and shear fracture of 800MPa dual phase steel sheet. Materials & Design 2014; 56:907-913.

Wayne SF, Rice SL. The role of microstructure in wear of selected steels. Wear 1983; 85:93-106.

Welsh N C. Philosophical Transactions of the Royal Society A of London. 1965; 257: 51-70

Williams J A, Wear and wear particles-some fundamentals, Tribology International 2005; 38: 863-870.

Wu P Q, Drees D, Stals L, Celis J -P, Comparison of wear and corrosion wear of TiN coatings under uni- and bidirectional sliding, Surface and Coatings Technology 1999, 113: 251-258.

Wu-rong W, Chang-wei H, Zhong-hua Z, Xi-cheng W. The limit drawing ratio and formability prediction of advanced high strength dual-phase steels. Materials & Design 2011; 32:3320-3327

Zhang J, Alpas AT. Transition between mild and severe wear in aluminium alloys. Acta Materialia 1997; 45:513-528.

Zhang J. Detection and monitoring of wear using imaging methods. Doctoral Thesis. University of Twente, Endschede, The Netherlands. 2006

Dissemination Of Results

Publications

Ruiz-Andres M, Conde A, De Damborenea J, Garcia I. Friction and wear behaviour of dual phase steels in discontinuous sliding contact conditions as a function of sliding speed and contact frequency. *Tribology International 2015; 90: 32-42.*

Ruiz-Andres M, Conde A, De Damborenea J, Garcia I. Wear behaviour of aluminium alloys at slow sliding speeds. *Tribology Transactions. 2015. DOI: 10.1080 /10402004.2015.1027432*

Ruiz-Andres M, Conde A, De Damborenea J, Garcia I.Microstructural and micromechanical effects of cold roll-forming on high strength dual phase steels. *Accepted manuscript. Materials Research*.

Ruiz-Andres M, Conde A, De Damborenea J, Garcia I. Influence of sliding direction changes, contact frequency and Bauschinger Effect on the wear of Dual Phase steels. *Accepted manuscript. Tribology International.*

Ruiz-Andres M, Conde A, De Damborenea J, Garcia I. Analysis of the contact frequency on reciprocating sliding wear tests using the energy wear approach. *Submitted*.

Communications

Garcia I, Rementeria R, Garcia-Caballero F, Ruiz-Andres M, Conde A. Wear behaviour of HSS in discontinuous sliding contact conditions. Advanced Steels 2014. Challenges in Steel Science & Technology. Madrid (Spain), 18th-19th September 2014. *Oral Presentation*.

Ruiz-Andres M, Conde A, De Damborenea J, Garcia I. Wear behaviour of aluminium alloys at very low sliding speeds. Conference on Tribology. Oporto (Portugal), 20th -21st June 2013.*Oral Presentation*.

Ruiz-Andres M, Conde A, De Damborenea J, Garcia I. Caracterización del desgaste discontinuo por deslizamiento en ensayos tipo bola-sobre-disco. XII Congreso Nacional de Materiales. Alicante (Spain), 30th–31st May and 1st-2nd June